

DESY 90-019
March 1990



Some Topics in ep Scattering at HERA:
I. Parton Distributions in the Nucleon

K. Charchula, M. Krawczyk

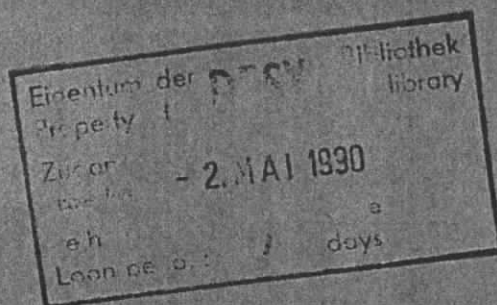
Institute of Theoretical Physics, Warsaw University

H. Abramowicz

Deutsches Elektronen-Synchrotron DESY, Hamburg

A. Levy

School of Physics, Tel-Aviv University



ISSN 0418-9833

NOTKESTRASSE 85

2 HAMBURG 52

Preface

High energy accelerators are to provide us with new information on possible extensions of the fundamental forces and/or fundamental constituents of matter. They provide us also with extensions of phase space domain where the predictions of the Standard Model may be tested further.

Independently of the problem under consideration, one has to refer to the Standard Model whether to test its validity or to estimate its contribution as background.

Although the Standard Model is rightly claimed to describe existing data, quantitative predictions - especially those related to the QCD part, are limited in precision. Whenever in need of an estimation of a physical quantity (i.e. structure function, cross section) from first principles, one is faced with a choice of parton distributions, Λ parameters, evolution equations, threshold effects, etc..., not to mention structure function definition, radiative corrections and many others. Because of the variety of existing data and approaches to extract information from measured physical quantities, it is extremely hard to make an objective choice.

The purpose of our activities is to create a program which allows to calculate inclusive differential cross section for ep scattering in the most general approach, so as to match the future experimental observations. In doing so, we must access the proton, electron and photon structure functions, parton-parton and photon-parton luminosities as well as cross section formulae for all the various processes that build up the ep total cross section.

In our approach we decided to collect "all" the available information, as to be able to estimate the systematic (shall we say theoretical) error of our cross section calculation.

We have encountered many problems in understanding the consistency of various approaches (i.e. leading order or next to leading order determination and evolution of parton densities), in the definition of parton densities beyond the leading order, in the treatment of exceptional kinematic regimes (i.e. low x), in the treatment of threshold effects, etc...

In this note and all the ones to follow, we intend to report the present status of the main ingredients that we need in the determination of physical quantities for ep scattering at the HERA collider. Our final goal, that we hope to achieve at a certain point, is to take into account the experimental conditions for the ZEUS detector, hoping that this step will lead to a realistic estimation of observable physical quantities. Needless to say that if we manage to achieve this goal, we should be able to propose a good strategy for determining structure functions, in the accessible kinematic region. At HERA, this

region will be up to a maximum square momentum transfer $Q^2 \sim 10^5 \text{ GeV}^2$ and down to $x \sim 10^{-4}$.

In the first note, we report our investigations of various parametrizations of parton densities for the nucleon. The next note, in preparation, will deal with the electron and photon structure functions. In the near future we plan to consider parton luminosities, kinematic limits, heavy quark thresholds. We also keep in mind the need to implement radiative corrections. In parallel we want to investigate some aspects of small x physics at HERA.

I. Parton distributions in the nucleon

Abstract

This is the first of a series of reports that we intend to present under a common title of "Some topics in ep scattering at HERA". This one deals with a comprehensive review of available parton parametrizations for the nucleon.

1 Introduction

High statistics experiments on deep inelastic scattering and experiments with hadron hadron beams have been performed in the last decade giving detailed information on the structure functions of the nucleon [1]. This information was used to derive the individual quark and gluon distributions in the framework of the QCD improved parton model [2-9].

Parton distributions play a basic role in studies of inclusive hadronic processes at present and future ranges of energy. Their specific features determine the behaviour of hadronic cross sections at high energies. Any reliable estimation of a possible signal of new physics will also depend on these ingredients. Therefore it is very important to realize what we know presently about parton densities and to what accuracy. The level of uncertainty attached to the parton densities depends of course on the experimental errors. Another source of uncertainty is associated with theoretical methods used in extraction of parton densities at some reference energy scale and in the calculation of their evolution to higher energies, beyond those currently available.

A variety of parton parametrizations exist in the literature. They differ among themselves in many respects, which results in sets of parton distributions with quite different features.

The largest variation can be observed for the gluon distribution which is partly due to the fact that there is still no direct measurement of gluons at present experiments. This uncertainty is getting even larger if an extrapolation over a wide kinematical range is performed. And this is precisely what is needed in order to describe high energy hadronic processes which, as we expect, are dominated by gluon initiated subprocesses.

Recent studies have pointed out the limitation of QCD calculations based on the leading order analysis [5-10]. The inclusion of corrections beyond the leading ones, seems

to be necessary to make reliable predictions for future accelerator energies, especially in such kinematic regions as the one defined by small x . In the calculations based on the next to leading order approximation one deals with quantities which depend on the renormalization scheme. Therefore in order to obtain a meaningful result for physical cross sections it is necessary to proceed with care in a selfconsistent manner.

For all these reasons, it is of interest to make an extended comparison of parton densities obtained according to the different parton parametrizations available in the literature. The purpose of this paper is to present a useful review of the existing sets of parton distributions and their comparisons in interesting kinematic regions. We would like to pay special attention to the theoretical assumptions used in their derivations. We would also like to clarify the experimental input used for individual parametrizations, since it influences the final results for parton distributions.

We have investigated the most popular parametrizations, listed below:

- P1.** Duke and Owens (DO) [4]-sets 1,2
- P2.** Eichten, Hinchliffe, Lane and Quigg (EHLQ) [5]-sets 1,2
- P3.** Martin, Roberts and Stirling (MRS) [6]-sets 1,2,3 and [7]-sets E',B'
- P4.** Diemoz, Ferroni, Longo and Martinelli (DFLM) [8]- set 1 (FXAVER), set 2 (FXN-LLA)
- P5.** Glück, Godbole and Reya (GGR) [10]-sets 1,2.

We describe in details the assumptions underlying each parametrization. This will allow to use them with understanding in a systematic and selfconsistent manner in future applications. We present the comparison of parton densities obtained according to the prescriptions **P1-P5** in a wide range of x and Q^2 . This can be used for estimation of the uncertainty of the predicted hadronic cross sections due to the different choice of parametrizations of parton distribution functions. Last but not least it will also constitute some reference for the experimental results still to come, on parton distributions within nucleons, e.g. at HERA.

We start by defining the kinematic variables which appear in deep-inelastic scattering (Sec. 2). Section 3 contains some general remarks on the QCD improved parton model analysis of the structure of the nucleon. In sections 4 and 5 a detailed description of parametrizations **P1-P5** and their comparison with each other is presented. Results of this work are finally summarized in Sec. 6.

The Fortran code for calculating parton densities according to prescriptions **P1-P5** is available via BITNET from the authors (F1PCHA at DHHDESY3).

2 Deep inelastic ep scattering

The inelastic scattering process

$$e + p \longrightarrow l + X \quad (1)$$

where l is the scattered lepton and X stands for the final hadronic state, can be illustrated as in fig. D1.

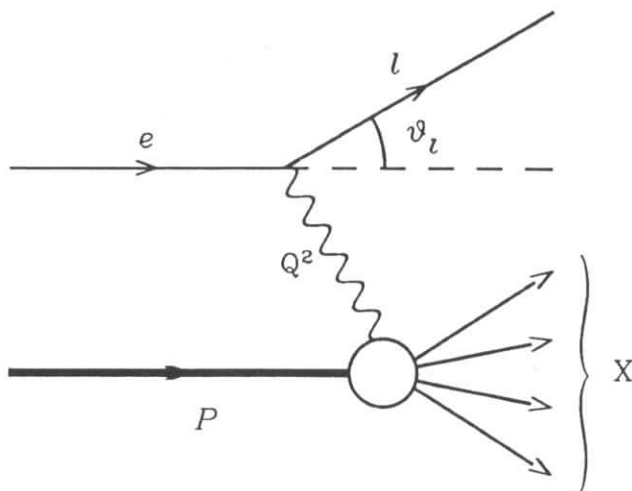


Fig. D1. The deep inelastic process $ep \longrightarrow lX$.

The wavy line in the diagram denotes the exchanged vector bosons: γ/Z^0 for neutral current (NC) interactions and W^\pm for charged current (CC) interactions.

At fixed incoming energy the kinematics of this process is determined by two independent variables only. From the experimental point of view the most natural ones are: the energy (E_l) and the angle (θ_l) of the final lepton state. There are also other, often used, variables. Let p_e be the four-momentum of the incoming electron, p_l of the scattered lepton and P that of the incoming proton. The total invariant mass squared is equal to

$$s = (p_e + P)^2. \quad (2)$$

The momentum transfer variable Q^2 is defined so as to be positive:

$$Q^2 \equiv -q^2 = -(p_e - p_l)^2 \simeq 4E_e E_l \sin^2(\theta_l/2) \quad (3)$$

where ' \simeq ' means that the masses of the electron and the scattered lepton are neglected (a good approximation at HERA energies).

The next variable, which can be interpreted as the energy transfer to the final-state hadronic system in the nucleon rest frame, is given by the relation:

$$\nu \equiv \frac{P \cdot q}{M_p} \simeq \frac{2E_p}{M_p} (E_e - E_l \cos^2(\theta_l/2)) \quad (4)$$

The dimensionless variables Bjorken- x and y are defined as:

$$x \equiv \frac{Q^2}{2P \cdot q} = \frac{Q^2}{2M_p \nu} \simeq \frac{E_e E_l \sin^2(\theta_l/2)}{E_p (E_e - E_l \cos^2(\theta_l/2))} \quad (5)$$

$$y \equiv \frac{P \cdot q}{P \cdot p_e} = \frac{2P \cdot q}{s} \simeq \frac{E_e - E_l \cos^2(\theta_l/2)}{E_l} \quad (6)$$

The invariant mass W of the hadronic system takes the form

$$W^2 \equiv (q + P)^2 = Q^2 \frac{1-x}{x} + M_p^2. \quad (7)$$

The physical region defined by $M_p^2 \leq W^2 \leq s$ implies some kinematic limits on the variables defined above:

$$0 \leq x \leq 1, \quad 0 \leq y \leq 1, \quad 0 \leq Q^2 \leq 2M_p \nu, \quad 0 \leq \nu \leq (s - M_p^2)/2M_p \quad (8)$$

In principle any two of those variables may be used for the description of deep inelastic processes, but (x, y) and (x, Q^2) are the most frequently used ones.

The cross sections for deep inelastic lepton-hadron scattering are commonly written in terms of structure functions which contain information about the internal structure of the hadron. For example, the differential cross section for ep scattering mediated by the neutral current is given in terms of the structure functions F_1, F_2, F_3 by the following formula:

$$\frac{d^2 \sigma_{NC}(e^\mp)}{dx dQ^2} = \frac{4\pi\alpha^2}{xQ^2} \left\{ y^2 x F_1(x, Q^2) + (1-y) F_2(x, Q^2) \pm \left(y - \frac{y^2}{2}\right) x F_3(x, Q^2) \right\}. \quad (9)$$

The above formula relating σ to F_1, F_2, F_3 suggests that measuring cross section is in fact equivalent to measuring structure functions. The extraction of F_i from the measured cross sections is relatively straightforward although some technical difficulties have to be solved, but those are not the only source of uncertainties influencing the determination of structure functions. A more serious problem arises because of the radiative corrections to the elementary upper vertex (see fig. D1), since those corrections change the relation

(9) between σ and F_i . Different approaches to radiative corrections used in the analysis of deep inelastic experiments lead to different structure functions independently of the initial data for cross sections. The determination of F_i involves quite a lot of theoretical ingredients in contrast to the otherwise directly measured σ .

The structure functions F_i depend on the process and in principle they may be very different (e.g. in ep and νp scattering) and not directly related to each other. In the quark-parton model they acquire an interpretation and can be expressed in terms of universal (process-independent) parton distributions.

A full description of the structure of hadrons in the theory of strong interactions is still missing. It is not possible to obtain absolute predictions for F_i from first principles until the confinement problem is solved. The quark-parton model as well as its QCD improved version describe only some aspects of the hadron structure which lead to relations between F_i , sum rules, asymptotic behaviour, etc. The QCD improved parton model predicts the Q^2 -dependence of structure functions, but the structure functions themselves have to be determined from some experimental input.

3 Parton densities in the QCD improved parton model

The parton model has offered a first insight into the structure of hadrons. In this model, in the infinite momentum frame, partons carrying a fraction x of the hadron (longitudinal) momentum are distributed in the hadron with densities which depend only on x [12]. This scaling behaviour of parton distributions was observed in early deep inelastic experiments [13].

More precise measurements have shown deviations from the above simple picture based on the (naive) parton model. A new attempt to describe the hadron structure at high energies led to the formulation of the so called QCD improved parton model, which provides the framework for most studies of high energy processes at current and future accelerators (see for example [14]).

In this approach partons—quarks and gluons are treated as elementary objects of the Quantum Chromodynamics (QCD) with the appropriate interactions. As a natural consequence one has to take into account the creation and annihilation processes which occur during the interaction of an external probe (e.g. virtual γ , Z , or W in deep inelastic scattering) with the hadron. In the deep inelastic scattering radiation of gluons and $q\bar{q}$ pairs leads to parton distributions which depend on Q^2 — the virtuality of the exchanged bosons ($Q^2 = -q^2 > 0$). These exchanged bosons (γ^* , Z or W) play a role of

a "partonometer" with a resolution

$$\Delta b \sim \frac{1}{\sqrt{Q^2}}. \quad (10)$$

The structure of hadron seen by the probe depends on the reference frame. It is greatly simplified in the infinite momentum frame, where the hadron has large momentum. For large Q^2 partons from long chains of subsequent radiations can be "registered" by the partonometer. There are many such partons and they are predominantly soft, since there is little chance that after many decays, the final partons will carry large energy. The partonometer with smaller Q^2 sees rather few energetic partons from the early stage of the parton cascade.

These features of parton distributions in the nucleon are described by the so called ladder diagrams (fig. D2) which give a dominant contribution to the deep inelastic cross section in perturbative QCD.

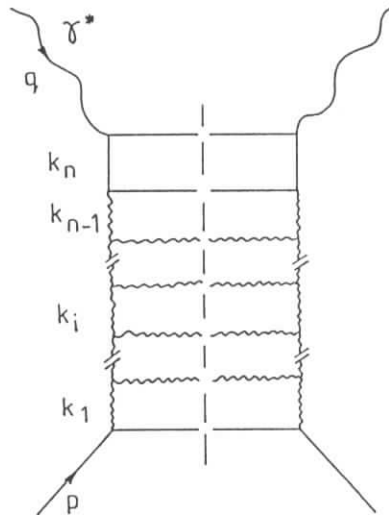


Fig. D2. The ladder diagram describing (in the physical gauge) the cross section for the γ^*q interaction in the LLA. Four momenta of the virtual photon, the initial quark and exchanged partons are equal to q , p and k_1, \dots, k_n , respectively. Gluons (quarks) are denoted by curly (solid) lines. The vertical dashed line means that the amplitude M for the process $\gamma^*q \rightarrow \{\text{partons}\}$ (left part of the diagram) is multiplied by the complex conjugated one: M^* (right part). The cross section is obtained after the integration of $|M|^2$ over the phase space allowed for the final particles.

The ladder diagram describes the development of one parton cascade interacting with a partonometer. (Note that the probabilistic parton interpretation requires the selection

of a special gauge). The large contribution to the cross section or structure function at large Q^2 arises from an integration with respect to virtualities of products from sequential decays with a strict order in a broad range of these virtualities:

$$\mu^2 \sim p^2 \sim p_{\perp}^2 \ll |k_1^2| \sim k_{1\perp}^2 \ll \dots \ll |k_{n-1}^2| \sim k_{n-1\perp}^2 \ll |k_n^2| \sim k_{n\perp}^2 \ll |q^2| \quad (11)$$

where we have introduced the numbering of the decay products (momentum) k_i from $i = 1$ to n ; p is the momentum of the original quark, μ^2 is a characteristic value of virtuality above which α_s may be assumed small, thus justifying the applicability of perturbation theory. The quark interacting directly with the photon is the one with momentum k_n .

For the longitudinal momentum fractions x_i we have

$$x_p \sim 1 \geq x_1 \geq x_2 \dots \geq x_n = x. \quad (12)$$

The leading contribution for large Q^2 and $x \sim \mathcal{O}(1)$ obtained in this way is of the type

$$\left(\alpha_s \ln(Q^2/\mu^2)\right)^n \quad (13)$$

where $x \sim \mathcal{O}(1)$ means that x may be small but not too small, say $10^{-2} \leq x \leq 1$. The procedure which relies on keeping only these dominant terms is called the leading logarithmic approximation (LLA) (see [14,15]). The logic of this approximation lies in selecting diagrams that contain the maximum power of $\ln Q^2$ in every order of perturbation theory¹. More precisely, for small α_s , we have

$$\frac{\alpha_s}{\pi} \ll 1, \quad \frac{\alpha_s}{\pi} \ln\left(\frac{1}{x}\right) \ll 1, \quad \frac{\alpha_s}{\pi} \ln\left(\frac{Q^2}{\mu^2}\right) \sim 1 \quad (14)$$

and all terms of order $(\alpha_s \ln(Q^2/\mu^2))^n$ must be taken into account. This means, that in fact not α_s , but $\alpha_s \ln(Q^2/\mu^2)$ becomes the real expansion parameter of the theory. This parameter is not small and could be even bigger than 1. Therefore, as we have mentioned above, we have to sum all terms containing this parameter and there exist appropriate methods [15] to do it to all orders.

So far we have discussed leading logarithmic terms depending only on Q^2 , since the other kinematic variable appropriate for deep inelastic scattering – x is large, $x \sim \mathcal{O}(1)$.

¹In a field theory with massless gauge bosons the maximum power of logarithms in each order of perturbation calculations, is equal to 2: $\alpha_s \ln^2 Q^2$. These so called double logarithmic terms arise in very specific physical situations and do not appear in the cross section for deep inelastic scattering.

Deep inelastic scattering at very small x ($x \ll 1$) and large Q^2 requires similar treatment of $\ln(Q^2/\mu^2)$ and $\ln(1/x)$ [16,17]. Keeping the leading logarithms of $1/x$ (i.e. $(\alpha_s \ln(1/x))^n$) leads to the leading logarithmic approximation in x – LLA(x) (in contrast to the previous one which could be called LLA(Q^2)). In the kinematic region of small x double logarithmic contribution of the type $(\alpha_s \ln(1/x) \ln(Q^2/\mu^2))^n$ appear as well. They will arise from ladder diagrams with strong ordering in virtualities and in x_j

$$1 \geq x_1 \gg x_2 \dots x_{n-1} \gg x_n = x. \quad (15)$$

We would like to discuss in this paper leading and next-to-leading logarithmic terms for the deep inelastic scattering for $x \sim \mathcal{O}(1)$, postponing the detailed discussion of small x for a further note. Therefore we will always use the names: leading and next-to-leading in respect to logarithms of Q^2 without further explanation.

In our discussion of deep inelastic scattering we discard all corrections due to parton and target masses and other so called higher twist effects which are expected to have $(\mu^2/Q^2)^n$ ($n = 1, 2, \dots$) behaviour, and should vanish for $Q^2 \rightarrow \infty$.

To make our language more transparent for non-experts we would like to compare different approximations used in the perturbative calculations in QCD or in QED. For a physical quantity R which depends on Q^2 and some other variables

- the calculation of **fixed order** corrections means that we calculate the following terms in sequence

$$R = R_0(\alpha_s^0 + \alpha_s^1 R_1 + \alpha_s^2 R_2 + \dots) \quad (16)$$

and keep the terms up to appropriate order. The first term is called the lowest or Born term. Then the first and the second order corrections appear. R_1, R_2, \dots are functions (usually very complicated ones) of Q^2 and other variables.

- the **leading logarithmic approximation** means that we keep all terms of the type $\alpha_s^n \ln^n Q^2$:

$$R = R_0(\alpha_s^0 + \alpha_s^1 \ln Q^2 \bar{R}_1 + \alpha_s^2 \ln^2 Q^2 \bar{R}_2 + \alpha_s^3 \ln^3 Q^2 \bar{R}_3 + \dots) \quad (17)$$

- the **next-to-leading logarithmic approximation** leads in addition to the series of terms $\alpha_s^n \ln^{n-1} Q^2$, and up to next-to-leading logarithmic accuracy we have:

$$R = R_0(\alpha_s^0 + \alpha_s^1(\ln Q^2 \bar{R}_1 + \bar{R}'_1) + \alpha_s^2(\ln^2 Q^2 \bar{R}_2 + \ln Q^2 R'_2) + \dots) \quad (18)$$

(all leading and next-to-leading terms must be summed).

- the **double logarithmic approximation** is based on the following perturbation expansion:

$$R = R_0(\alpha_s^0 + \alpha_s^1 \ln^2 Q^2 \check{R}_1 + \alpha_s^2 \ln^4 Q^2 \check{R}_2 + \alpha_s^3 \ln^6 Q^2 \check{R}_3 + \dots) \quad (19)$$

where the sum has to be performed to all orders.

In all above formulas functions $\bar{R}_i, \tilde{R}_i, \check{R}_i$ do not depend on Q^2 .

Going beyond LLA means taking into account also less dominant terms, e.g. NLL, NNLL corrections. This structure of higher order corrections is presented graphically in fig. D3.

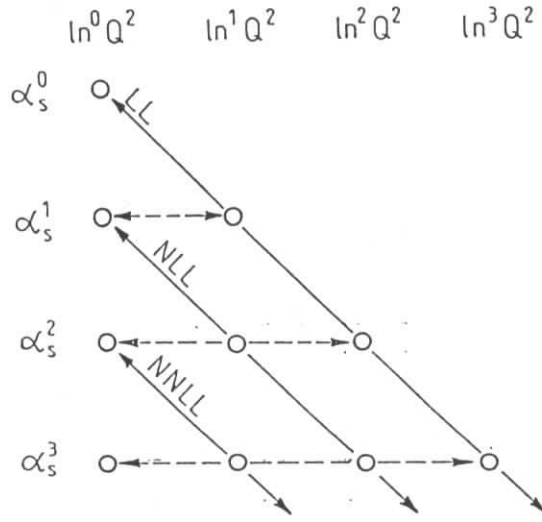


Fig. D3. Structure of perturbative corrections. The horizontal lines show the **fixed order** corrections. The **leading logarithmic** corrections LL are represented by the inclined line. Lines showing the **next-to-leading** NLL, the **next-to-next-to-leading** NNLL, are parallel to the LL line. Arrows indicate that the whole series has to be summed up for LL, NLL and NNLL approximations: $\sum \alpha_s^n \ln^n Q^2$, $\sum \alpha_s^n \ln^{n-1} Q^2$ and $\sum \alpha_s^n \ln^{n-2} Q^2$, respectively.

There is another widely used terminology which differs slightly from ours. Instead of leading logarithmic approximation one uses the name – the leading order (LO) approximation and the same for the next-to-leading terms.

3.1 Leading logarithmic approximation.

As we have discussed before, in the QCD improved parton model the parton densities appear as effective densities depending on the energy scale Q^2 .

For deep inelastic scattering the leading logarithmic approximation (LLA) means that [14]:

- 1) The measured structure functions $F_i(x, Q^2)$ are related to the Q^2 dependent parton densities by the naive parton model formulae.

In the LLA the original scaling parton densities are replaced by effective Q^2 dependent densities:

$$q(x) \rightarrow q(x, Q^2) = q(x) + \Delta q(x, Q^2), \quad (20)$$

where $\Delta q(x, Q^2)$ contains all leading logarithms. The relation to measured structure functions remains as for the parton model, namely:

$$2F_1(x, Q^2) = F_2(x, Q^2)/x = \sum e_q^2 q(x, Q^2) \quad (21)$$

or in a more compact form

$$\mathcal{F}_1(x, Q^2) = \mathcal{F}_2(x, Q^2) = \sum e_q^2 q(x, Q^2), \quad (22)$$

where we have introduced the notation [18]:

$$(\mathcal{F}_1, \mathcal{F}_2, \mathcal{F}_3) \equiv (2F_1, F_2/x, F_3). \quad (23)$$

- 2) The Q^2 dependent parton densities obey the first order (or in other words one-loop) Altarelli-Parisi (AP) evolution equations ² with first order (or one-loop) splitting functions $P_{ij}^{(1)}$:

$$\frac{dq_i(x, Q^2)}{d(\ln Q^2/\Lambda^2)} = \frac{\alpha_s(Q^2)}{2\pi} \int_x^1 \frac{dy}{y} \left[P_{qq}^{(1)}\left(\frac{x}{y}\right) q_i(y, Q^2) + P_{qG}^{(1)}\left(\frac{x}{y}\right) G(y, Q^2) \right] \quad (24)$$

$$\frac{dG(x, Q^2)}{d(\ln Q^2/\Lambda^2)} = \frac{\alpha_s(Q^2)}{2\pi} \int_x^1 \frac{dy}{y} \left[\sum_i P_{Gq}^{(1)}\left(\frac{x}{y}\right) q_i(y, Q^2) + P_{GG}^{(1)}\left(\frac{x}{y}\right) G(y, Q^2) \right] \quad (25)$$

where $q_i(x, Q^2)$ denotes a quark or antiquark distribution and $G(x, Q^2)$ —the gluon distribution. The splitting functions $P_{ab}(x/y)$ describe the probability for a parton b of momentum fraction y to emit another parton a with a fraction x/y of the parent parton momentum. In the LLA these functions are given by [14]:

$$P_{qq}^{(1)}(z) = \frac{4}{3} \left[\frac{1+z^2}{(1-z)_+} + \frac{3}{2} \delta(1-z) \right] \quad (26)$$

²These equations were introduced already in 1972 by V.Gribov and L.Lipatov [15].

$$P_{qG}^{(1)}(z) = \frac{1}{2} (1 - 2z + 2z^2) \quad (27)$$

$$P_{Gq}^{(1)}(z) = \frac{4}{3} \left(\frac{2 - 2z + z^2}{z} \right) \quad (28)$$

$$P_{GG}^{(1)}(z) = 6 \left[z(1-z) + \frac{1-z}{z} + \frac{z}{1-z} + \left(\frac{11}{12} - \frac{N_f}{18} \right) \delta(1-z) \right] \quad (29)$$

with the distribution $1/(1-z)_+$ being defined by

$$\int_0^1 dz \frac{f(z)}{(1-z)_+} \equiv \int_0^1 dz \frac{f(z) - f(1)}{1-z}. \quad (30)$$

The evolution equations (24,25) can be expressed in a more compact form as

$$\frac{df_A^a(x, Q^2)}{d(\ln Q^2/\Lambda^2)} = \frac{\alpha_s(Q^2)}{2\pi} [P^{(1)}(x)]_b^a \otimes f_A^b(x, Q^2), \quad (31)$$

where $f_A^a(x, Q^2)$ is the distribution of parton a in hadron A (here $A = \text{proton}$), and the symbol \otimes means the convolution integral

$$P \otimes f = \int_x^1 \frac{dy}{y} P\left(\frac{x}{y}\right) f(y, Q^2) = \int_x^1 \frac{dy}{y} P(y) f\left(\frac{x}{y}, Q^2\right). \quad (32)$$

In the LLA the running coupling constant is calculated by solving the first order (or one-loop) renormalization group equation

$$\frac{d\alpha_s}{d \ln(Q^2/\Lambda^2)} = -\frac{\beta_0}{4\pi} \alpha_s^2 \quad (33)$$

with

$$\beta_0 = 11 - \frac{2}{3} N_f, \quad (34)$$

where N_f denotes the number of flavours and Λ is the QCD scale. By using this approximation one obtains from the experimental data (see for example [9])

$$\Lambda_{LO} \simeq 200 \text{ MeV}. \quad (35)$$

By solving equations (33,34) one obtains the first order running coupling constant, which is equal to:

$$\alpha_s^{(1)} = \frac{4\pi}{\beta_0 \ln(Q^2/\Lambda^2)} \quad (36)$$

The solution of equations (24,25) together with formula (36) allow the computation of parton densities at any scale Q^2 once the initial conditions are known.

For hadron-hadron collisions the LLA involves the convolution of cross sections for hard subprocesses calculated in the lowest order of the perturbation series expansion (i.e. at the Born level) with the Q^2 dependent parton densities as described above in 1) and 2). To be more specific, the basic formula for a generic high energy inclusive hadronic process

$$A B \rightarrow C X \quad (37)$$

takes in the parton model the following form:

$$\sigma_{AB \rightarrow CX} = f_A^a \otimes \hat{\sigma}_{ab \rightarrow cX} \otimes f_B^b, \quad (38)$$

where $f_A^a(f_B^b)$ is the distribution function of parton $a(b)$ in hadron $A(B)$, and $\hat{\sigma}$ is the hard scattering cross section for the partonic subprocess. In the QCD improved parton model the cross section (38) is equal in the leading logarithmic approximation to:

$$\sigma_{AB \rightarrow CX} = f_A^a|_{LLA} \otimes \hat{\sigma}_{ab \rightarrow cX}^{Born} \otimes f_B^b|_{LLA} \quad (39)$$

where $f_A^a|_{LLA}$ denotes the distributions obeying the first order evolution equations (see point 2) above) ³.

3.2 Next-to-leading logarithmic approximation.

The importance of the next-to-leading logarithmic corrections arises at higher energies. In the next-to-leading logarithmic approximation (NLLA) besides the leading terms, also less dominant contributions of the type

$$\alpha_s^n \ln^{n-1}(Q^2/\mu^2) \quad (40)$$

are taken into account.

The existing analyses of deep inelastic scattering beyond LLA are limited to order α_s corrections to the parton densities and to the splitting functions. This means that we have here

$$q(x) \rightarrow q(x, Q^2) = q(x) + \Delta \bar{q}(x, Q^2) \quad (41)$$

³The terminology used here is in some sense misleading, since not all ingredients in (39) are really calculated in LLA—for example, for the parton cross section we take the lowest order formulae. One should rather say that eq. (39) is obtained in the leading order approach within the QCD improved parton model. The consistent application of the LLA cross section (38) should take into account the logarithmic structure also for $\hat{\sigma}$.

where now $\Delta\bar{q}(x, Q^2)$ contains leading and next-to-leading logarithms, and

$$P_{ij}^{(1)}(x) \rightarrow P_{ij}^{(1)}(x) + \frac{\alpha_s(Q^2)}{2\pi} P_{ij}^{(2)}(x). \quad (42)$$

In the next-to-leading logarithmic approximation applied to the deep inelastic scattering:

- 1) the expressions for the structure functions $\mathcal{F}_i(x, Q^2)$ in terms of parton densities deviate, in principle, from the parton model formulae, e.g. for \mathcal{F}_2 :

$$\mathcal{F}_2(x, Q^2) = \sum_{q, \bar{q}} e_q^2 q(x, Q^2) + \Delta\mathcal{F}_2 \quad (43)$$

- 2) the evolution equations include additional next-to-leading contributions $P_{ij}^{(2)}$ (second order or two-loop splitting functions) [14]:

$$\frac{df_A^a(x, Q^2)}{d(\ln Q^2/\Lambda^2)} = \frac{\alpha_s(Q^2)}{2\pi} \left[P^{(1)}(x) + \frac{\alpha_s(Q^2)}{2\pi} P^{(2)}(x) \right]_b^a \otimes f_A^b(x, Q^2) \quad (44)$$

The particular form of these next-to-leading logarithmic corrections depends on the (renormalization and factorization) scheme or in other words on the definition of parton densities. Going from parton model distributions to the effective ones by keeping the leading logarithmic contributions is a well defined procedure, since the coefficients of the maximum power of $\ln Q^2$ in each order of α_s do not depend on the method of calculations⁴. It is a matter of convention or definition how many other terms, which are less dominant from the point of view of the LLA approximation, are incorporated into the "renormalized" parton densities beyond leading logarithms. Let us discuss this point in more details, since it will play an important role in the forthcoming analysis.

The structure functions $F_i(x, Q^2)$ (or $\mathcal{F}_i(x, Q^2)$) are physical quantities which are determined in deep inelastic experiments. They can not and do not depend on the renormalization scheme used in the theoretical calculations. It is the quark or gluon densities which, as theoretical objects, have to be defined somehow and which are sensitive to the details of the calculation methods. In the QCD improved parton model we interpret structure functions in terms of parton densities. Of course the relations between the data of $F_i(x, Q^2)$ and parton densities depend on the definition used for $q(x, Q^2)$ or $G(x, Q^2)$.

⁴On the other hand in the LLA there is a strong dependence of parton densities on the scale parameter Λ (scale ambiguity), which cannot be compensated by the other theoretical ingredients as it happens in the NLLA.

In the leading logarithmic analysis we are dealing with a scheme independent part of higher order corrections and therefore we do not have to worry about renormalization scheme dependence. But for all next-to-leading considerations we must proceed in a self consistent manner in order to get predictions for physical cross sections.

For example, for the high energy process (37) the next to leading logarithmic approximation requires the use of hard cross section $\hat{\sigma}$ and parton densities defined in the same scheme and calculated to a consistent order, since both of these ingredients are scheme (and scale) dependent. To be more precise—the hard cross section calculated up to first order corrections should be convoluted with the distribution function obtained in NLLA (with second order splitting functions):

$$\sigma_{AB \rightarrow CX} = f_A^a|_{NLLA} \otimes \hat{\sigma}_{ab \rightarrow cX}^{1st\ order} \otimes f_B^b|_{NLLA} \quad (45)$$

It is necessary to use here parton distributions obtained according to the two-loop evolution equations since only in this way leading and next-to-leading terms are evaluated properly. In particular, at order α_s , the parton distributions will contain full *1st order* corrections derived with the same accuracy as $\hat{\sigma}$ ⁵.

For consistency in the calculation performed in NLLA one should also use the appropriate running coupling constant including two loop contributions. We will give the NLLA formula for α_s later.

One of the definitions [11] of parton distributions used in an analysis performed beyond leading logarithmic approximation, is based on the requirement that in terms of the 'renormalized' scale dependent parton densities $q(x, Q^2)$, the naive parton model formula holds for the structure function $\mathcal{F}_2(x, Q^2)$ with no corrections proportional to $\alpha_s(Q^2)$:

$$\mathcal{F}_2(x, Q^2) \equiv F_2(x, Q^2)/x = \sum \epsilon_q^2 q(x, Q^2) \quad (46)$$

with the following relations between bare (parton) and renormalized quark densities:

$$q_i(x, Q^2) = q_i(x) + \int_x^1 \frac{dy}{y} \left\{ \left[\frac{\alpha_s}{2\pi} \ln\left(\frac{Q^2}{\Lambda^2}\right) P_{qq}\left(\frac{x}{y}\right) + \alpha_s f_{q,2}\left(\frac{x}{y}\right) \right] q(y) + \left[\frac{\alpha_s}{2\pi} \ln\left(\frac{Q^2}{\Lambda^2}\right) P_{qG}\left(\frac{x}{y}\right) + \alpha_s f_{G,2}\left(\frac{x}{y}\right) \right] G(y) \right\}, \quad (47)$$

where $f_{q,2}$ and $f_{G,2}$ are so called constant (i.e. independent on Q^2) terms. Other structure functions receive α_s corrections. For example, in terms of these densities, the electropro-

⁵The more consistent treatment of all next-to-leading logarithmic corrections will require calculation of NLL terms also for $\hat{\sigma}$ (see the footnote on page 13, where this point is discussed for LLA).

duction structure function $\mathcal{F}_1(x, Q^2)$ may be written as

$$\mathcal{F}_1(x, Q^2) = \sum_{q, \bar{q}} e_q^2 q(x, Q^2) + \alpha_s \Delta f_1 + \mathcal{O}(\alpha_s^2), \quad (48)$$

where

$$\begin{aligned} \Delta f_1 = & \int_x^1 \frac{dy}{y} \left\{ \sum_i \left[f_{q,1}\left(\frac{x}{y}\right) - f_{q,2}\left(\frac{x}{y}\right) \right] q_i(x, Q^2) \right. \\ & \left. + \left(\sum_i e_q^2 \right) \left[f_{G,1}\left(\frac{x}{y}\right) - f_{G,2}\left(\frac{x}{y}\right) \right] G(x, Q^2) \right\}. \end{aligned} \quad (49)$$

This definition, called the DIS scheme, is a very natural one for quark densities since a large fraction of the information on the structure of nucleons comes from measurements of F_2 in deep inelastic scattering experiments. It has also further theoretical advantages.

For the gluon distribution DIS does not offer any appropriate definition. Usually, together with the above convention for quark distributions, one fixes the gluon density beyond the LLA by demanding momentum conservation:

$$\int_0^1 dx \, x \left\{ \sum_f \left[q_f(x, Q^2) + \bar{q}_f(x, Q^2) \right] + G(x, Q^2) \right\} = 1. \quad (50)$$

It has been stressed (see, e.g. [8,14]) that the definition of the gluon should be taken from some strong interaction process, for example the two jet cross section in hadron—hadron collision, which is not measured yet precisely enough.

The other convention or renormalization scheme for parton distribution beyond LLA is called universal or $\overline{\text{MS}}$ renormalization scheme since it is based on the modified minimal subtraction scheme [19]. In this approach no specific process or quantity is favoured. In all of them there are corrections of order α_s (or higher) to the naive parton model formulae. The applicability to all orders of perturbation expansion is straightforward⁶. In this scheme one obtains the second order coupling constant:

$$\alpha_s^{(2)}(Q^2) = \alpha_s^{(1)}(Q^2) \left[1 - \frac{\alpha_s^{(1)}(Q^2) \beta_1}{4\pi \beta_0} \ln \ln(Q^2/\Lambda^2) \right], \quad (51)$$

where $\alpha_s^{(1)}(Q^2)$ is the first order α_s , given by eq.(36),

$$\beta_1 = 102 - 38N_f/3 \quad (52)$$

and

$$\Lambda_{\overline{\text{MS}}} = 300 \text{ MeV}. \quad (53)$$

⁶The second order $\overline{\text{MS}}$ splitting functions can be found in refs [19,11].

4 Parton parametrizations

In order to describe the hadronic processes at high energies it is necessary to know the individual parton distributions as functions of x and Q^2 . Since theory does not give absolute predictions for parton distributions, they have to be obtained from some experimental input and then the AP equations allow to determine those parton distributions at any Q^2 , even not accessible experimentally. However parton distributions are not directly measured in the experiment; it is the structure functions or hadronic cross sections that are measured, although in a limited range of x and Q^2 ($0.015 < x < 0.75, 0.5 < Q^2 < 250 \text{ GeV}^2$). Individual quark and gluon distributions in the nucleon may be usually determined in a simple analytical form from those data with some additional experimental and theoretical information.

The purpose of parametrizing the evolved parton distributions is to provide the user with an easy access to the solutions of the AP equations in any kinematic region, including the one covered by the experimental data.

Several such parametrizations with analytical approximations for parton distributions are available, for example the DO and EHLQ ones. In other parametrizations the resulting parton densities are in the form of (x, Q^2) grids with interpolation, e.g. the MRS sets.

The parton parametrizations presented in this note have been obtained in two different approaches and with different sets of available data. One of the approaches is to introduce the parton distribution at the level of the global fit. It means that the structure functions are parametrized at some reference value Q_0^2 and then evolved numerically in Q^2 through the AP equations in the kinematic regions where they are measured. A global fit is then performed to determine the best values for the starting parameters, as well as for the QCD scale parameter Λ . A by-product of these fits performed on the singlet structure function F_2 is a parametrization of the gluon distribution at the reference scale Q_0^2 . Because deep inelastic scattering does not constrain significantly the gluon distribution, a large variety of gluon behaviour is proposed in the literature. The parameters describing the gluon distribution are usually strongly correlated with the Λ value obtained from the fit. It is a matter of taste which parametrization of gluon distributions is chosen—typically a “hard” or a “soft” one, each with its own Λ value (see for example the MRS parametrization). This is the approach of DO and MRS.

The other approach, e.g. the one of EHLQ and DFLM is to take the parametrization of structure functions as obtained in various experiments and disentangle the contribution

of parton distributions at a reference Q_0^2 value. The evolution is then independent of the data, and relies on the Λ value and gluon distribution as determined from the original fit.

A very comprehensive discussion of the influence of various assumptions used for the evolution and the determination of structure functions, and the impact of systematic uncertainties on the parametrizations is given by Wu-Ki Tung et al. in [11]. A weak point of all the global parametrizations is that they include systematic errors in an approximate way, or not at all, since the experimentalists are the only ones to know the point-to-point correlations which are of prime importance for the slopes of structure functions. The relative normalization of various data is another source of uncertainty and it is a question of taste which data to trust. This influences directly the overall normalization of parton densities.

All in all, part of the disagreement observed in various parametrizations is certainly due to the choice of data. It makes it even more interesting to look at the results, since the observed differences are a measure of our knowledge and cannot be sorted out without additional new data, which hopefully, thanks to the tremendous theoretical and experimental effort, will allow us to explore new domains with less uncertainty.

4.1 Duke-Owens (DO)

This is a leading order (LO) type of parametrization. It is a simple, convenient one — available in a compact, analytic form. In the fitting procedure at the reference scale $Q_0^2 = 4 \text{ GeV}^2$ the following deep inelastic data were used: SLAC'79, CDHS'83 and EMC'81, as well as dimuon: CFS'81, ISR'82 and J/Ψ '79 data. Because of systematic overall normalization disagreement between different data sets, all of them were renormalized to the EMC'81 data. In addition, cuts of $x \geq 0.1$ and $Q^2 \geq Q_0^2$ were imposed. The other assumptions were:

- $N_f = 4$, i.e. bottom and top quark distributions were not provided;
- the charm content at the reference scale was neglected: $c = \bar{c} = 0$ at Q_0^2 ;
- an $SU(3)$ symmetric sea was assumed, i.e. the strange quark distribution $s(x)$ was set equal to the light sea distribution.

Two sets of parton distributions are provided, corresponding to different shapes of the gluon distribution and consequently different values of $\alpha_s(\Lambda)$:

Set 1 (soft) with $\Lambda = 200$ MeV and $xG(x, Q_0^2) \sim (1 + 9x)(1 - x)^6$;

Set 2 (hard) with $\Lambda = 400$ MeV and $xG(x, Q_0^2) \sim (1 + 9x)(1 - x)^4$.

The Q^2 -dependence enters into formulae for parton distributions through the variable

$$\bar{s} = \ln[\ln(Q^2/\Lambda^2)/\ln(Q_0^2/\Lambda^2)]$$

which varies slowly with changing Q^2 . The valence quark distributions are expressed in the form:

$$\begin{aligned} x(u_v + d_v) &= N_{ud}x^{\eta_1}(1-x)^{\eta_2}(1 + \gamma_{ud}x) \\ xd_v &= N_d x^{\eta_3}(1-x)^{\eta_4}(1 + \gamma_d x) \end{aligned}$$

while sea and gluon distributions are parametrized as follows:

$$Ax^a(1-x)^b(1 + dx + \beta x^2 + \gamma x^3).$$

All parameters appearing in the above formulae are polynomials in \bar{s} up to the 2-nd order.

The range of applicability is as follows:

$$\begin{aligned} 0 &< x < 1 \\ 4 \text{ GeV}^2 &< Q^2 < \sim 10^6 \text{ GeV}^2. \end{aligned}$$

According to the authors the accuracy is

at a few-percent level for Q^2 up to about 1 TeV² for the bulk of the x range from 0 to 1. The only exception to this is for the gluon and sea distributions at large x values where the distributions are already extremely small.

4.2 Eichten-Hinchliffe-Lane-Quigg (EHLQ)

This is also a leading order (LO) parametrization. Primarily CDHS'83 data were used in the fitting procedure at the input scale $Q_0^2 = 5 \text{ GeV}^2$. The integration of the evolution equations was performed numerically, therefore no full range of x was required. The parametrization is based on the expansion in terms of orthogonal polynomials $P_n(y)$. The small x region, which is very important for applications at high energies, was treated

separately. For this reason the x range has been divided at $x = 0.1$. For $x > 0.1$ the distribution functions were parametrized as

$$f(x, Q^2) = x^{-1}(1-x)^a \sum_{i,j} c_{ij} P_i(x) P_j(\ln(Q^2/\Lambda^2))$$

For smaller x ($x < 0.1$), polynomials in $\ln(x)$ were used instead of polynomials in x . Depending on the shape of the gluon distribution, there are two sets:

$$\text{Set 1 (soft) with } \Lambda = 200 \text{ MeV; } xG(x, Q_0^2) \sim (2.62 + 9.17x)(1-x)^{5.9};$$

$$\text{Set 2 (hard) with } \Lambda = 290 \text{ MeV; } xG(x, Q_0^2) \sim (1.25 + 15.57x)(1-x)^{6.03}.$$

This parametrization provides parton distributions for $N_f = 6$. At $Q_0^2 = 5 \text{ GeV}^2$ heavy quarks (c, b, t) are neglected and the value of Λ has been determined for $N_f = 4$. Distributions of heavy quarks above their production threshold $Q^2(1-z)/z > 4m^2$ were obtained by including explicit heavy quark mass dependence in the corresponding gluon to quark splitting functions. The masses of the heavy quarks are: $M_b = 5.5 \text{ GeV}$ and $M_t = 30 \text{ GeV}$. The range of applicability is as follows:

$$10^{-4} < x < 1 \\ 5 \text{ GeV}^2 < Q^2 < 10^8 \text{ GeV}^2.$$

4.3 Martin-Roberts-Stirling (MRS)

This parametrization uses next to leading order QCD (NLLA) in the \overline{MS} scheme. The original version [6] was based on EMC'85,'86,'87 data, together with those from CDHSW'86 and CCCFRR'84 with appropriate renormalization (of order 10 %). It consist of three sets that differ in the form of the gluon distribution at the reference scale $Q_0^2 = 4 \text{ GeV}^2$, where $N_f = 3$:

$$\text{MRS1 (soft); } xG(x, Q_0^2) \sim (1-x)^5 \text{ and } \Lambda_{\overline{MS}} = 107 \text{ MeV ;}$$

$$\text{MRS2 (hard); } xG(x, Q_0^2) \sim (1-x)^4(1+9x) \text{ and } \Lambda_{\overline{MS}} = 250 \text{ MeV;}$$

$$\text{MRS3 (1/}\sqrt{x}\text{); } xG(x, Q_0^2) \sim 1/\sqrt{x}(1-x)^4(1+9x) \text{ and } \Lambda_{\overline{MS}} = 178 \text{ MeV.}$$

In addition, the sea is $SU(3)$ symmetric i.e. $x\bar{q} = x\bar{u} = x\bar{d} = x\bar{s} = xs$.

Recently [7] the authors have refined set 1 (MRS1), using the BCDMS data instead of the EMC ones. They found that neutrino (CDHSW'86) and muon (BCDMS'87) data are compatible—no renormalization of the former is needed. New sets, including either EMC'86,'87 or BCDMS'87 data, were derived:

MRSE' with $\Lambda_{\overline{MS}} = 100$ MeV;

MRSB' with $\Lambda_{\overline{MS}} = 200$ MeV.

In the fitting procedure, for both sets of parton parametrizations also the new NMC'88 measurements of F_2^n/F_2^p , as well as neutrino (CDHSW'86, CFRR'88) and dimuon (E605'89) data were used. The gluon distribution at $Q_0^2 = 4$ GeV² is taken to be: $xG(x, Q_0^2) \sim (1-x)^{4.4}$. For the bottom quark a fixed threshold in Q^2 at $4M_b^2 = 100$ GeV² for all x is assumed. The range of applicability is as follows:

$$10^{-4} < x < 1$$
$$5 \text{ GeV}^2 < Q^2 < 1.31 * 10^6 \text{ GeV}^2.$$

The authors conclude that

... the comparison with Drell-Yan data appears to favour the 'BCDMS' parton distributions (i.e. MRSB').

4.4 Diemoz-Ferroni-Longo-Martinelli (DFLM)

This parametrization consists of several sets of parton densities corresponding to different assumptions concerning the input parton densities (uncertainties from deep inelastic data) and to different order of perturbative QCD calculations (LO or NLLA). The next-to-leading order version of this parametrization is formulated in the DIS scheme. As input for the QCD evolution of the gluon, the valence and the sea densities, the data from the neutrino experiments: BEBC'85, CCFRR'83, CHARM'83 and CDHS'83 at $Q_0^2 = 10$ GeV² were used. There are some specific assumptions:

- $d_v/u_v = r(1-x)$, where r was fitted to be $r = 0.57$;
- $\bar{s} = 0.2(\bar{u} + \bar{d}) = 0.4\bar{u}$;
- $xG \sim (1 - 0.18x)(1-x)^{5.06}$.

In the evolution procedure, corrections due to threshold effects for heavy flavours were included. Particularly, at Q_0^2 charm threshold was already opened ($N_f = 4$) but $c(x, Q_0^2) \approx 0$. Masses of the heavy quarks are as follows: $M_b = 4.5$ GeV and $M_t = 40$ GeV. The heavy flavour distributions are valid only for values of Q^2 larger than the threshold ($Q^2 > M_h^2$) in spite of the fact that this parametrization may give in any case results also for lower Q^2 .

Depending on the order, in which QCD evolution was performed, the authors favour two sets:

FXAVER (LO) with $\Lambda_{\overline{MS}} = 200$ MeV;

FXNLLA (NLL0) with $\Lambda_{\overline{MS}} = 300$ MeV.

The parton densities are available in the following range:

$$\begin{aligned} 5. * 10^{-5} < x < 0.95 \\ 10 \text{ GeV}^2 < Q^2 < 10^8 \text{ GeV}^2. \end{aligned}$$

4.5 Glück-Godbole-Reya (GGR)

The last parametrization discussed here provides two qualitatively different sets. The first one, GGR1, has been evaluated dynamically using the assumption that at some low resolution scale the nucleon consists of valence quarks only. The valence quarks in turn generate radiatively the gluons and the sea quark pairs, and their distributions are described by the leading-order Renormalization Group evolution equation. In this scheme only input valence densities $u_v(x, Q_0^2)$ and $d_v(x, Q_0^2)$ are required and they are taken the same as determined by DFLM at $Q_0^2 = 10 \text{ GeV}^2$. The resulting predictions for $G(x, Q^2)$ and $q_{sea}(x, Q^2)$ do not involve any additional assumptions.

The second set, GGR2, was produced in the conventional manner, i.e. with input $G(x, Q_0^2)$ and $\bar{q}(x, Q_0^2)$ distributions (taken from [8]). At the input scale the strange quark distribution was taken to be $s = \bar{s} = 0.4\bar{u}$.

In the Q^2 evolution for both of these sets only three light ($N_f = 3$) flavours were included. The distributions for the heavy quarks $h = c, b, t$ were calculated from the formula:

$$h(x, Q^2) = \bar{h}(x, q^2) = \frac{\alpha_s(Q^2)}{2\pi} \ln \left(\frac{Q^2}{M_h^2} \right) \int_x^1 \frac{dy}{y} P_{qG} \left(\frac{x}{y} \right) G(y, Q^2)$$

which gives a good description of processes involving heavy quarks for $Q^2 \geq 100 M_h^2$.

This parametrization is valid for:

$$\begin{aligned} 10^{-5} < x < 0.95 \\ 10 \text{ GeV}^2 < Q^2 < 10^6 \text{ GeV}^2. \end{aligned}$$

As was pointed out in [10]:

... the dynamically predicted $G(x, Q^2)$ and $\bar{q}(x, Q^2)$ turn out to be much steeper and larger in the very small x region ($x < 10^{-2}$) than the conventional distributions.

The two sets differ distinctly in the predictions for F_2^{ep} in the low- x region. Recent preliminary data from the EMC collaboration (EMC'89) support the results of the conventional one.

5 Results of different parametrizations

5.1 Parton densities

Before we start a detailed comparison of predictions of various parametrizations some words of caution are needed, since parton densities are not physical observables and additional theoretical assumptions have to be used in their determination. All existing parametrizations can be divided into two main groups depending on the approach used – LLA or NLLA. It is in principle meaningless to compare parton densities obtained in NLLA in different renormalization schemes since they are not physical observables. Only after convolution with hard processes cross sections, which also depend on the scheme, one obtains scheme independent predictions for physical quantities. For example, the proper formula for the cross section would be (schematically)

$$\sigma = f_{DIS} \otimes \hat{\sigma}_{DIS} = f_{\overline{MS}} \otimes \hat{\sigma}_{\overline{MS}}. \quad (54)$$

On the other hand there is a unique transformation of one set of quark distribution functions into another one, defined in a different manner, e.g.

$$f_{DIS}^q = \left(1 + \frac{\alpha_s}{2\pi} C_q^2(x)\right) \otimes f_{\overline{MS}}^q + \frac{\alpha_s}{2\pi} C_G^2(x) \otimes f_{\overline{MS}}^g \quad (55)$$

where C_q^2 and C_G^2 are known coefficients. Only after this transformation, a proper comparison between different parametrizations can be made (see for example [11]).

There are also objections against the procedure in which one uses distribution functions obtained in the NLLA, but with the lowest order (Born) expressions for $\hat{\sigma}$ in the prediction for hadronic cross sections:

$$\sigma = f|_{NLLA} \otimes \hat{\sigma}_{Born} \quad (\text{wrong}). \quad (56)$$

Although not all of the existing approaches are theoretically consistent, they have been used in many applications. Therefore it seems to be useful to estimate the actual size of

the differences between the commonly used schemes for various parton distributions in important kinematic regions.

The significance of the second order evolution in the small x region was pointed out in Ref.[11]. Therefore it is of interest to compare the LLA approach with the NLLA in order to gain confidence in the predictions at high energies. A very useful comparison has been made in Ref.[11], where the results of different evolutions (leading and next-to-leading) are presented with a fixed input parametrization.

Now we will start to present the predictions of parametrizations P1—P5 for parton densities of the proton for $10 \text{ GeV}^2 \leq Q^2 \leq 10^4 \text{ GeV}^2$ and for $10^{-4} \leq x \leq 1$. The x -dependence of parton distributions is compared at $Q^2 = 10, 100$ and 10^4 GeV^2 and is shown in figures I.1–I.8, II.1–II.9 and III.1–III.10, respectively. In figures IV.1–IV.7 the Q^2 -dependence of parton distributions is presented only in the DFLM2 parametrization at fixed values of $x = 10^{-4}, 10^{-3}, 10^{-2}, 10^{-1}$. After the main part of our study was finished, a new MRS parametrization appeared (MRSE' and MRSB') which differs substantially from the older ones. In the figs. V.1–V.6 we compare the previous predictions of the MRS1 parametrization with new MRSE', MRSB' versions for parton distributions at $Q^2 = 10, 10^2, 10^3, 10^4 \text{ GeV}^2$.

The individual parton contributions, i.e. the valence up quark at $Q^2 = 10 \text{ GeV}^2$, are presented in the way which allows to compare the different sets within each parametrization P1–P5 (see four windows in fig. I.1a). In a separate picture the comparison is made for the same parton distribution of the different parametrizations P1–P4 by taking the set favoured by the authors (see fig. I.1b). We take usually the DO1, EHLQ1, MRS1 and DFLM2 parametrizations as a representative sample. In this "mixed" picture we do not include the GGR parametrization since it is shown in the previous figure (window 4) together with the DFLM1,2 parametrizations. From this comparison one can easily figure out some of the specific features of different parametrizations.

This method of presentation was used for all distributions at $Q^2 = 10, 10^2, 10^4 \text{ GeV}^2$. In figures I–III the x -dependence of respective parton distributions at each value of Q^2 is shown as follows:

- valence up quark $xu_v(x, Q^2)$ —figs.: I.1a,b, II.1a,b, III.1a,b;
- valence down quark $xd_v(x, Q^2)$ —figs.: I.2a,b, II.2a,b, III.2a,b;
- light sea $xu_s(x, Q^2) = xd_s(x, Q^2) = x\bar{u}(x, Q^2) = x\bar{d}(x, Q^2)$ —figs.: I.3a,b, II.3a,b, III.3a,b;

- strange quark $x s(x, Q^2)$ —figs.: I.4a,b, II.4a,b, III.4a,b;
- charm quark $x c(x, Q^2)$ —figs.: I.5a,b, II.5a,b, III.5a,b;
- bottom quark $x b(x, Q^2)$ —figs.: II.6a,b, III.6a,b;
- top quark $x t(x, Q^2)$ —figs.: III.7a,b;
- gluon $x G(x, Q^2)$ —figs.: I.6a,b, II.7a,b, III.8a,b.

The ratio d_v/u_v is compared for the representative sets of the parametrizations in figs. I.7, II.8, III.9a,b. For one particular parametrization—the DFLM2, the comparison of the valence quarks, the sea and the gluon content of the proton is presented in figs. I.8, II.9, III.10a,b. Note that for higher energies we used both linear and logarithmic scales.

The valence quark distributions $x u_v$ and $x d_v$ peak at x around 0.15 for $Q^2 = 10 \text{ GeV}^2$ (figs I.1b, I.2b). The position of the peak differs slightly for different parametrizations. The differences in the height are much bigger. The same may be observed at higher Q^2 . There is an expected shift of the position of the peak towards smaller values of x with increasing Q^2 , e.g. for $Q^2 = 10^4 \text{ GeV}^2$ the peaks in $x u_v$ and $x d_v$ occur at $x < 0.01$ (figs III.1b, III.2b). The biggest value of $x u_v$ at the peak is predicted by the EHLQ1 parametrization and the smallest by the DO1. For $x d_v$ the situation is reversed. Predictions given by other parametrizations lie between these two.

The plots for light sea distributions show that the EHLQ parametrization predicts lower values than the other three—especially at very small- x .

Large differences may be observed in the strange quark distributions (see figs I.4b, II.4b). For lower $Q^2 = 10 \text{ GeV}^2$ the EHLQ and the DFLM parametrizations give similar results whereas MRS1 is close to DO1. This is due to the underlying assumption of $x s = x \bar{u} = x \bar{d}$ in the latter ones. At higher Q^2 they start to split up leading to a factor 2 difference between MRS1 and EHLQ1 at $(x, Q^2) = (10^{-4}, 10^2 \text{ GeV}^2)$. For MRSE', and especially MRSEB', the difference is much smaller (fig.V.3).

The charm distribution for $Q^2 = 10 \text{ GeV}^2$ is rather large at small x in the MRS1 parametrization—much larger than in the EHLQ1. But MRSE' gives smaller values (fig.V.4). At this scale the charm distribution in the DFLM parametrization is negligible. At higher Q^2 DFLM2 and MRS1 tend to give similar results, a bit bigger than EHLQ1. Predictions of the DO parametrization with respect to other ones vary quite much for different Q^2 .

The bottom quark distribution is not parametrized in the DO sets and for the EHLQ it is negligible at $Q^2 = 10^2 \text{ GeV}^2$. The predictions of the MRS1 and DFLM2 parametriza-

tions differ at this scale very much—by a factor of 9 at $x = 10^{-4}$ (and by a factor of 22 for MRSE³). It is mainly related to the different assumptions concerning threshold effects.

For the top quark distribution there are only results in the EHLQ, DFLM and GGR parametrizations. As is seen from fig.III.7b, DFLM predicts bigger values than EHLQ.

As we expected, very different answers for the gluon distributions can be obtained even within the same parametrization. At larger Q^2 the differences become more transparent (figs II.7b, III.8b) since we enter here the small x -region. This region is particularly sensitive to the type of analysis: leading or next-to-leading order. We would expect (see Tung paper [11])

that the well known rapid growth of the gluon distribution at small x seen in the usual leading order will be dumped by inclusion of next to leading terms.

This can be seen in the comparison of the EHLQ and the DFLM gluon distributions. As for the MRS behaviour, an error recently was found in this parametrization ([7]) which affects the $x \leq 10^{-2}$ region. So the correct behaviour of this parametrization (especially in the small- x region) for the gluon as well as for other distributions should be invoked from figs V.1–V.6.

The comparison of the d_v/u_v ratio (figs I.7, II.8, III.9a,b) shows that different assumptions concerning valence quark distribution at the input scale Q_0^2 lead to large differences in this ratio. For example, at $Q^2 = 10^4 \text{ GeV}^2$ the two extreme distributions (EHLQ1 and DO1) differ by a factor of 4 at $x = 10^{-4}$.

Finally, we compare valence, sea and gluon contributions to the proton structure functions in the DFLM2 scheme. At $Q^2 = 10 \text{ GeV}^2$ the first crossover between valence and sea distributions occurs at $x \sim 0.05$, the second one between the valence and gluon terms may be seen at $x \sim 0.2$ (fig.I.8). With increasing Q^2 the first crossover shifts to larger values of x , whereas the second one to smaller x (figs II.9, II.10a).

Plots of parton distributions as a function of Q^2 at fixed x (figs IV.1–IV.7) illustrate the general behaviour of these functions in the range of $10 \text{ GeV}^2 \leq Q^2 \leq 10^4 \text{ GeV}^2$. The behaviour of heavy flavours (figs IV.4–IV.6) should be taken with some caution, because of the threshold effects, which are included differently by different authors.

In summary, all discussed parametrizations behave similarly in the medium and large- x region but differ significantly for small- x . Since the small- x region gives a large contribution to the hadronic cross sections at high energy it is extremely important clarify the situation here. HERA is especially suitable for this purpose since it extends the accessible range of x down to $x \sim 10^{-4}$.

5.2 Structure function F_2

It is of interest to compare the predictions of various parametrizations for the F_2 structure function with data. As mentioned previously, the F_2 can be determined directly from the data as opposed to parton densities, and the predictions for F_2 should not depend on the renormalization scheme. This means that the next-to-leading parametrizations obtained within different schemes should lead to the same results for F_2 . In principle they should describe the data with a better accuracy than the leading logarithmic parametrization with a much lesser dependence on the scale parameter Λ .

In practice the situation is not so clear since different parametrizations follow different fitting procedures and are based on different data sets. It is in general expected that the parton parametrizations based on more precise data fitted with next-to-leading approach should be of better quality.

The comparison between the predictions for the electromagnetic and weak F_2 given by parametrizations **P1–P5** and the appropriate data is presented in figs VI.1, VI.2. The interest of this comparison lies in the fact that those data, but for the EMC data, have not been used in the determination of these parametrizations.

In figs VI.1a,b we present the F_2^{em} from deep inelastic charged lepton interactions and in figs VI.2a,b we show the F_2^ν as a function of Q^2 at several x values. A large spread of data is observed, especially in the small x regions. The same is true for the predictions of the different parametrizations. The spread in the experimental results is due to large systematic errors and therefore makes it difficult to conclude which parametrization to prefer. The band of the parametrization results overlap with most of the data. It seems to be difficult to describe the behaviour of the neutrino data for the smallest x region ($x = 0.015$). For both F_2^{em} and F_2^ν none of the predictions can reproduce the strong Q^2 dependence shown by the data in the region of small Q^2 ($Q^2 \leq 20 \text{ GeV}^2$) and large x ($x \geq 0.5$). This may suggest the necessity to include some additional mechanism such as higher-twist effects.

The HERA experiments will provide information about the structure function in a new domain of x and Q^2 . The kinematic limits will be extended enormously, reaching a maximum square momentum transfer of $Q^2 \sim 10^4 \text{ GeV}^2$ and x as low as 10^{-4} . Unfortunately there will be no overlap region with the present day deep inelastic experiments.

6 Conclusions

The purpose of this note was to get more insight into the results of different parametrizations of parton distributions in the nucleon, as obtained by various groups in a QCD analysis of existing data. It is quite clear that the differences observed among those parametrizations are due partially to the different approaches at the level of perturbative QCD and partially to the different sets of available structure function measurements. This can be seen in figs VI.1,2 where the F_2 structure function has been reconstructed from the parton densities, following the prescriptions of the authors of various parametrizations, and compared to the latest experimental results [20]. The differences in slopes arise from the underlying QCD approximations. The difference in the overall normalization depends on the set of data used for the determination of structure functions. A comparison of the predictions for the F_2 and the data show clearly that there is no way to choose objectively any of the available parametrizations as the inherent differences are compatible with experimental uncertainties.

The size of the differences among various parametrizations of parton densities is impressive enough as to take it seriously into consideration in those analyses which use parton distributions as their input.

Acknowledgements

We would like to thank especially E.Levin from Leningrad Nuclear Physics Institute and A.K.Wroblewski from Warsaw University for carefully reading the manuscript, critical remarks and many useful suggestions. We would like to acknowledge helpful discussions with J.Kalinowski, S.Pokorski, R.Walczak and J.Zakrzewski from Warsaw University, and E.Gotsman from Tel-Aviv University. We would like to thank also G.Ingelman, G.Martinelli and J.Stirling for the access to their Fortran codes of parton distributions and for permission for further distribution and B.Badelek for providing us with useful information on the small x region. Two of us (KCh and MK) acknowledge the support of the Polish Government Research Programs CPBP 01.03 and CPBP 01.06 as well as the DESY Directorate for supporting their visit at DESY. One of us (HA) would like to thank the Alexander von Humboldt Stiftung for supporting her stay at DESY. AL would like to thank the Minerva Foundation for the financial support which made his stay at DESY possible.

References

- [1] **SLAC'79** , A.Bodek et al.: Phys. Rev. D20 (1979) 1471;
EMC'81 , J.Aubert et al.: Phys. Lett. 105B (1981) 315;
EMC'85 , J.Aubert et al.: Nucl. Phys. B259 (1985) 189;
EMC'86 , J.Aubert et al.: Nucl. Phys. B272 (1986) 158;
EMC'87 , J.Aubert et al.: Nucl. Phys. B293 (1987) 740;
EMC'89 , M.Arneodo et al.: submitted to Nucl. Phys. B, (1989);
NMC'88 , M.Botje: report at the 19th Symposium on Multiparticle Dynamics, Arles, 1988;
BCDMS'87 , A.Benvenuti et al.: in Proc. of the Int. EPS Conf. on High Energy Physics, Uppsala 1987, ed. O.Botner, p.437; Phys. Lett. 195B (1987) 91;
CDHS'83 , H.Abramowicz et al.: Z. Phys. C17 (1983) 283;
CDHSW'86 , P.Perez: in Proc. of the 12th Int. Conf. 'Neutrino'86: Neutrino Physics and Astrophysics', Sendai Japan, 1986, ed. by T.Kitagaki and H.Yuto (World Scientific, Singapore, 1986), p.341;
CDHSW'89 , P.Berge et al.: CERN-EP/89-103;
CHARM'83 , F.Bergsma et al.: Phys. Lett. 123B (1983) 269;
CCFRR'83 , D.MacFarlane et al.: Fermilab-pub-83, 108-Exp(83);
CCCFRR'84 , D.MacFarlane et al.: Z. Phys. C26 (1984) 1.;
CFRR'88 , F.Sciulli: report at the 19th Symposium on Multiparticle Dynamics, Arles, 1988;
BEBC'85 , D.Alasia et al.: Z. Phys. C28 (1985) 321;
CFS'81 , A.Ito et al.: Phys. Rev. D23 (1981) 604;
ISR'82 , D.Antreasyan et al.: Phys. Rev. Lett. 48 (1982) 302;
J/ Ψ '79 , J.Branson et al.: Phys. Rev. Lett. 38 (1977) 1331; K.Anderson et al.: ibid. 42 (1979) 944.
- [2] A.J.Buras, K.J.F.Gaemers: Nucl. Phys. B132 (1978) 249.
- [3] M.Glück, E.Hoffmans, E.Reya: Z. Phys. C13 (1982) 119.
- [4] D.Duke, J.Owens: Phys. Rev. D30 (1984) 49.

- [5] E.Eichten, I.Hinchliffe, K.Lane, Ch.Quigg: *Rev. Mod. Phys.* 56 (1984) 579; revised *ibid.* 58 (1986) 1047.
- [6] A.Martin, R.Roberts, J.Stirling: *Phys. Rev.* D37 (1988) 1161.
- [7] A.Martin, R.Roberts, J.Stirling: *Phys. Lett.* B206 (1988) 327; *ibid.* B207 (1988) 205 (MRSE.B);
A.Martin, R.Roberts, J.Stirling: *Mod. Phys. Lett.* A4 (1989) 1135 (MRSE',B').
- [8] M.Diemoz, F.Ferroni, E.Longo, G.Martinelli: *Z. Phys.* C39 (1988) 21.
- [9] M.Diemoz, F.Ferroni, E.Longo: *Phys. Rep.* 130 (1986) 293.
- [10] M.Glück, R.Godbole, E.Reya: DO-TH 88/18; *Z. Phys.* C41 (1989) 667.
- [11] Wu-Ki Tung: *Nucl. Phys.* B315 (1989) 378; Wu-Ki Tung et al.: ANL-HEP-CP-89-01.
- [12] R.Feynman: *Phys. Rev. Lett.* 23 (1969) 1415; J.Bjorken: *Phys. Rev.* 179 (1969) 1547.
- [13] SLAC-MIT Coll.: 14th Int. Conf. High Energy Physics, Vienna, 1968; J.Friedman, H.Kendall: *Ann. Rev. Nucl. Science* 22 (1972) 203.
- [14] A.Buras: *Rev. Mod. Phys.* 52 (1980) 199; Yu.Dokshitzer, D.Dyakonov, S.Troyan: *Phys. Rep.* 58 (1980) 269; G.Altarelli: *Phys. Rep.* 81C (1982) 1.
- [15] V.Gribov, L.Lipatov: *Yad. Fiz.* 15 (1972) 78, 1218; L.Lipatov: *Yad. Fiz.* 20 (1974) 181.
- [16] L.Gribov, E.Levin, M.Ryskin: *Phys. Rep.* 100 (1983) 1.
- [17] J.Collins, J.Kwiecinski: *Nucl. Phys.* B316 (1989) 307; E.Levin: in *Proceedings of the XII Warsaw Symposium on Elementary Particle Physics, Kazimierz, 1989.*
- [18] G.Altarelli, K.Ellis, G.Martinelli: *Nucl. Phys.* B157 (1979) 461.
- [19] W.Furmanski, R.Petronzio: *Z. Phys.* C11 (1982) 293.
- [20] J.Feltesse: in *Proceedings of the XIV Int.Symposium on Lepton and Photon Interactions, Stanford, 1989.*

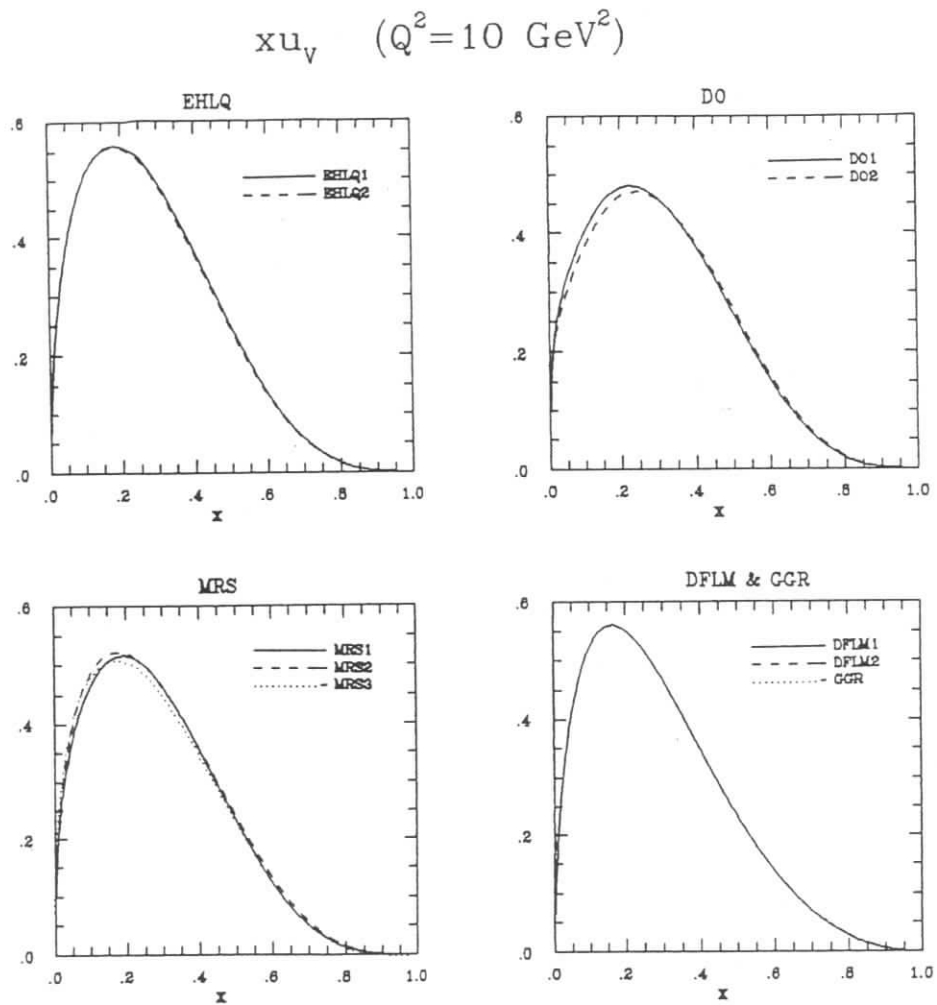


Fig. 1.1a. The valence up quark distribution $xu_v(x, Q^2)$ at $Q^2 = 10 \text{ GeV}^2$ as a function of x , for various parametrizations: EHLQ1,2, DO1,2, MRS1,2,3, DFLM1,2 and GGR.

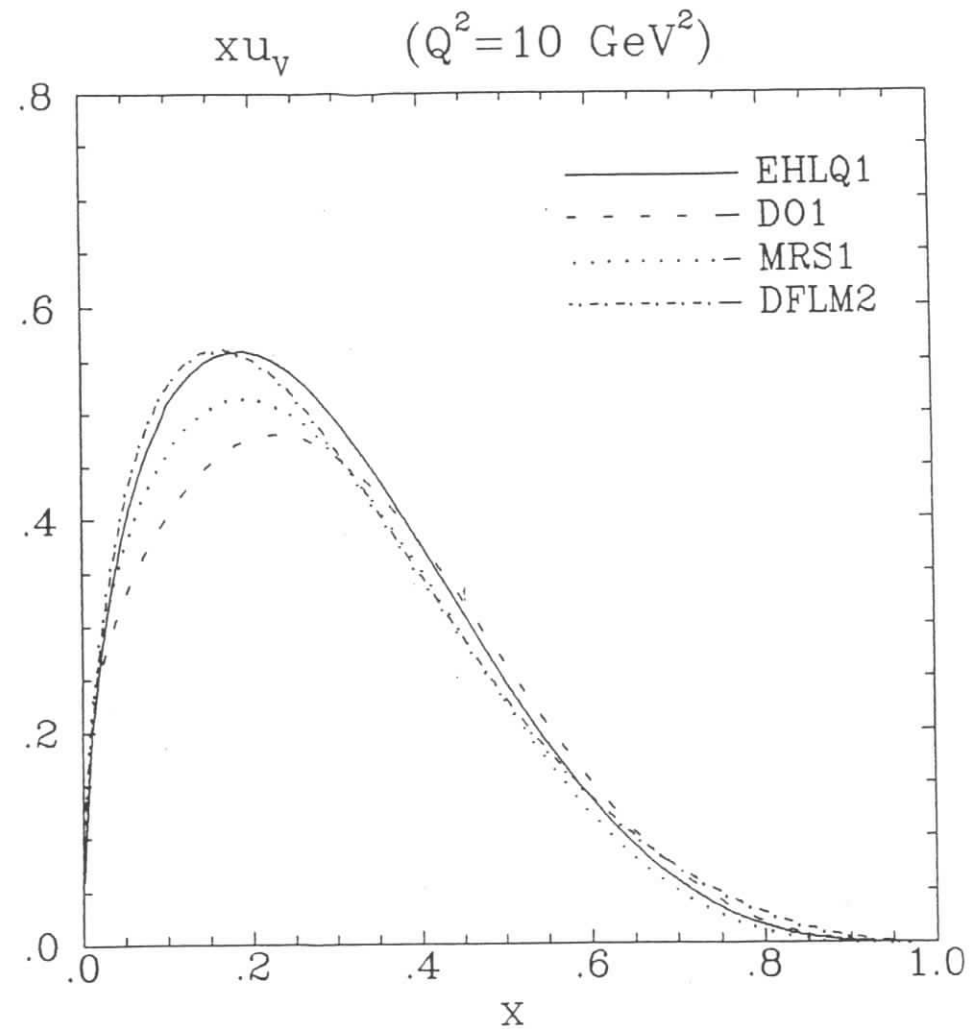


Fig. 1.1b. Comparison of the valence up quark distributions $xu_v(x, Q^2)$ at $Q^2 = 10 \text{ GeV}^2$ obtained in various parametrizations: EHLQ1, DO1, MRS1, DFLM2.

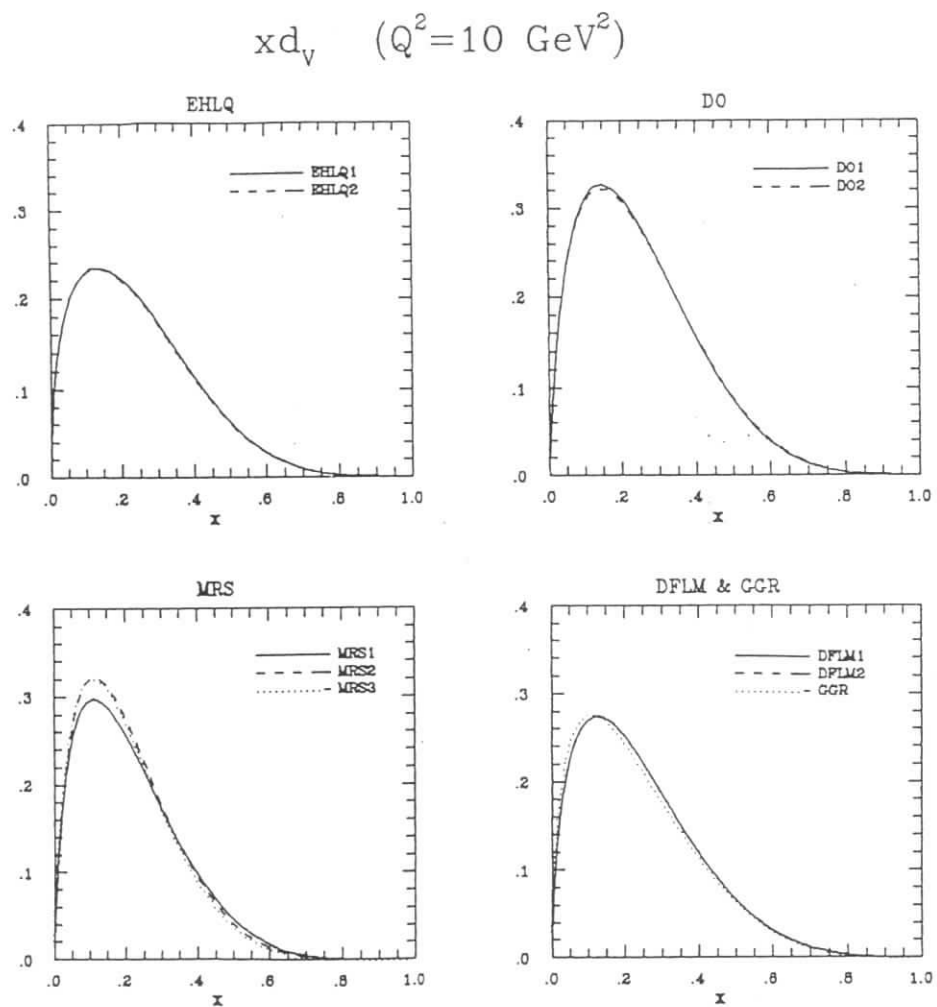


Fig. 1.2a. The valence down quark distribution $x d_v(x, Q^2)$ at $Q^2 = 10 \text{ GeV}^2$ as a function of x , for various parametrizations: EHLQ1,2, DO1,2, MRS1,2,3, DFLM1,2 and GGR.

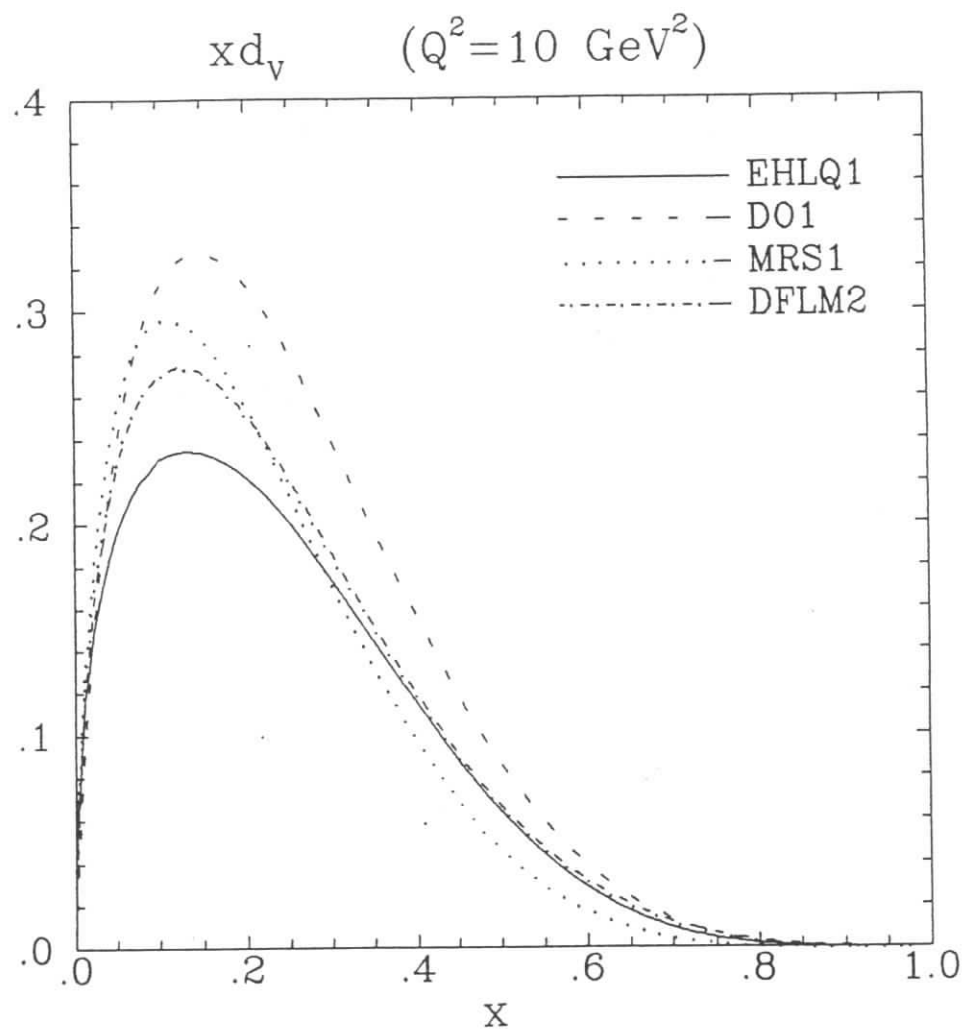


Fig. 1.2b. Comparison of the valence down quark distributions $x d_v(x, Q^2)$ at $Q^2 = 10 \text{ GeV}^2$ obtained in various parametrizations: EHLQ1, DO1, MRS1, DFLM2.

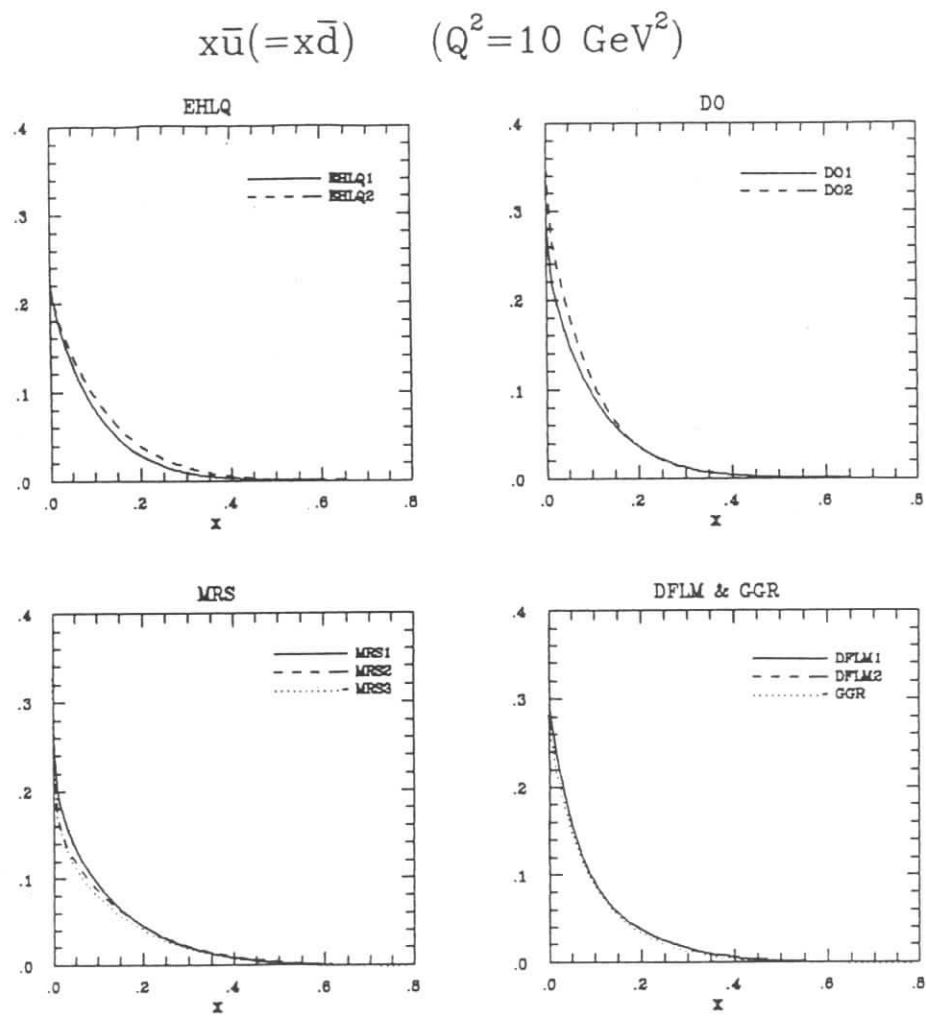


Fig. I.3a. The up(down) antiquark distribution $x\bar{u}(x, Q^2)(x\bar{d}(x, Q^2))$ at $Q^2 = 10\text{GeV}^2$ as a function of x , for various parametrizations: EHLQ1,2, DO1,2, MRS1,2,3, DFLM1,2 and GGR.

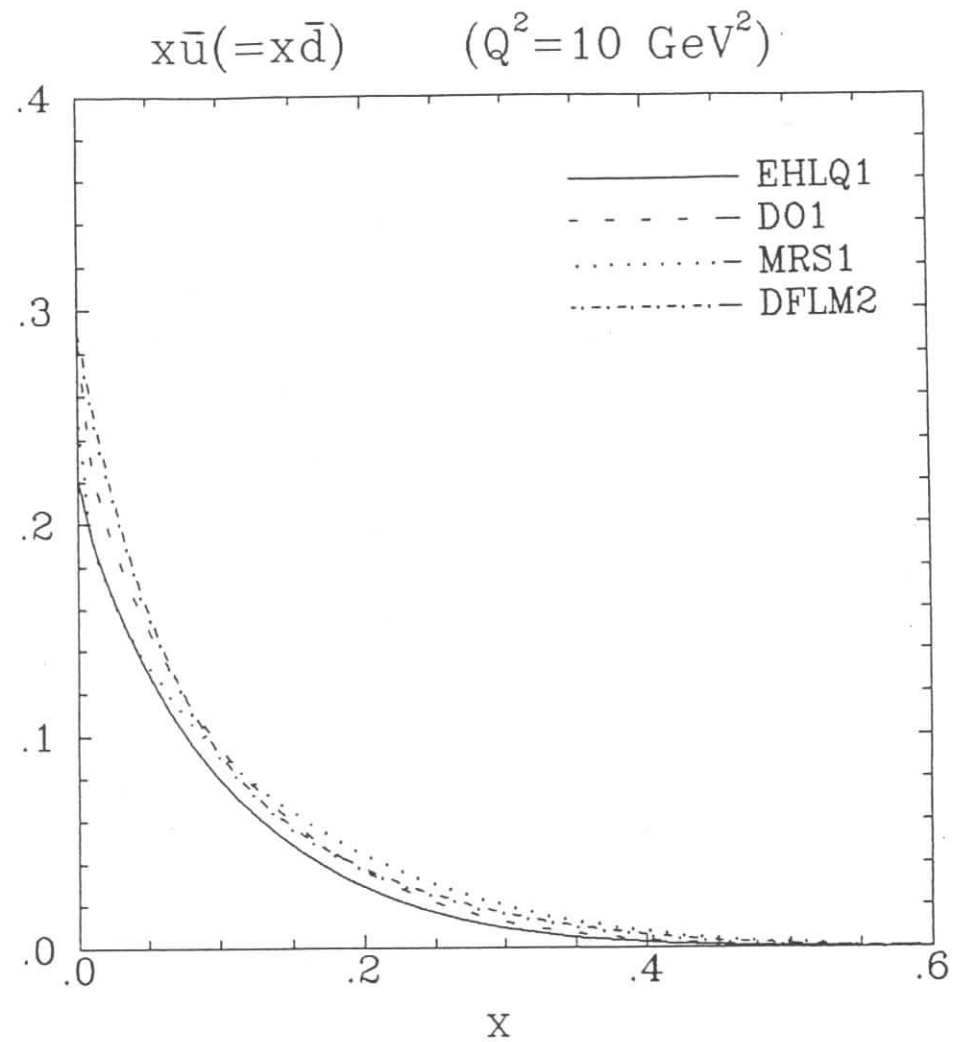


Fig. I.3b. Comparison of the up (down) antiquark distributions $x\bar{u}(x, Q^2) (x\bar{d}(x, Q^2))$ at $Q^2 = 10 \text{ GeV}^2$ obtained in various parametrizations: EHLQ1, DO1, MRS1, DFLM2.

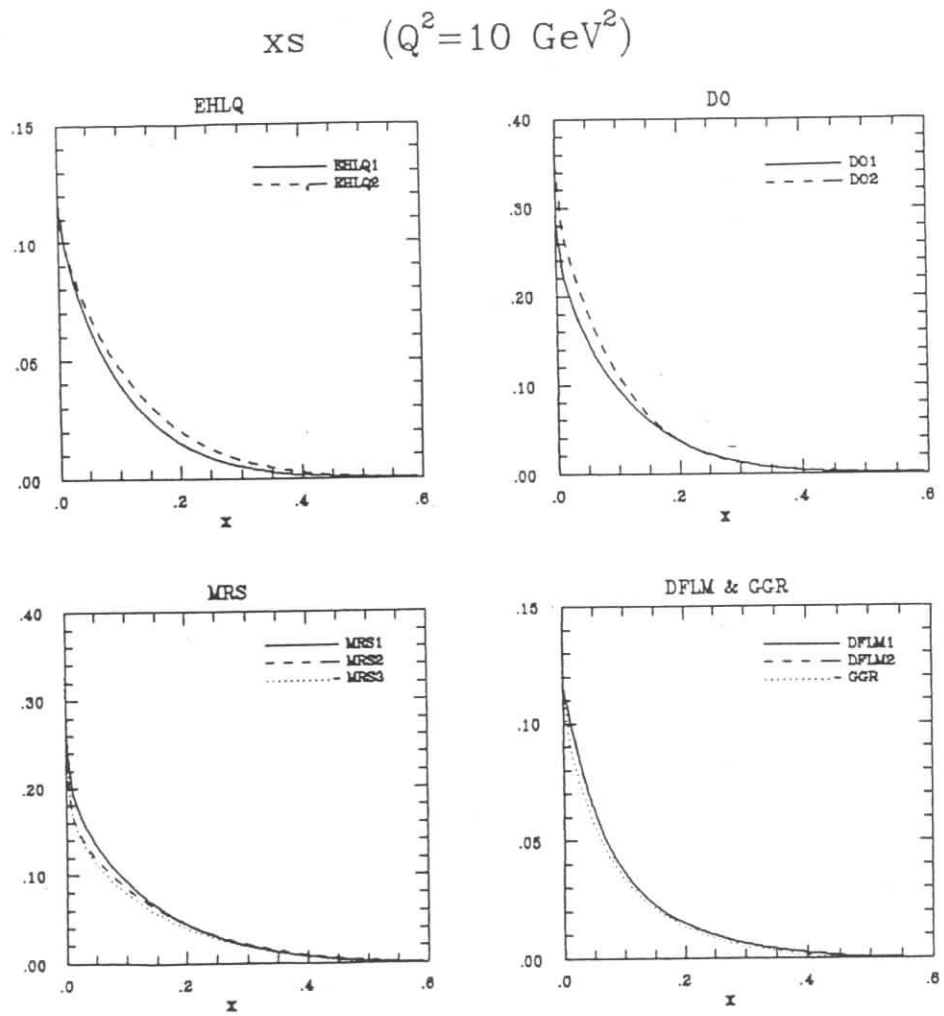


Fig. I.4a. The strange quark distribution $x s(x, Q^2)$ at $Q^2 = 10 \text{ GeV}^2$ as a function of x , for various parametrizations: EHLQ1,2, DO1,2, MRS1,2,3, DFLM1,2 and GGR.

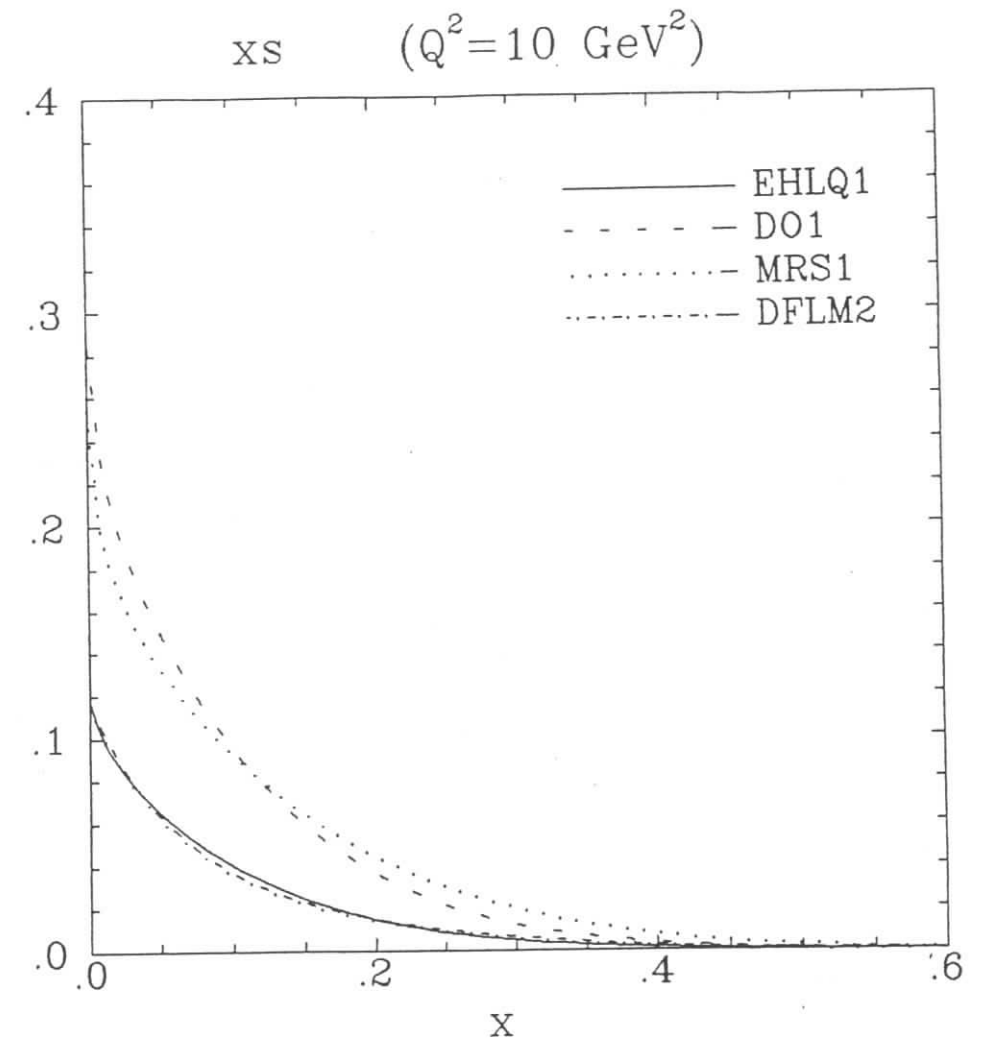


Fig. I.4b. Comparison of the strange quark distributions $x s(x, Q^2)$ at $Q^2 = 10 \text{ GeV}^2$ obtained in various parametrizations: EHLQ1, DO1, MRS1, DFLM2.

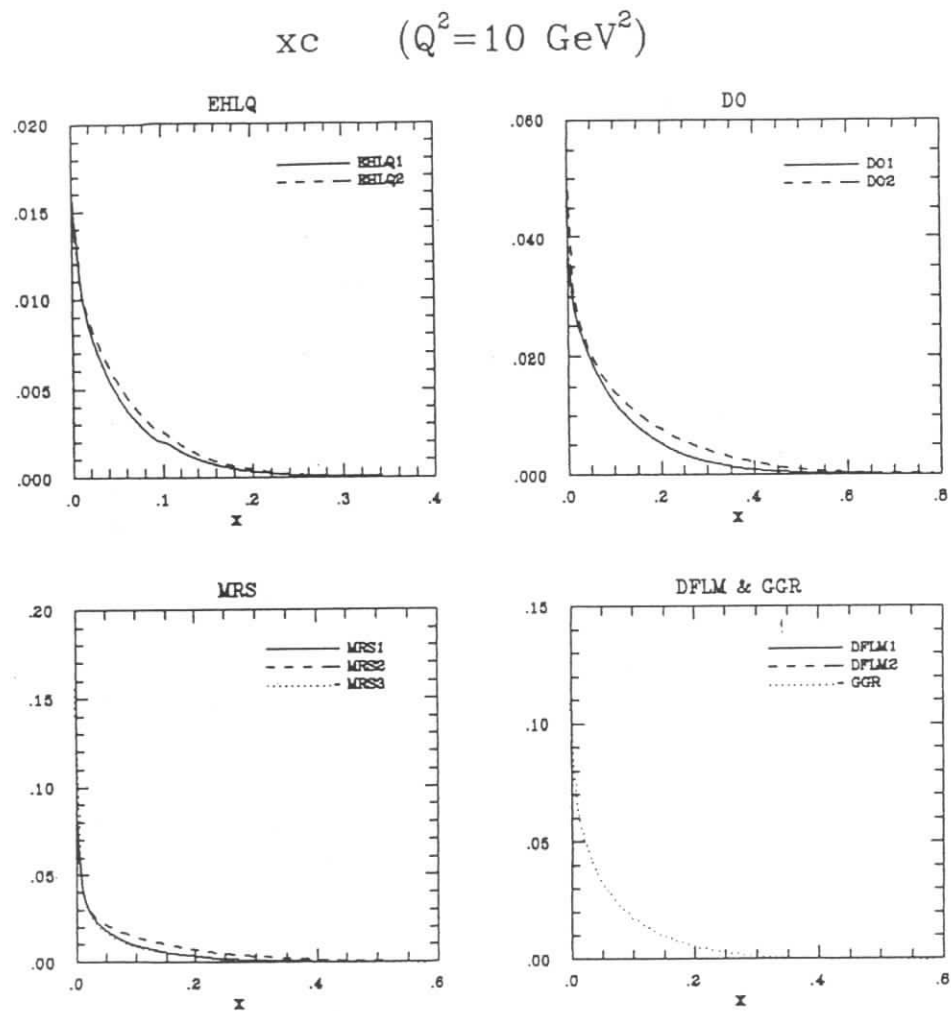


Fig. 1.5a. The charm quark distribution $x_c(x, Q^2)$ at $Q^2 = 10 \text{ GeV}^2$ as a function of x , for various parametrizations: EHLQ1,2, DO1,2, MRS1,2,3, DFLM1,2 and GGR.

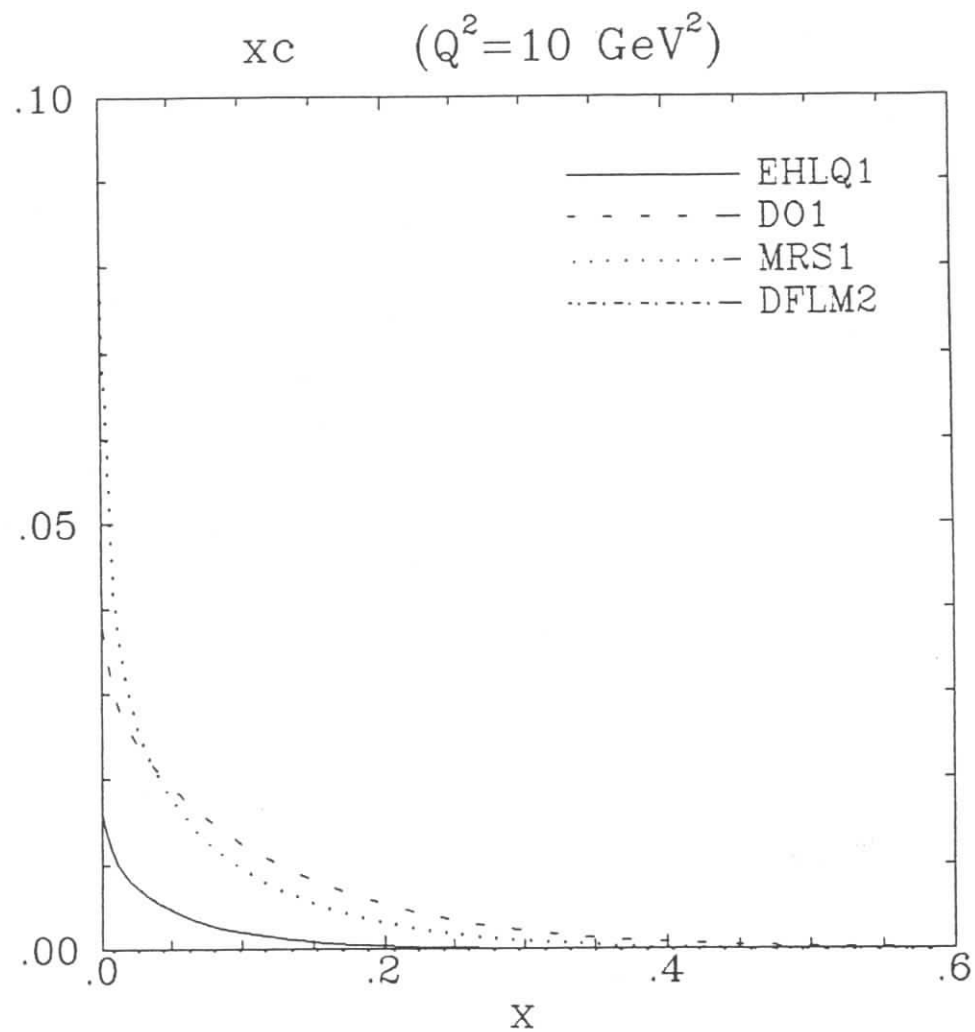


Fig. 1.5b. Comparison of the charm quark distributions $x_c(x, Q^2)$ at $Q^2 = 10 \text{ GeV}^2$ obtained in various parametrizations: EHLQ1, DO1, MRS1, DFLM2.

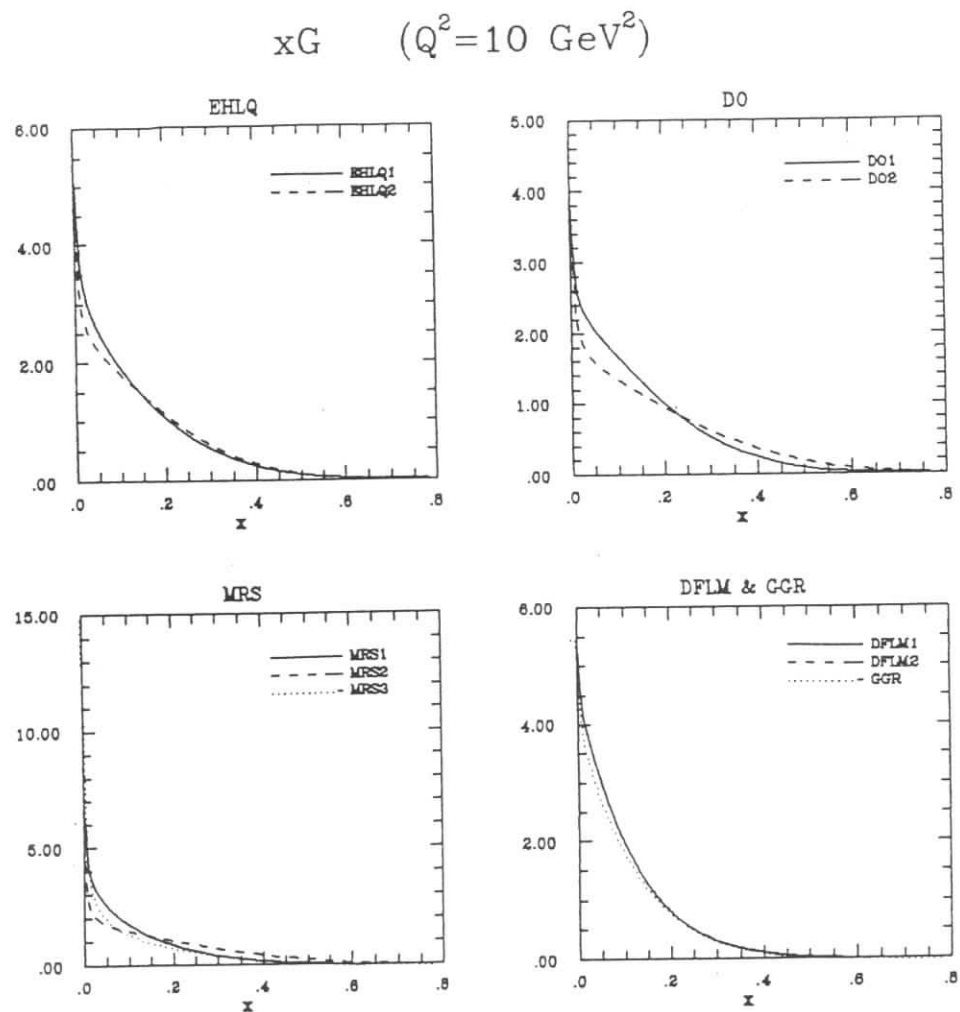


Fig. I.6a. The gluon distribution $xG(x, Q^2)$ at $Q^2 = 10 \text{ GeV}^2$ as a function of x , for various parametrizations: EHLQ1,2, DO1,2, MRS1,2,3, DFLM1,2 and GGR.

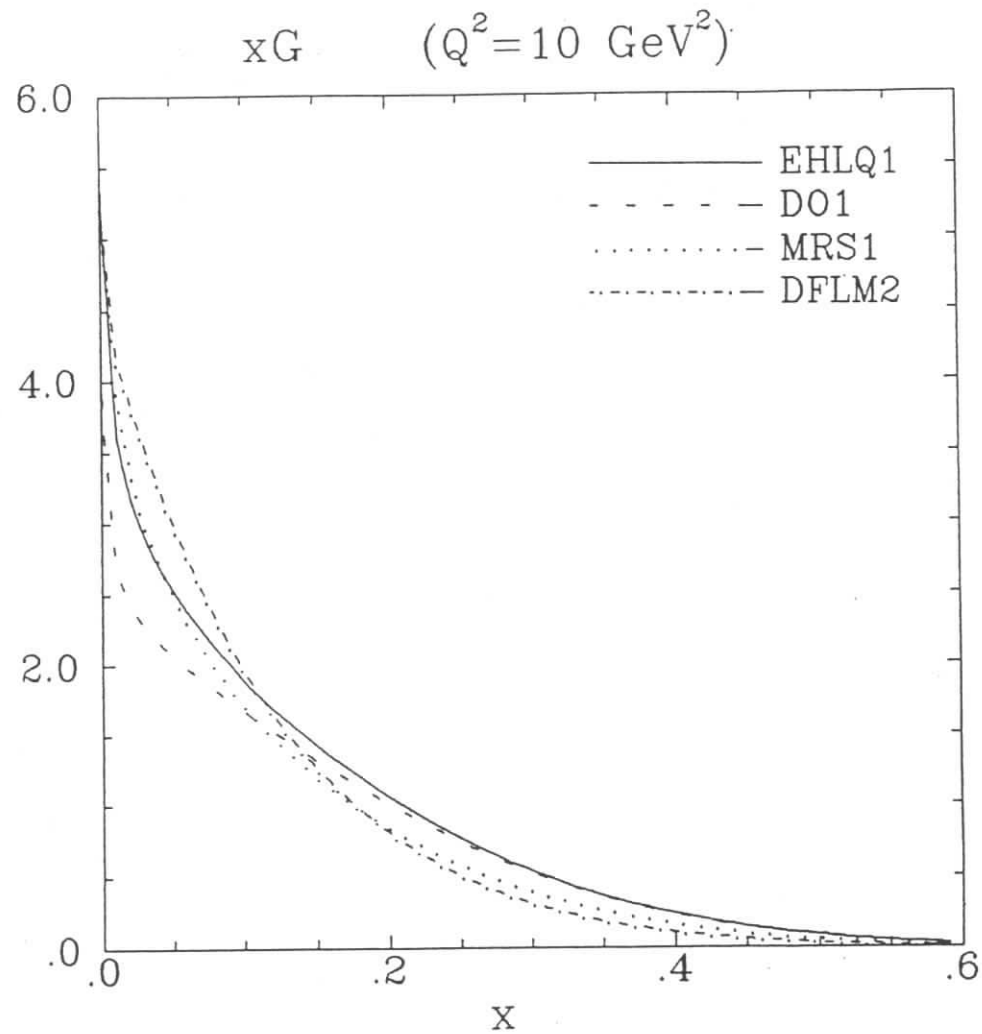


Fig. I.6b. Comparison of the gluon distributions $xG(x, Q^2)$ at $Q^2 = 10 \text{ GeV}^2$ obtained in various parametrizations: EHLQ1, DO1, MRS1, DFLM2.

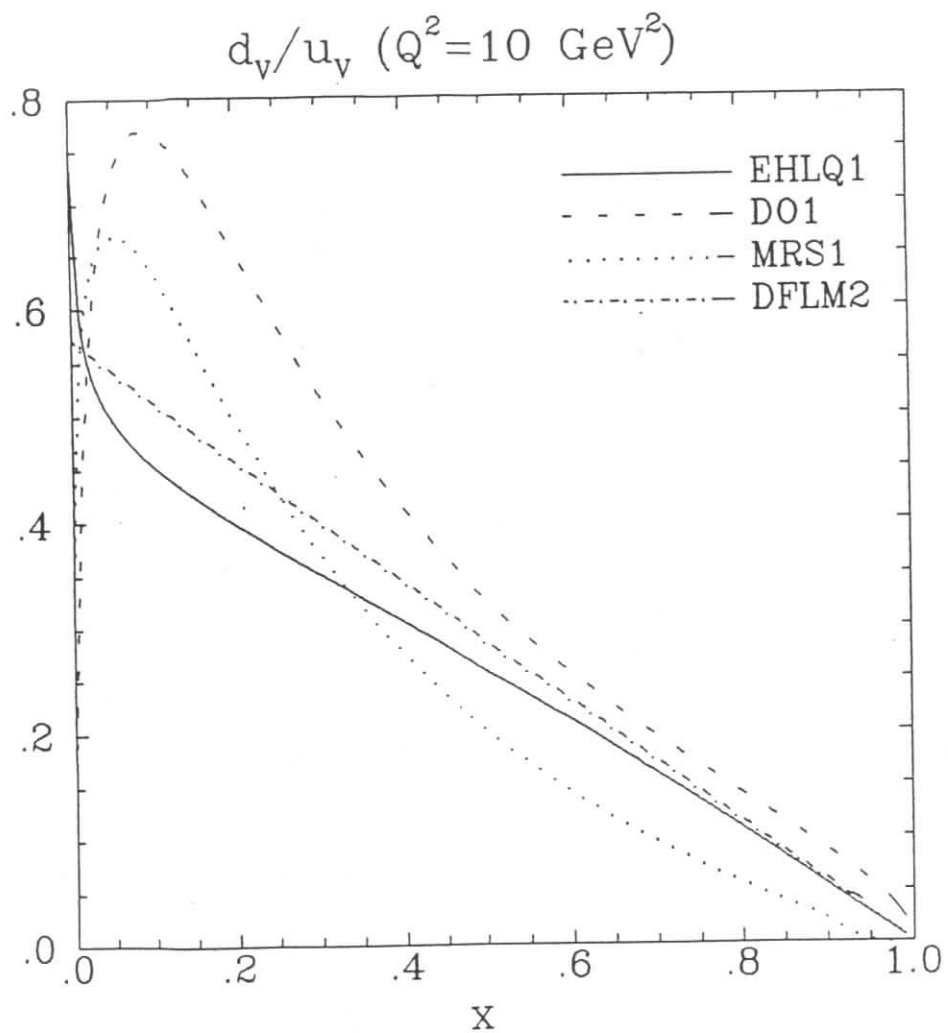


Fig. I.7. The ratio for valence down and up quarks distributions $d_v(x, Q^2)/u_v(x, Q^2)$ at $Q^2 = 10 \text{ GeV}^2$ predicted by various parametrizations: EHLQ1, DO1, MRS1 and DFLM2.

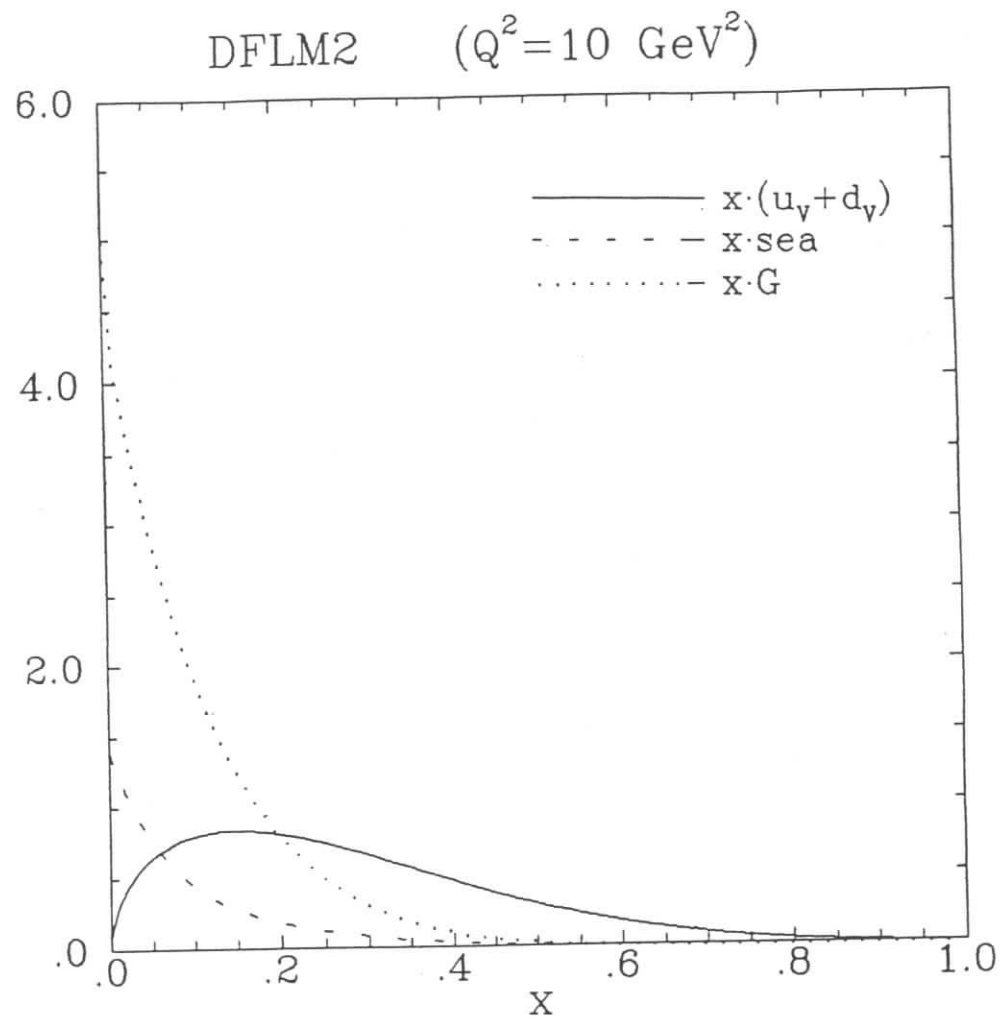


Fig. I.8. Comparison of the valence quark distribution $x[u_v + d_v]$, the sea quark distribution $2x[\bar{u} + \bar{d} + s + c + b + t]$ and the gluon distribution xG of DFLM2 parametrization at $Q^2 = 10 \text{ GeV}^2$

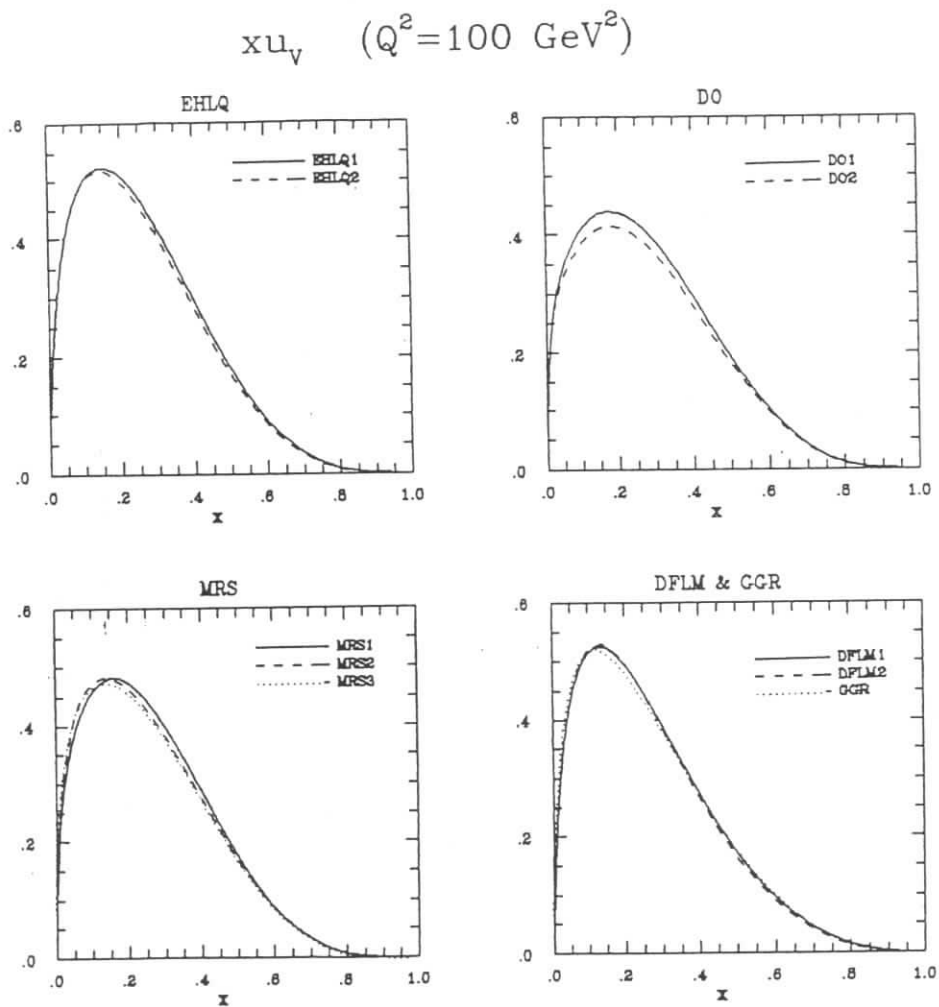


Fig. II.1a. The valence up quark distribution $xu_v(x, Q^2)$ at $Q^2 = 10^2 \text{ GeV}^2$ as a function of x , for various parametrizations: EHLQ1.2, DO1.2, MRS1.2.3, DFLM1.2 and GGR.

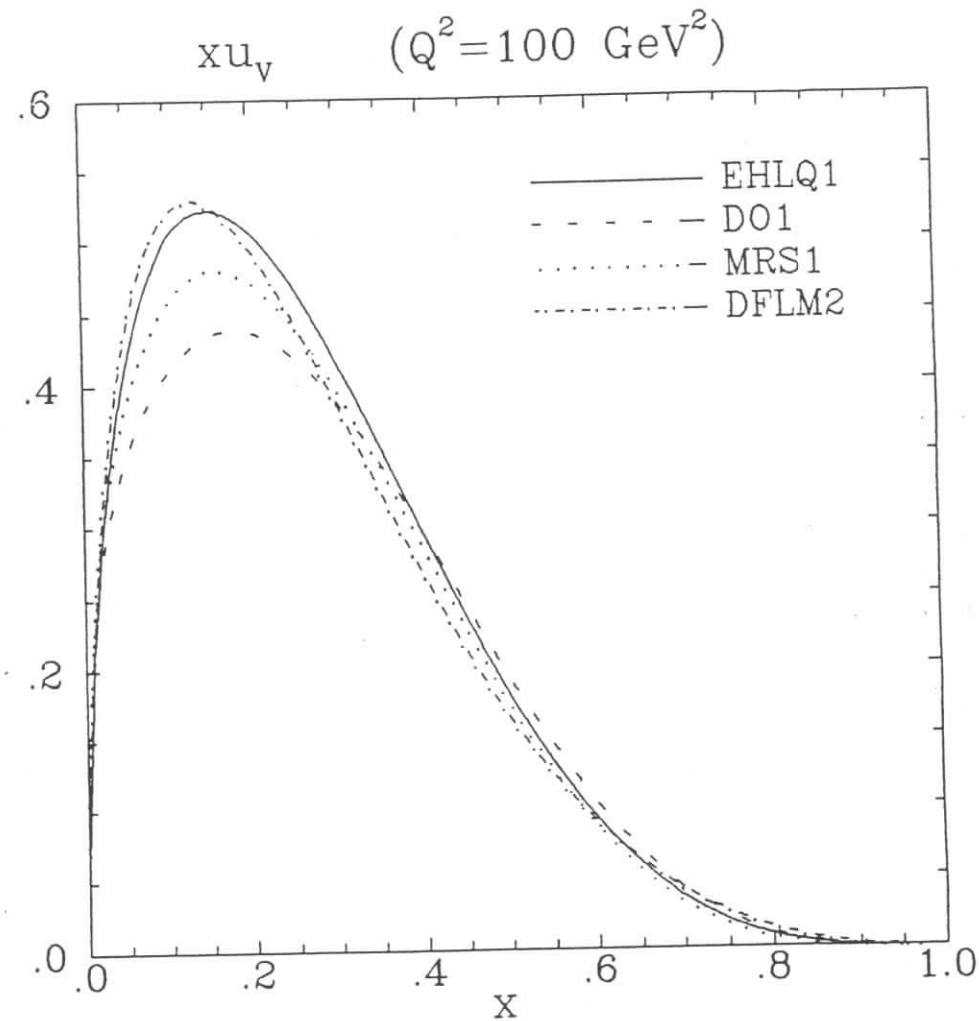


Fig. II.1b. Comparison of the valence up quark distributions $xu_v(x, Q^2)$ at $Q^2 = 10^2 \text{ GeV}^2$ obtained in various parametrizations: EHLQ1, DO1, MRS1, DFLM2.

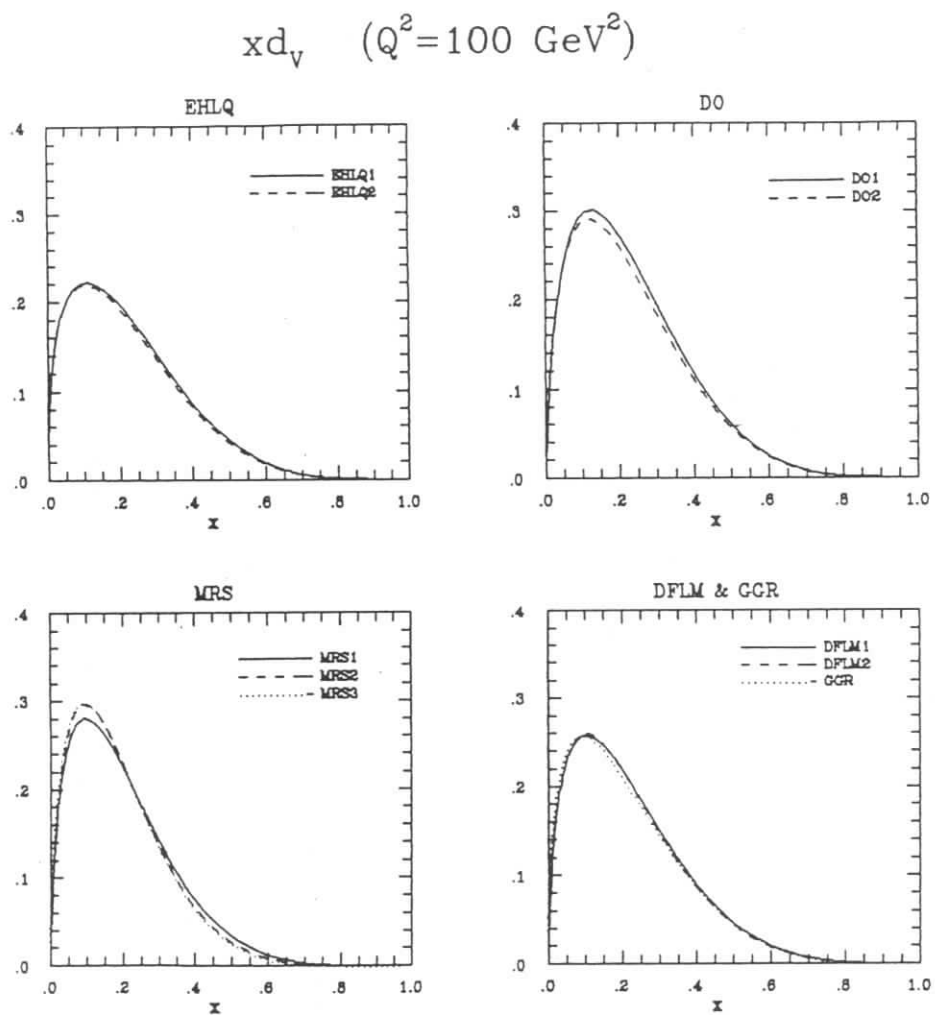


Fig. II.2a. The valence down quark distribution $x d_v(x, Q^2)$ at $Q^2 = 10^2 \text{ GeV}^2$ as a function of x , for various parametrizations: EHLQ1.2, DO1.2, MRS1.2,3, DFLM1.2 and GGR.

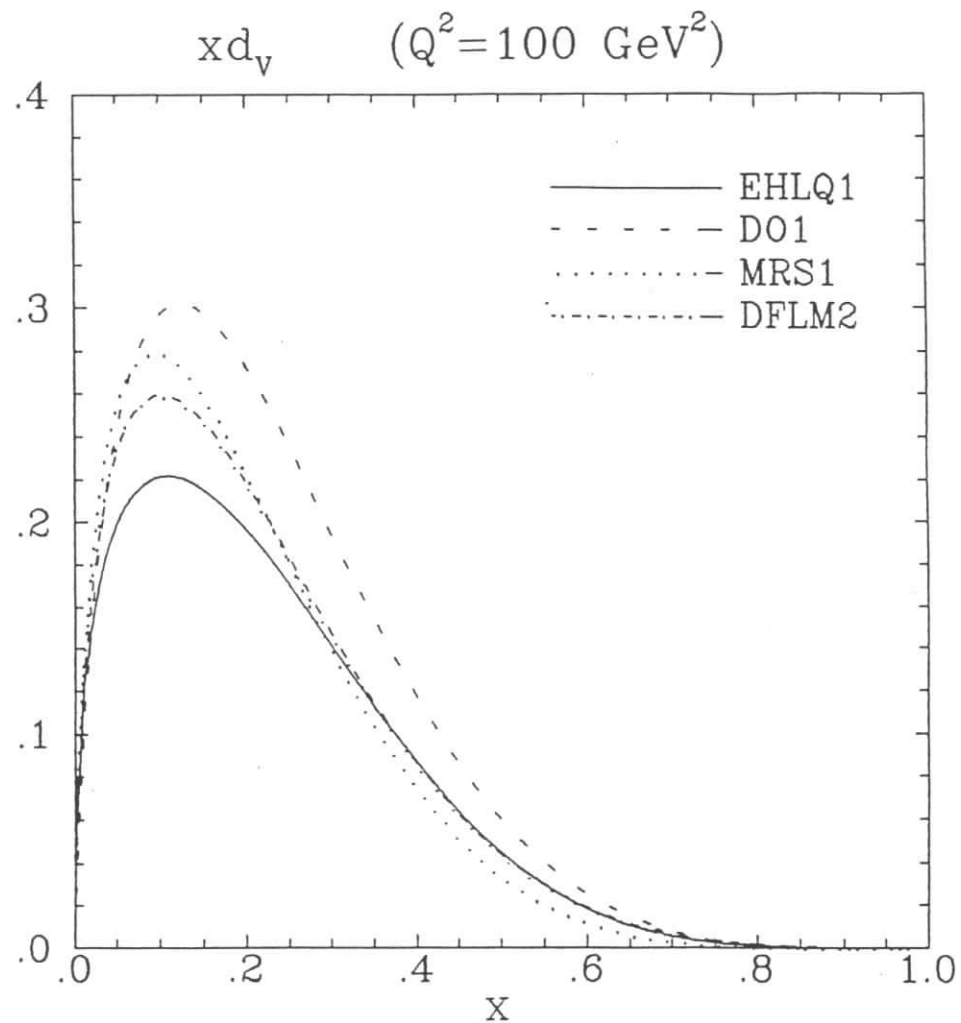


Fig. II.2b. Comparison of the valence down quark distributions $x d_v(x, Q^2)$ at $Q^2 = 10^2 \text{ GeV}^2$ obtained in various parametrizations: EHLQ1, DO1, MRS1, DFLM2.

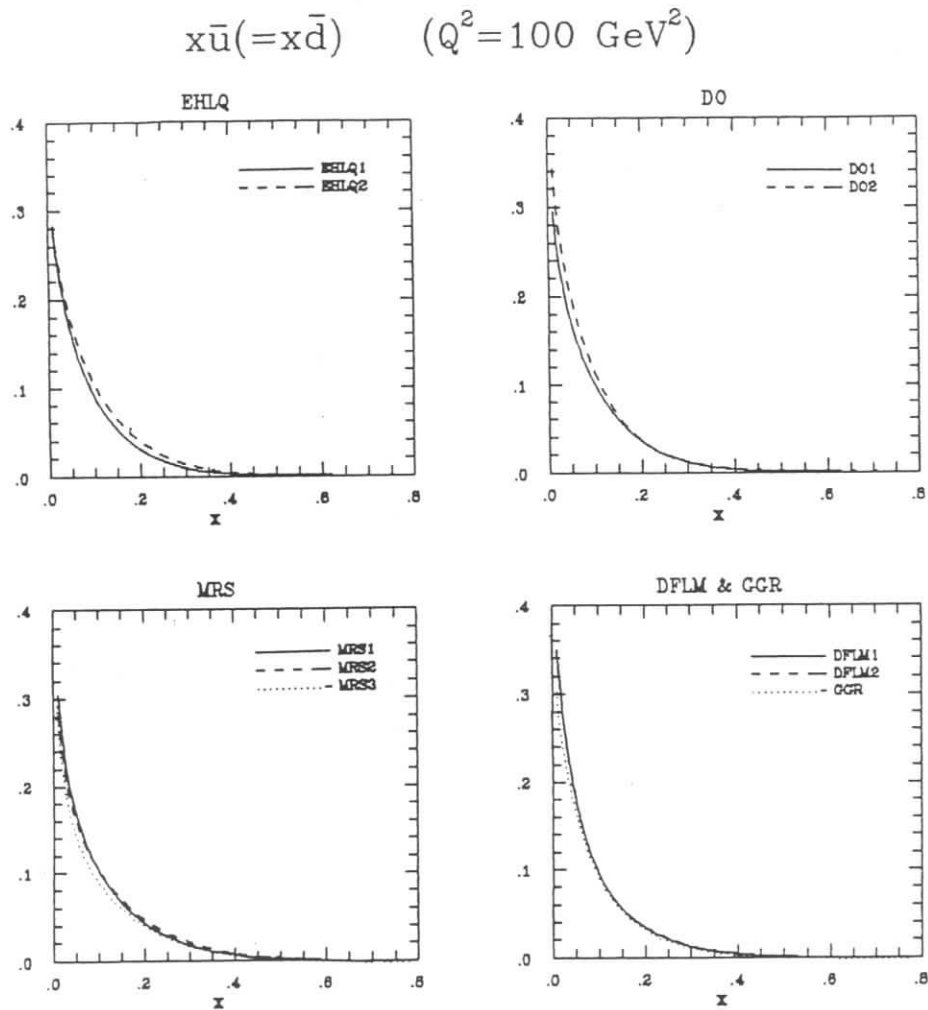


Fig. II.3a. The up(down) antiquark distribution $x\bar{u}(x, Q^2)(x\bar{d}(x, Q^2))$ at $Q^2 = 10^2 \text{ GeV}^2$ as a function of x , for various parametrizations: EHLQ1,2, DO1,2, MRS1,2,3, DFLM1,2 and GGR.

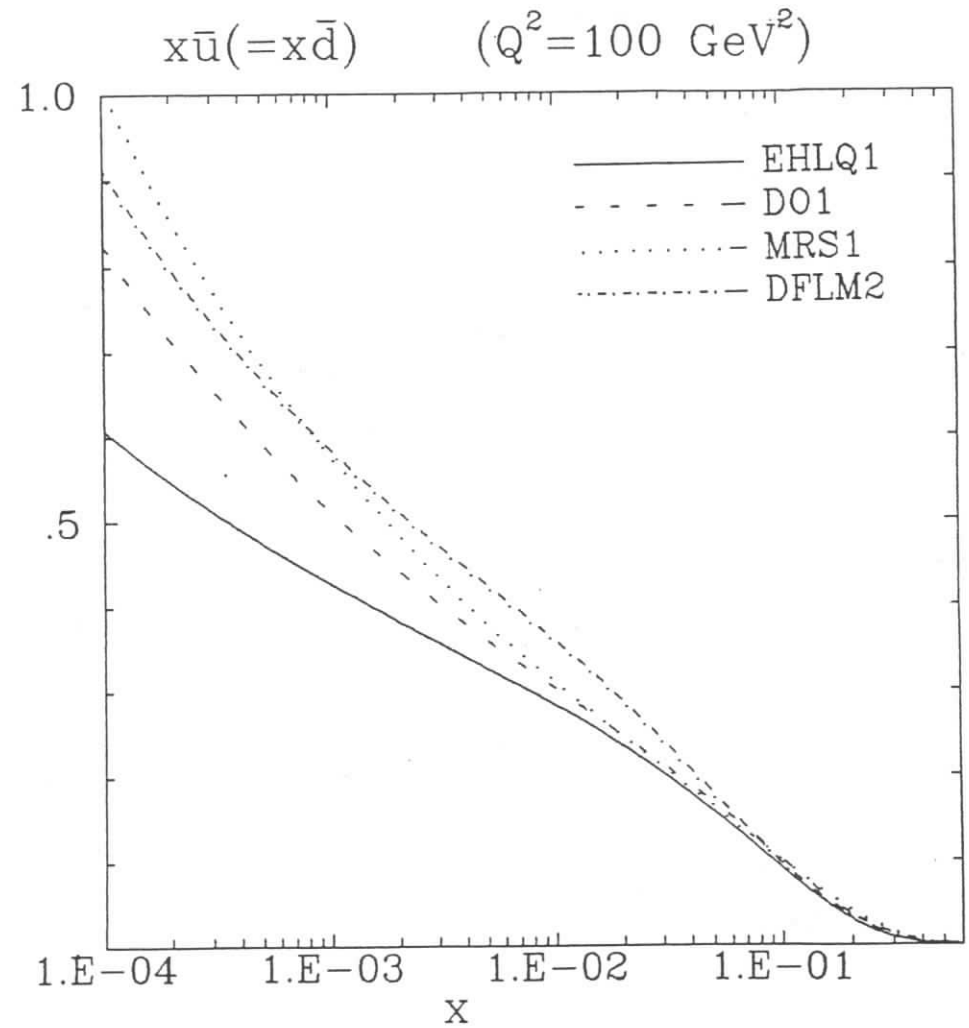


Fig. II.3b. Comparison of the up (down) antiquark distributions $x\bar{u}(x, Q^2) (x\bar{d}(x, Q^2))$ at $Q^2 = 10^2 \text{ GeV}^2$ obtained in various parametrizations: EHLQ1, DO1, MRS1, DFLM2.

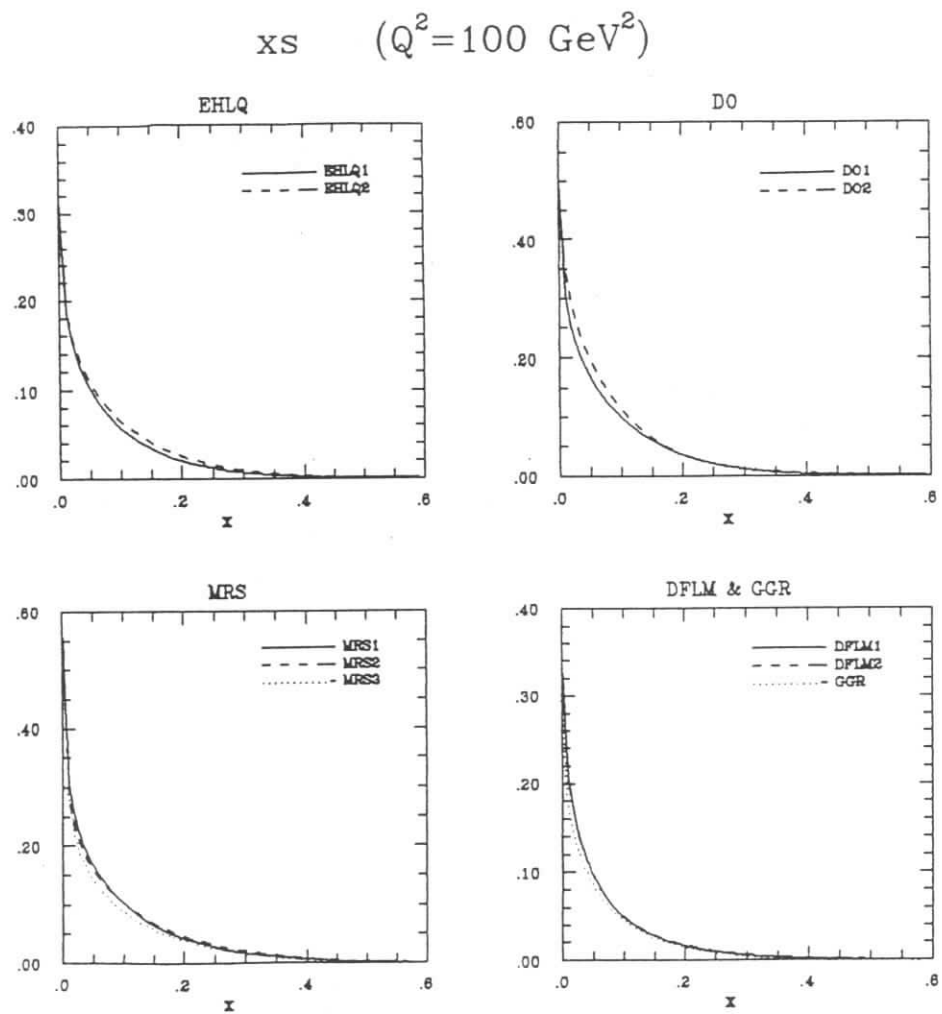


Fig. II.4a. The strange quark distribution $x s(x, Q^2)$ at $Q^2 = 10^2 \text{ GeV}^2$ as a function of x , for various parametrizations: EHLQ1,2, DO1,2, MRS1,2,3, DFLM1,2 and GGR.

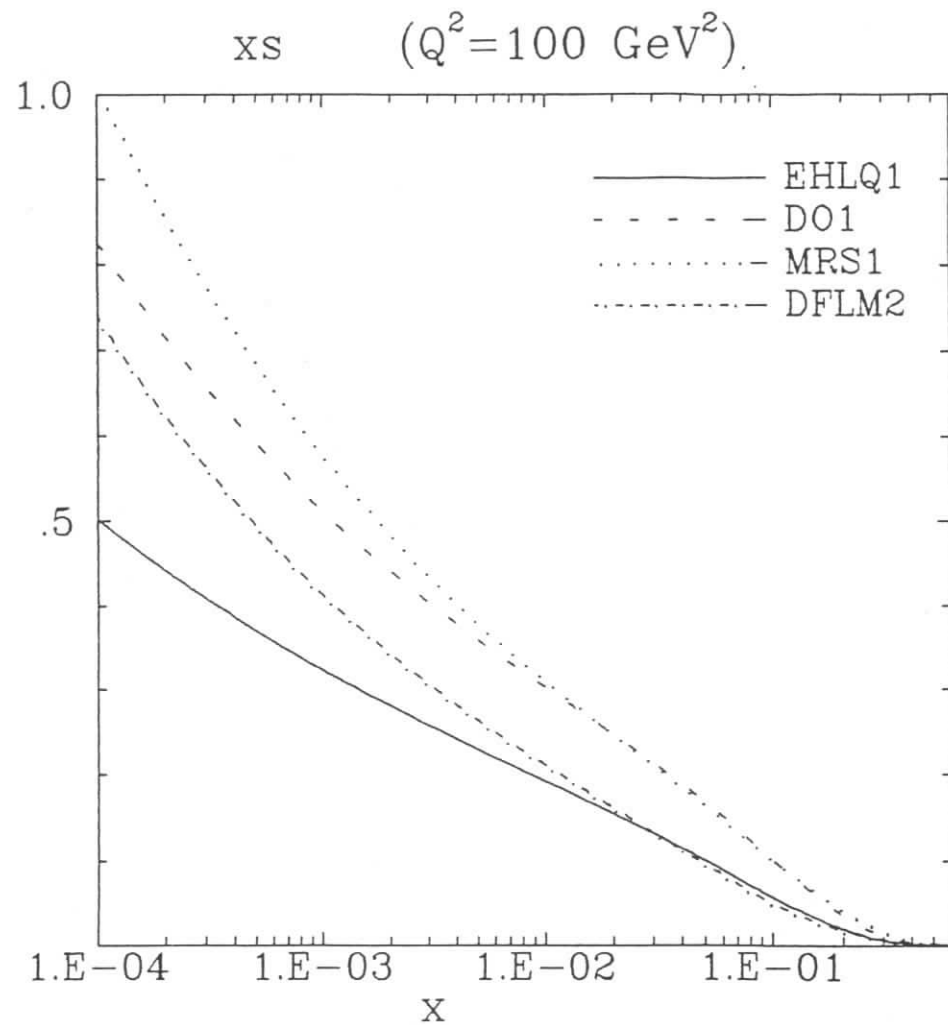


Fig. II.4b. Comparison of the strange quark distributions $x s(x, Q^2)$ at $Q^2 = 10^2 \text{ GeV}^2$ obtained in various parametrizations: EHLQ1, DO1, MRS1, DFLM2.

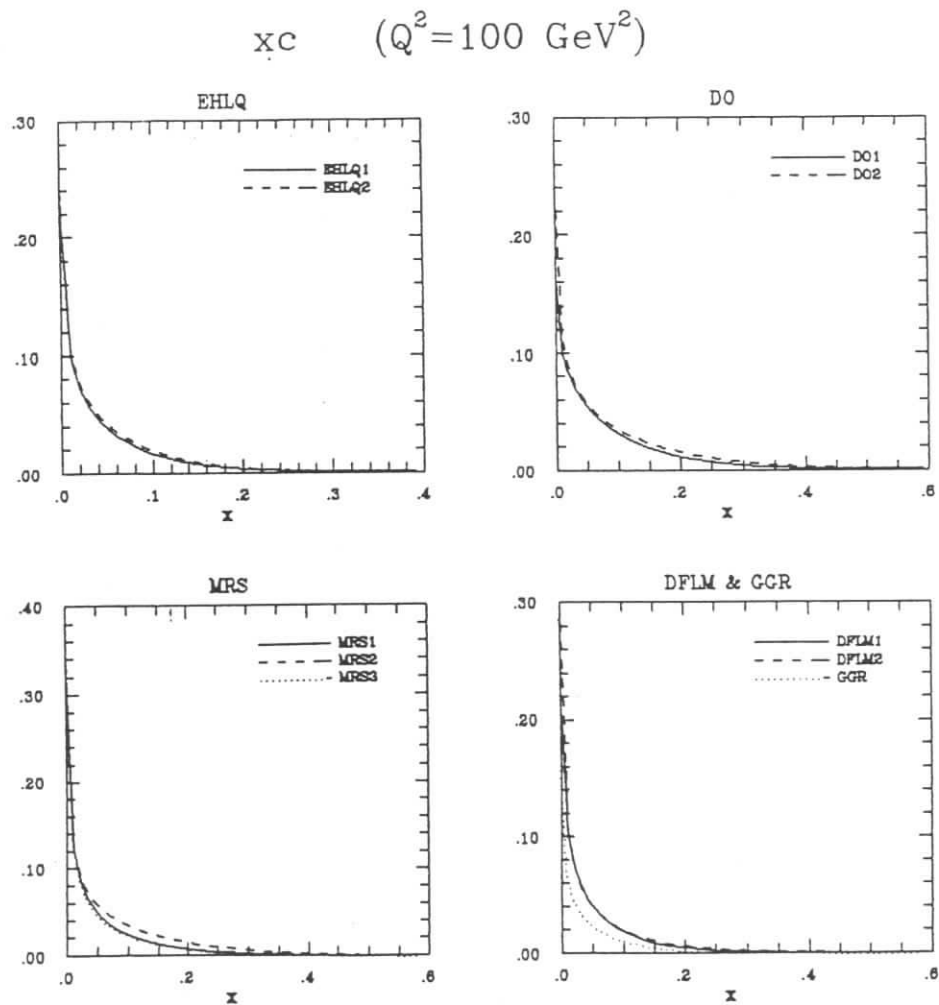


Fig. II.5a. The charm quark distribution $x_c(x, Q^2)$ at $Q^2 = 10^2 \text{ GeV}^2$ as a function of x , for various parametrizations: EHLQ1,2, DO1,2, MRS1,2,3, DFLM1,2 and GGR.

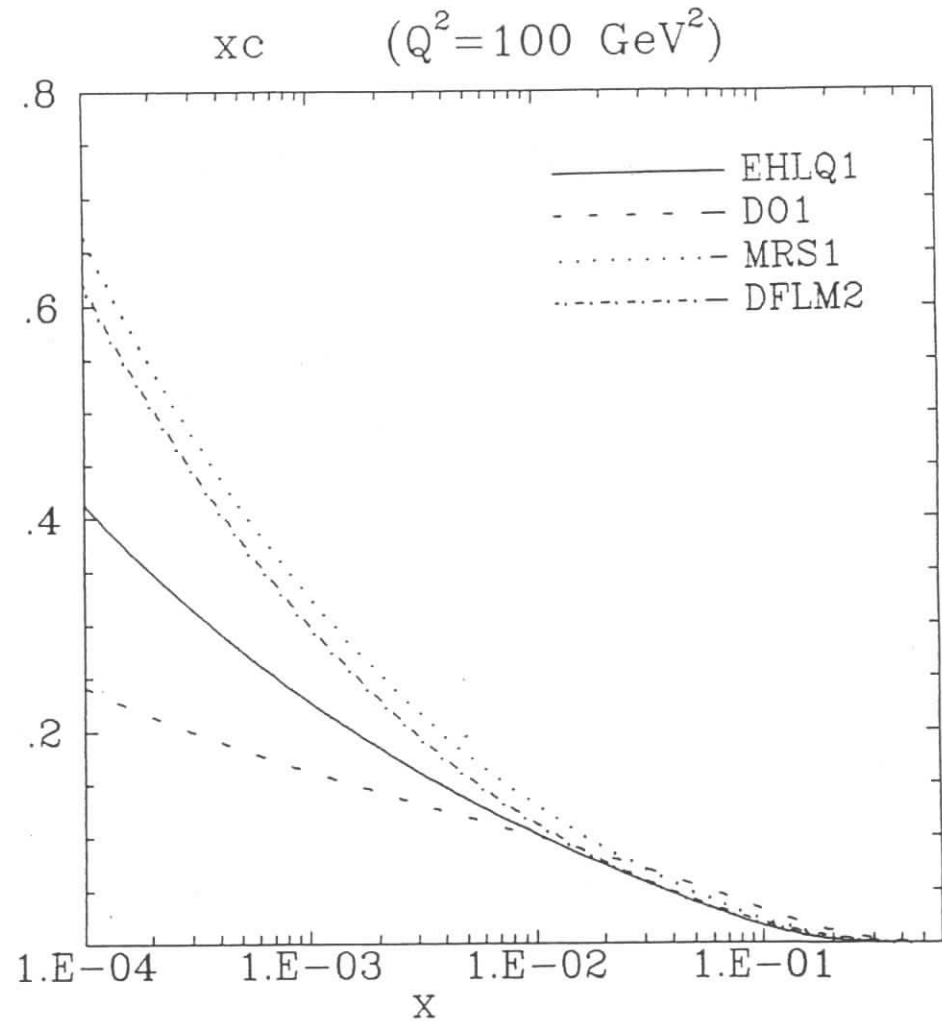


Fig. II.5b. Comparison of the charm quark distributions $x_c(x, Q^2)$ at $Q^2 = 10^2 \text{ GeV}^2$ obtained in various parametrizations: EHLQ1, DO1, MRS1, DFLM2.

$x b \quad (Q^2 = 100 \text{ GeV}^2)$

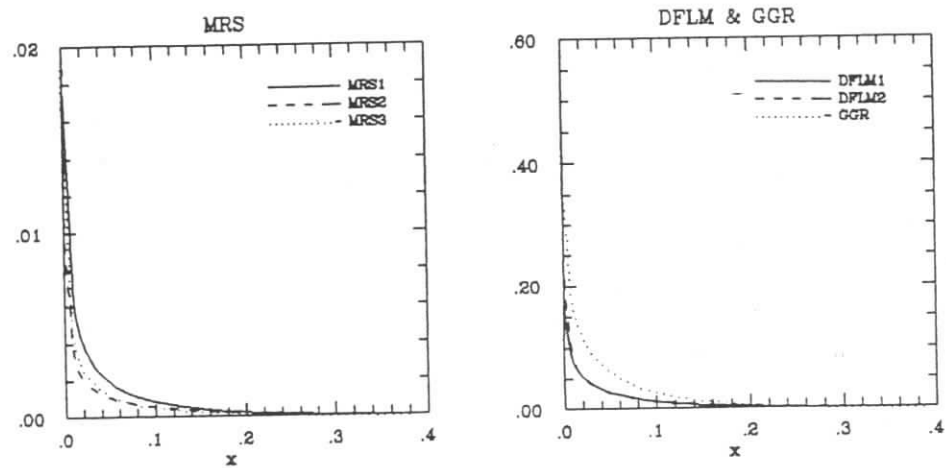


Fig. II.6a. The bottom quark distribution $x b(x, Q^2)$ at $Q^2 = 10^2 \text{ GeV}^2$ as a function of x , for various parametrizations: MRS1,2,3, DFLM1,2 and GGR.

$x b \quad (Q^2 = 100 \text{ GeV}^2)$

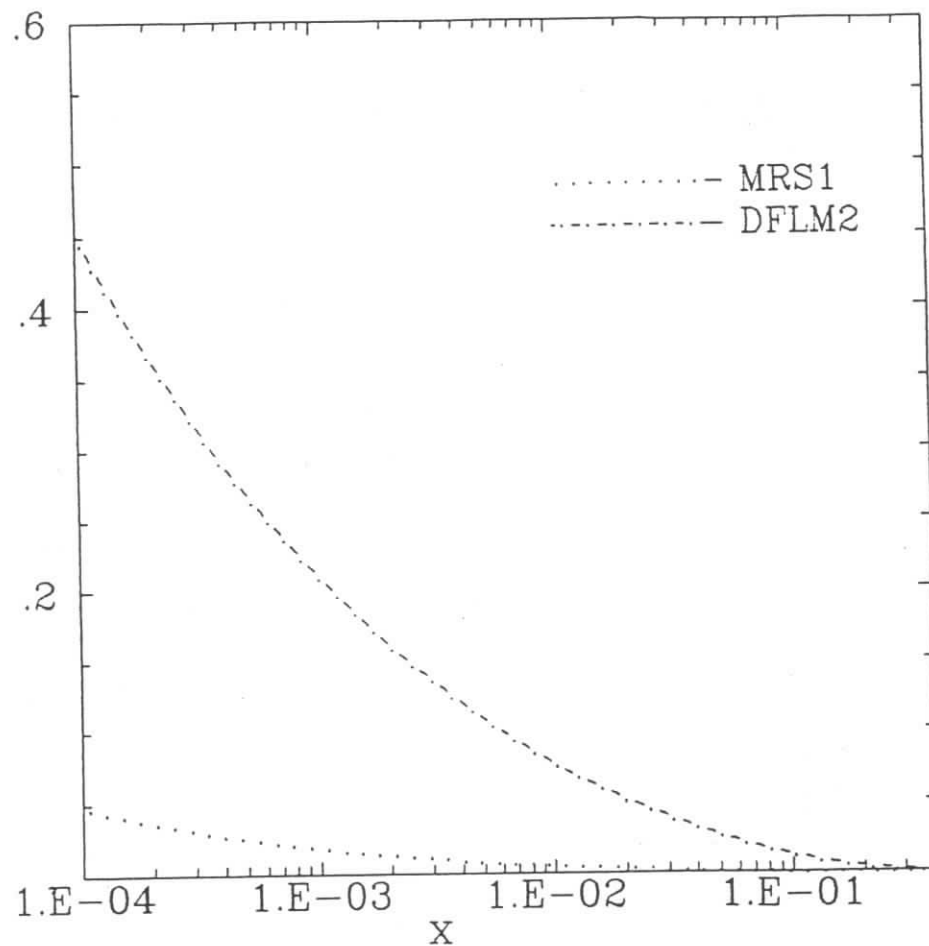


Fig. II.6b. Comparison of the bottom quark distributions $x b(x, Q^2)$ at $Q^2 = 10^2 \text{ GeV}^2$ obtained in MRS1, DFLM2 parametrizations.

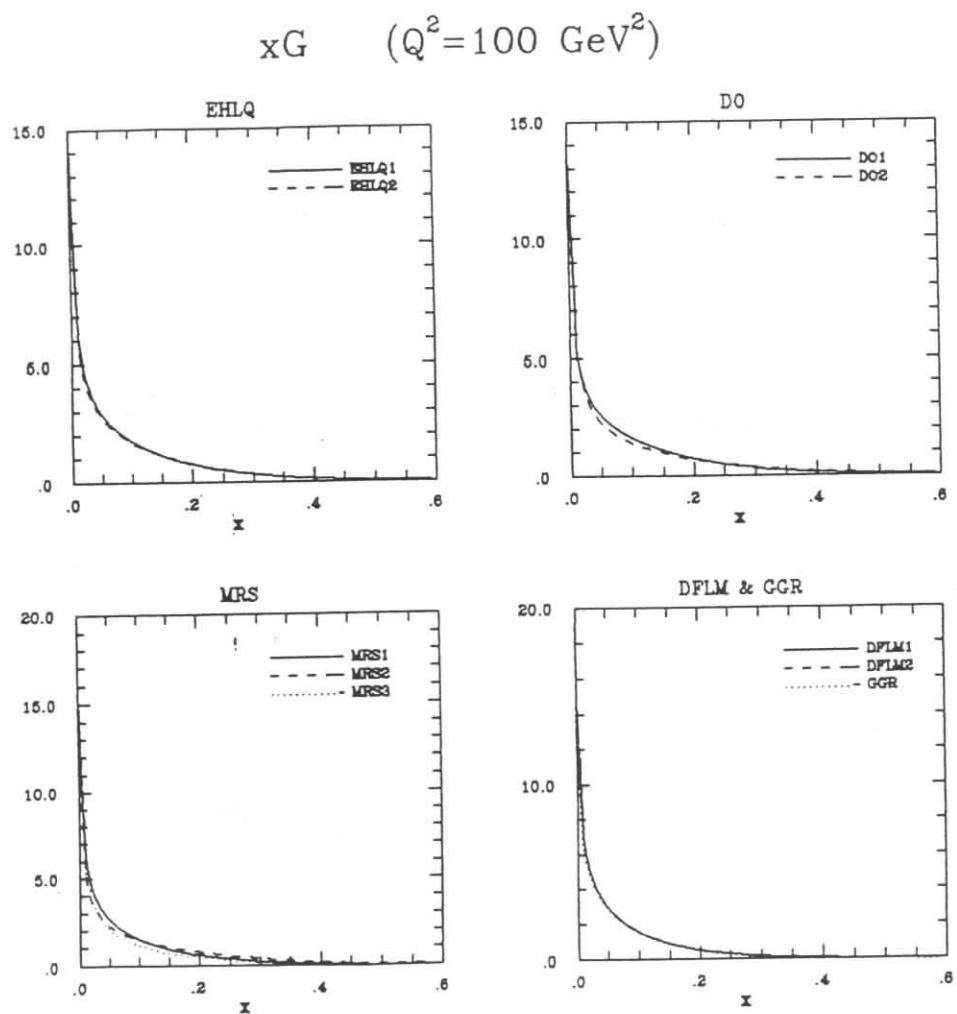


Fig. II.7a. The gluon distribution $xG(x, Q^2)$ at $Q^2 = 10^2 \text{ GeV}^2$ as a function of x , for various parametrizations: EHLQ1,2, DO1,2, MRS1,2,3, DFLM1,2 and GGR.

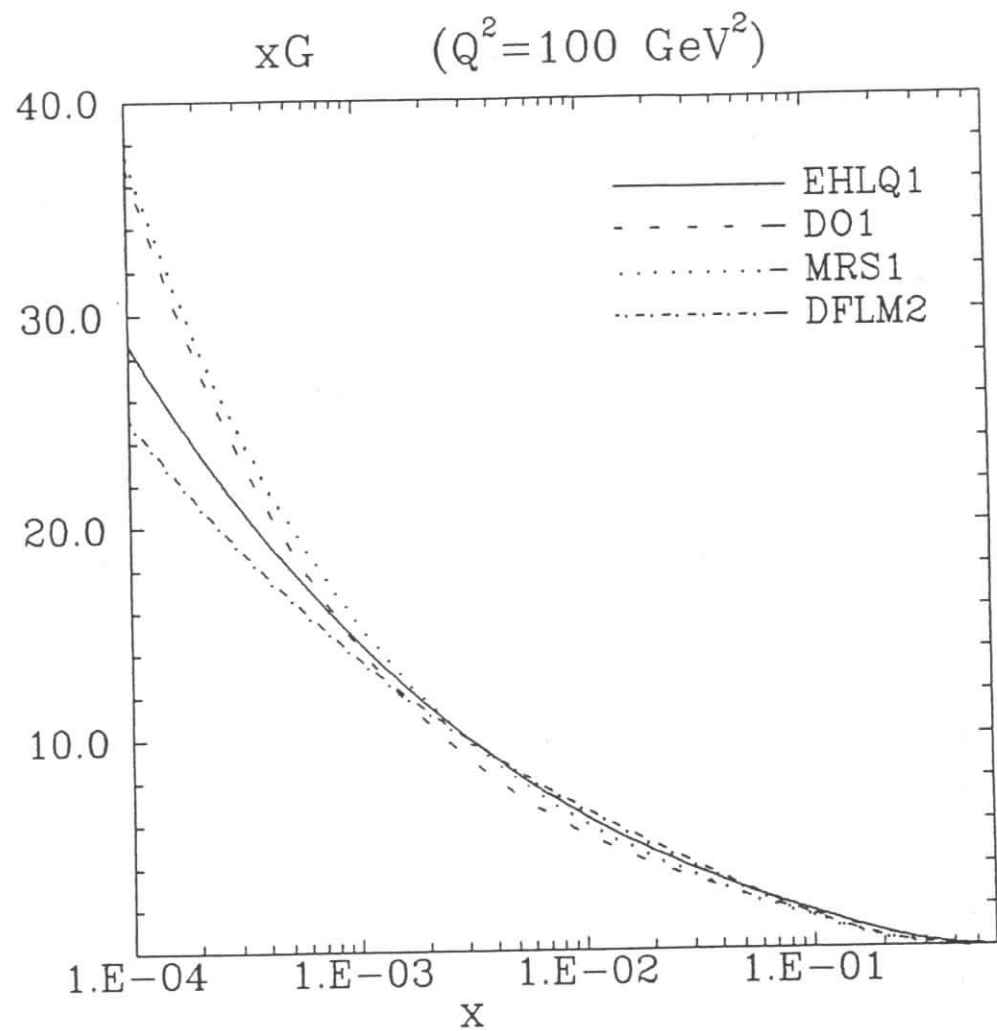


Fig. II.7b. Comparison of the gluon distributions $xG(x, Q^2)$ at $Q^2 = 10^2 \text{ GeV}^2$ obtained in various parametrizations: EHLQ1, DO1, MRS1, DFLM2.

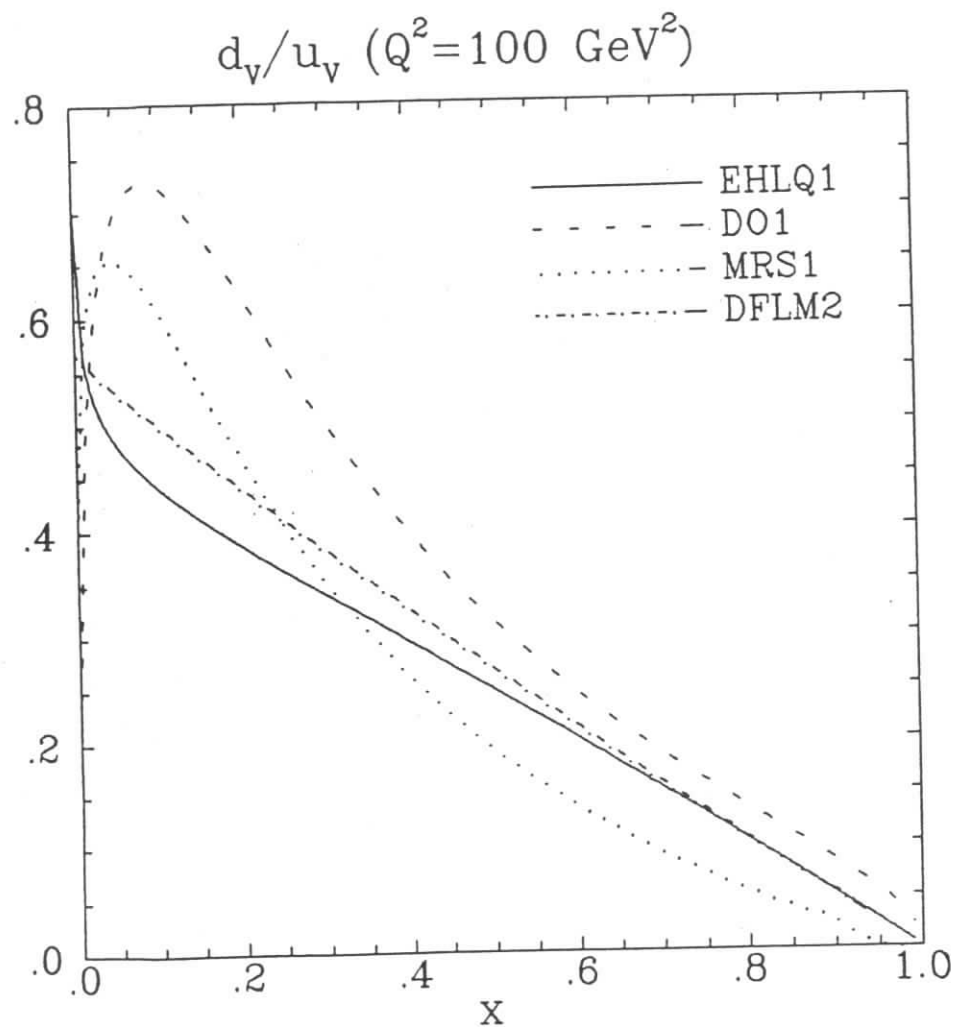


Fig. 11.8. The ratio for valence down and up quarks distributions $d_v(x, Q^2)/u_v(x, Q^2)$ at $Q^2 = 10^2 \text{ GeV}^2$ predicted by various parametrizations: EHLQ1, DO1, MRS1 and DFLM2.

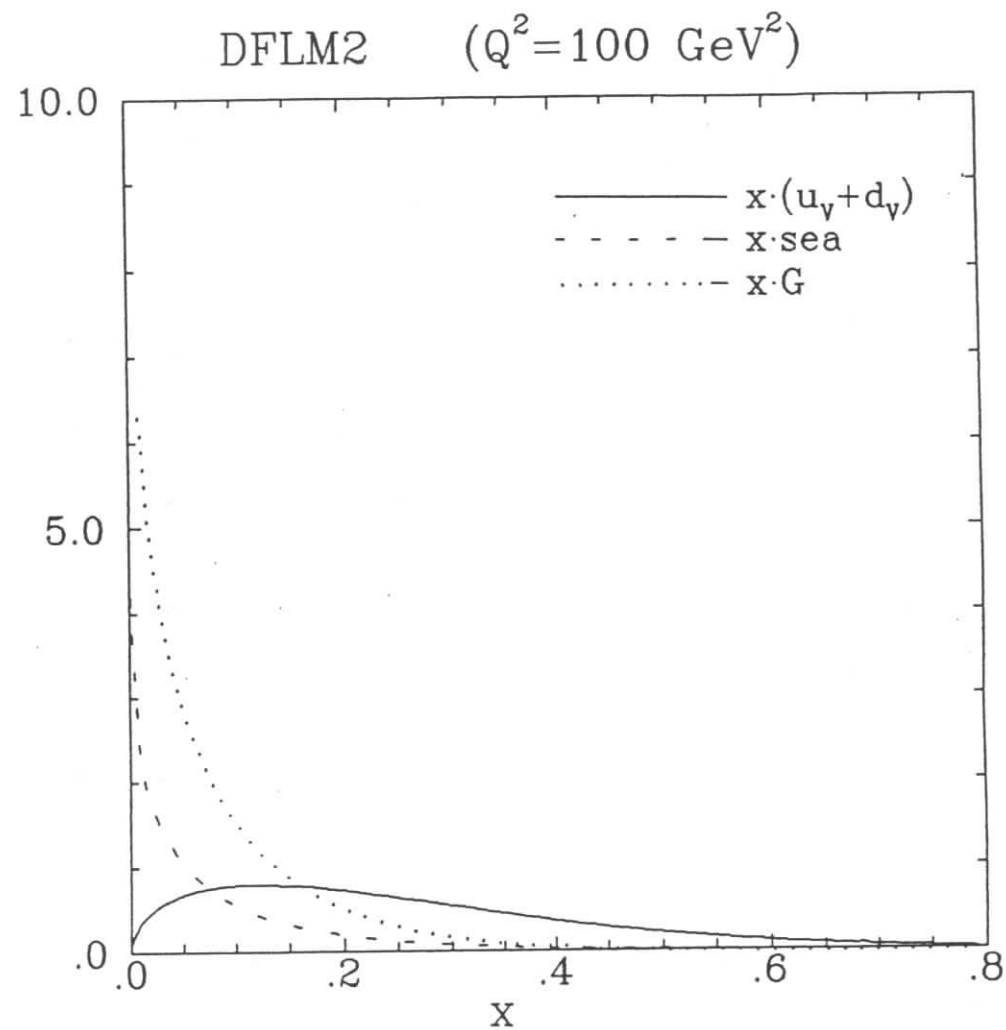


Fig. 11.9. Comparison of the valence quark distribution $x[u_v + d_v]$, the sea quark distribution $2x[\bar{u} + \bar{d} + s + c + b + t]$ and the gluon distribution xG of DFLM2 parametrization at $Q^2 = 10^2 \text{ GeV}^2$.

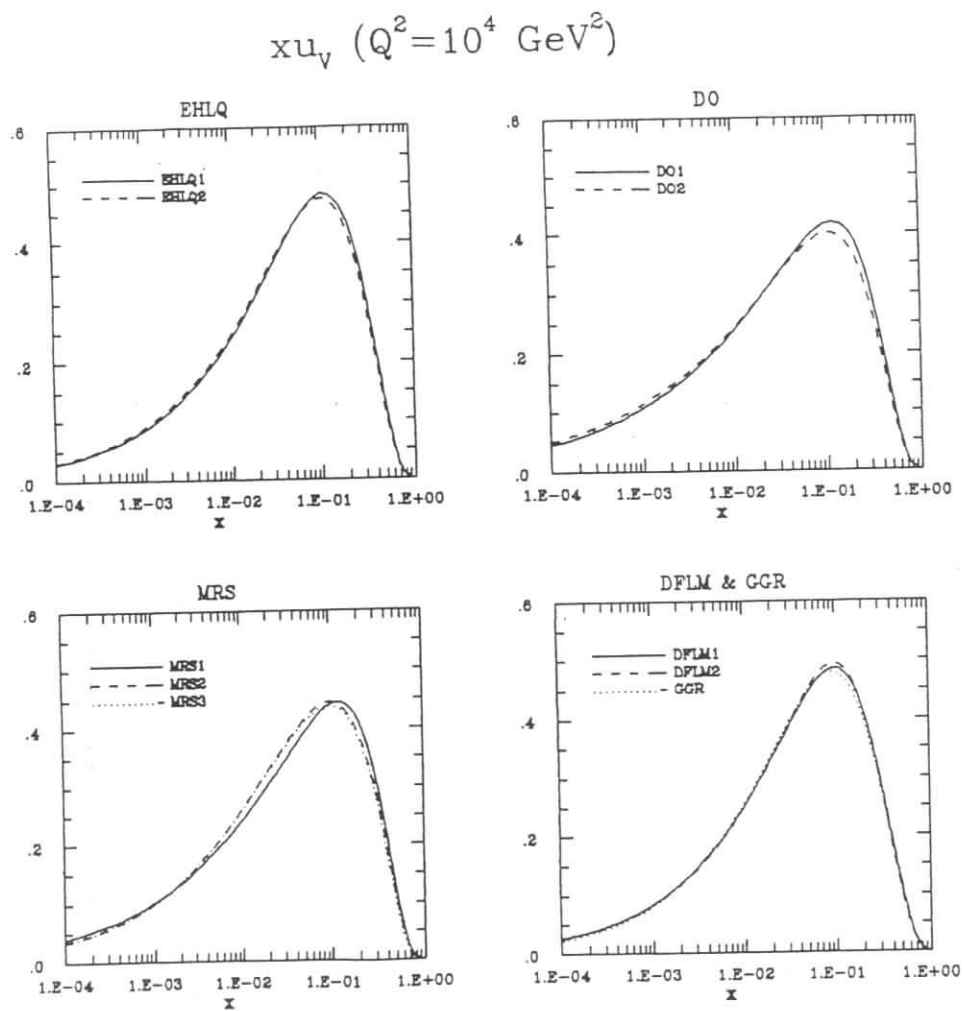


Fig. III.1a. The valence up quark distribution $xu_v(x, Q^2)$ at $Q^2 = 10^4 \text{ GeV}^2$ as a function of x , for various parametrizations: EHLQ1.2, DO1.2, MRS1,2,3, DFLM1.2 and GGR.

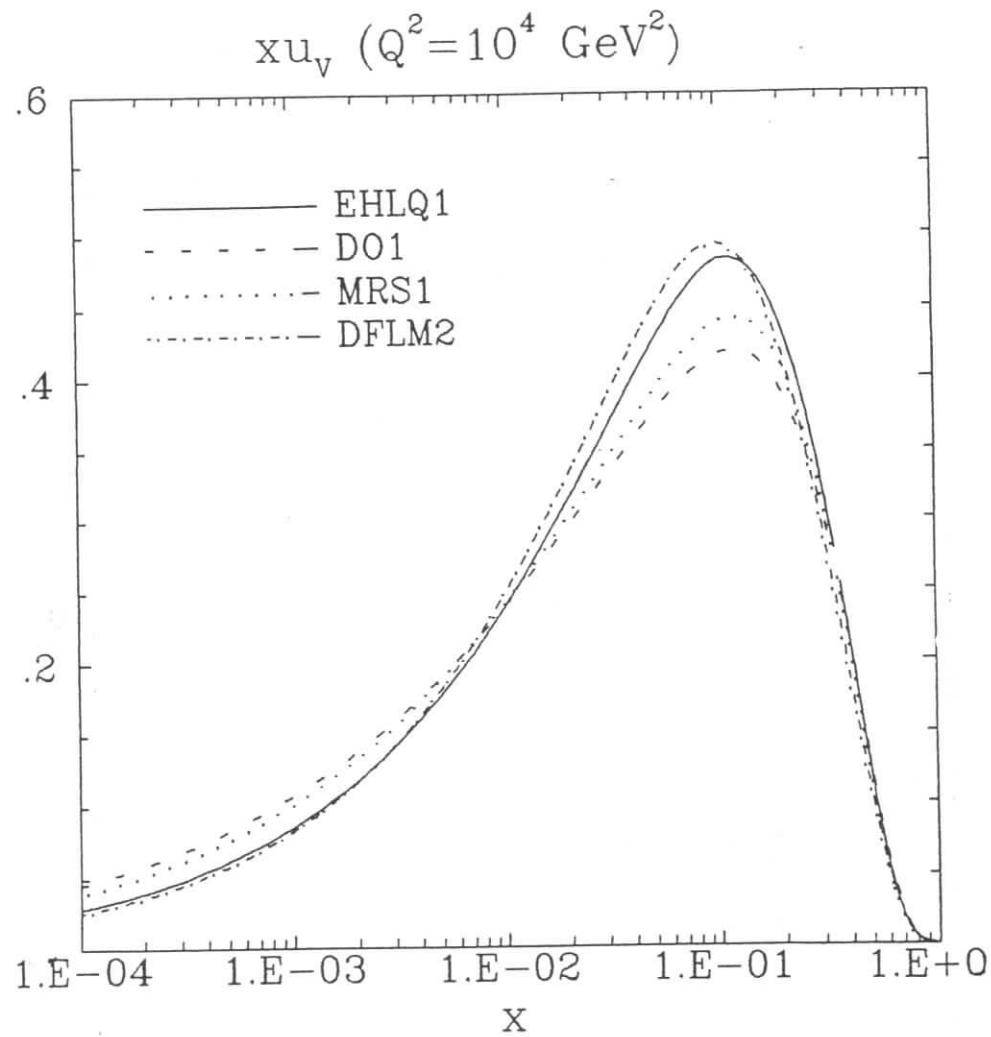


Fig. III.1b. Comparison of the valence up quark distributions $xu_v(x, Q^2)$ at $Q^2 = 10^4 \text{ GeV}^2$ obtained in various parametrizations: EHLQ1, DO1, MRS1, DFLM2.

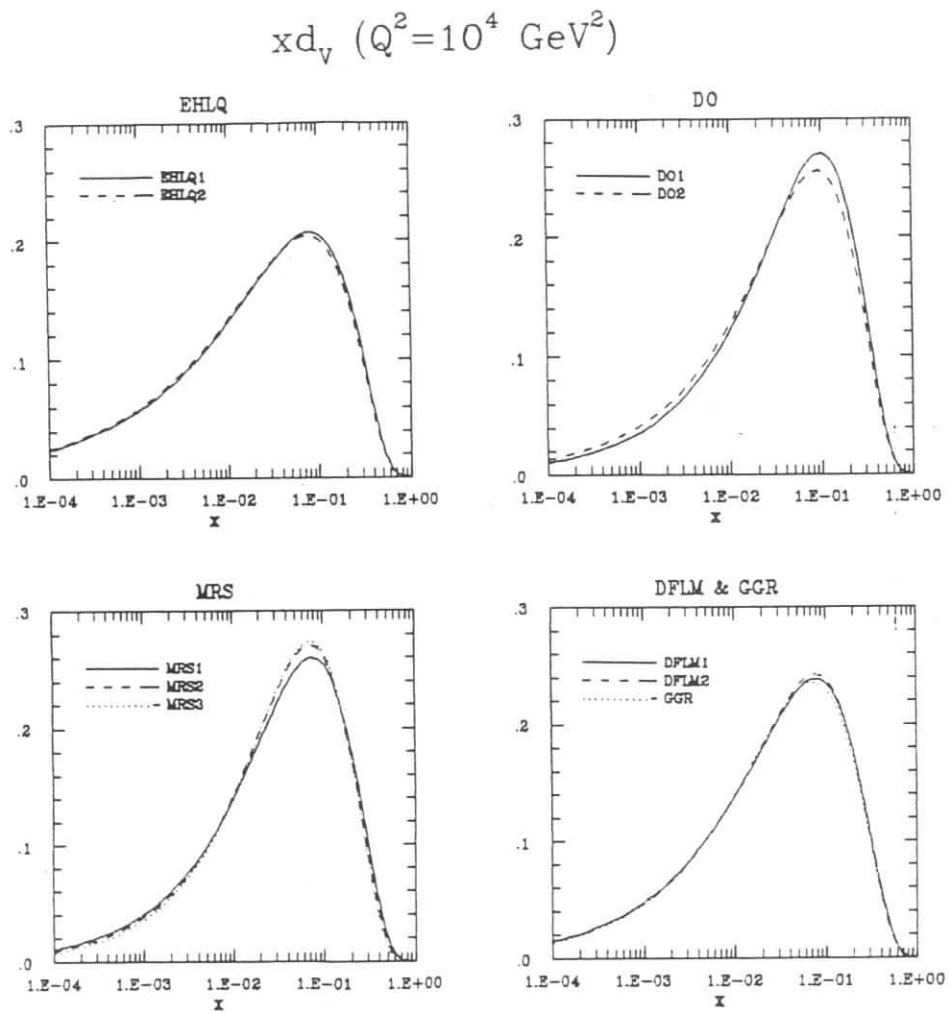


Fig. III.2a. The valence down quark distribution $x d_v(x, Q^2)$ at $Q^2 = 10^4 \text{ GeV}^2$ as a function of x , for various parametrizations: EHLQ1.2, DO1.2, MRS1,2,3, DFLM1.2 and GGR.

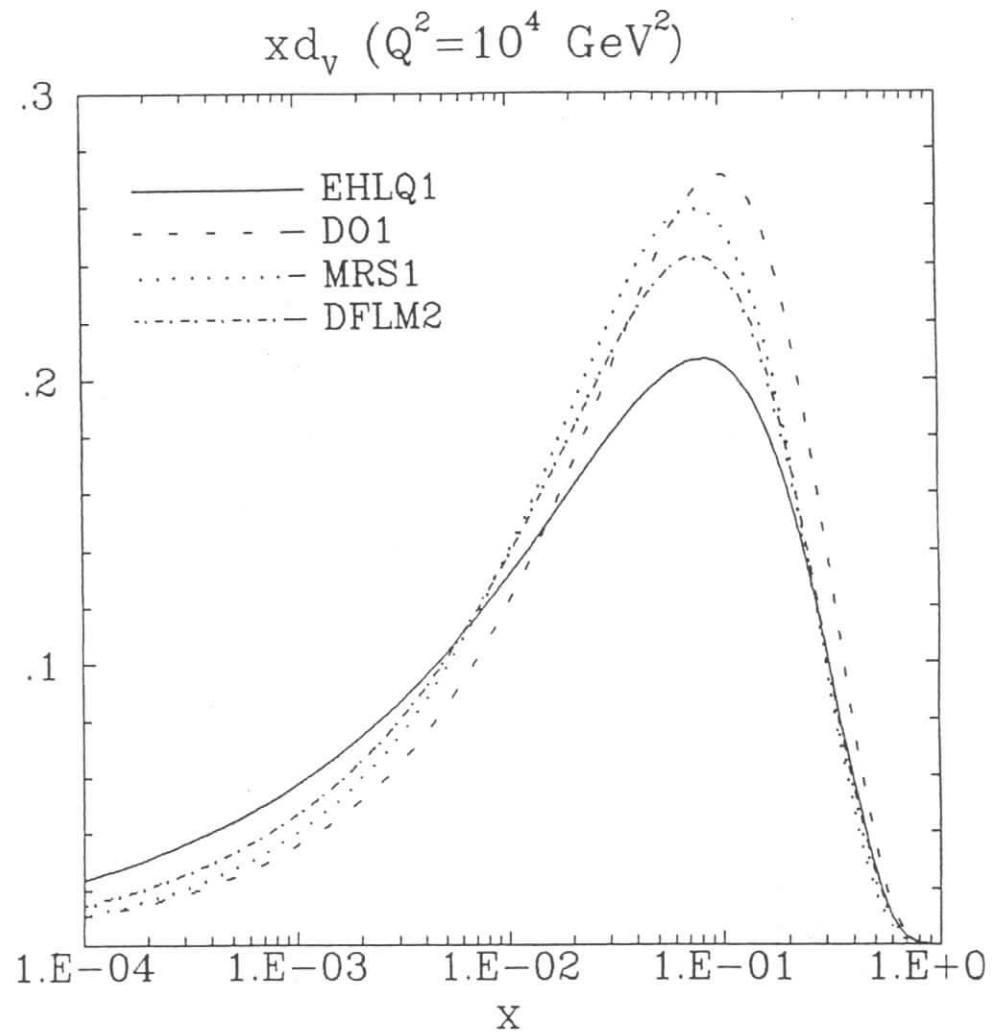


Fig. III.2b. Comparison of the valence down quark distributions $x d_v(x, Q^2)$ at $Q^2 = 10^4 \text{ GeV}^2$ obtained in various parametrizations: EHLQ1, DO1, MRS1, DFLM2.

$$x\bar{u}(=x\bar{d}) \quad (Q^2=10^4 \text{ GeV}^2)$$

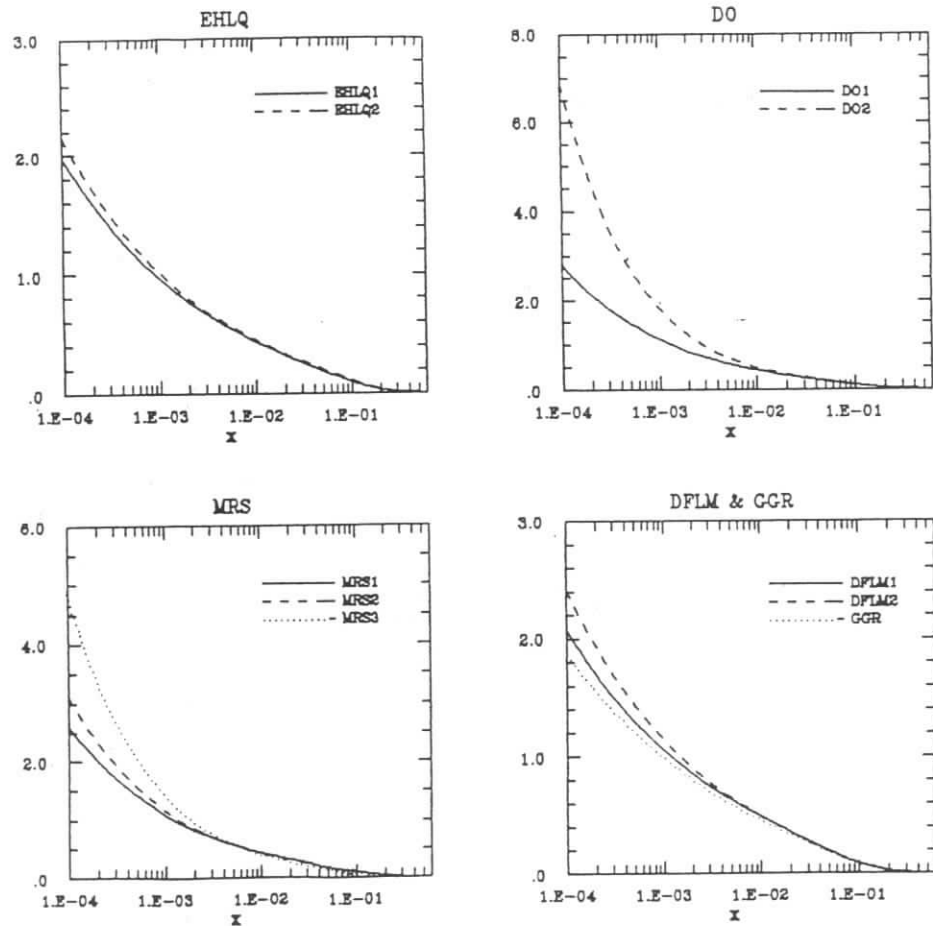


Fig. III.3a. The up(down) antiquark distribution $x\bar{u}(x, Q^2)(x\bar{d}(x, Q^2))$ at $Q^2 = 10^4 \text{ GeV}^2$ as a function of x , for various parametrizations: EHLQ1,2, DO1,2, MRS1,2,3, DFLM1,2 and GGR.

$$x\bar{u}(=x\bar{d}) \quad (Q^2=10^4 \text{ GeV}^2)$$

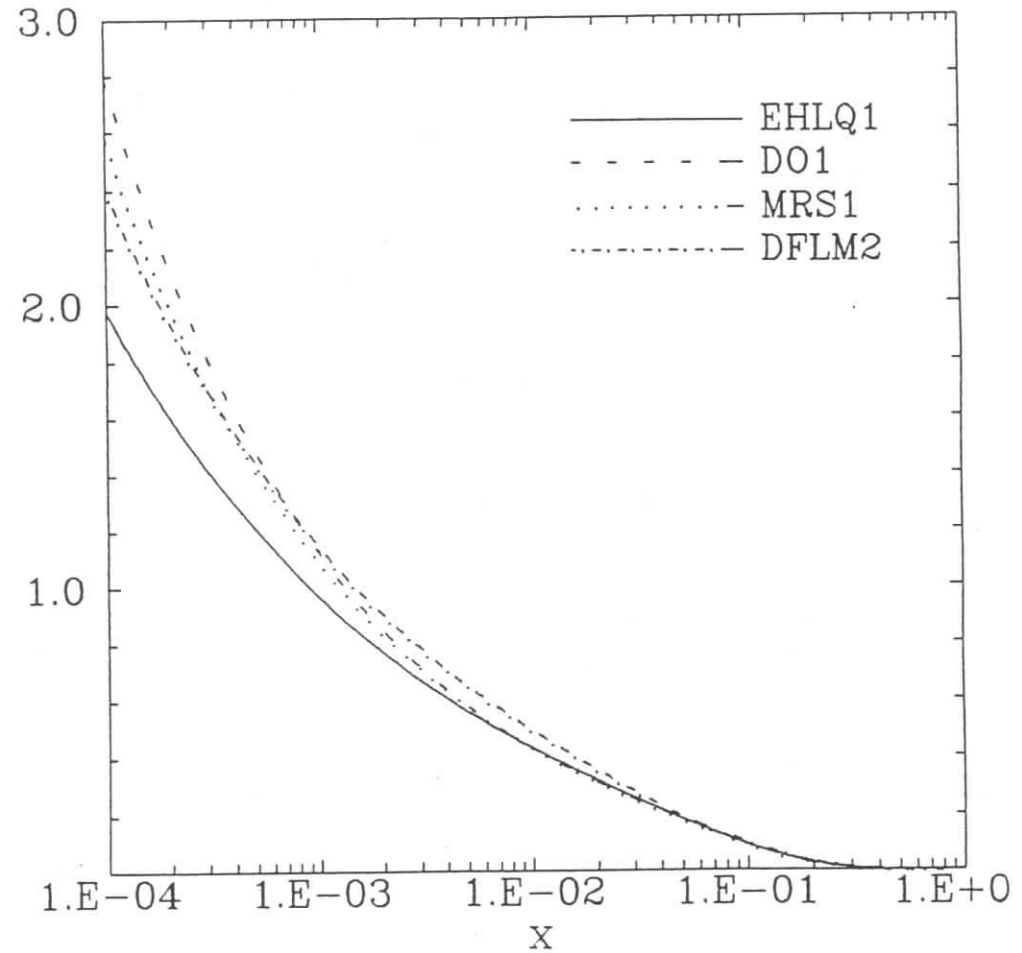


Fig. III.3b. Comparison of the up (down) antiquark distributions $x\bar{u}(x, Q^2)(x\bar{d}(x, Q^2))$ at $Q^2 = 10^4 \text{ GeV}^2$ obtained in various parametrizations: EHLQ1, DO1, MRS1, DFLM2.

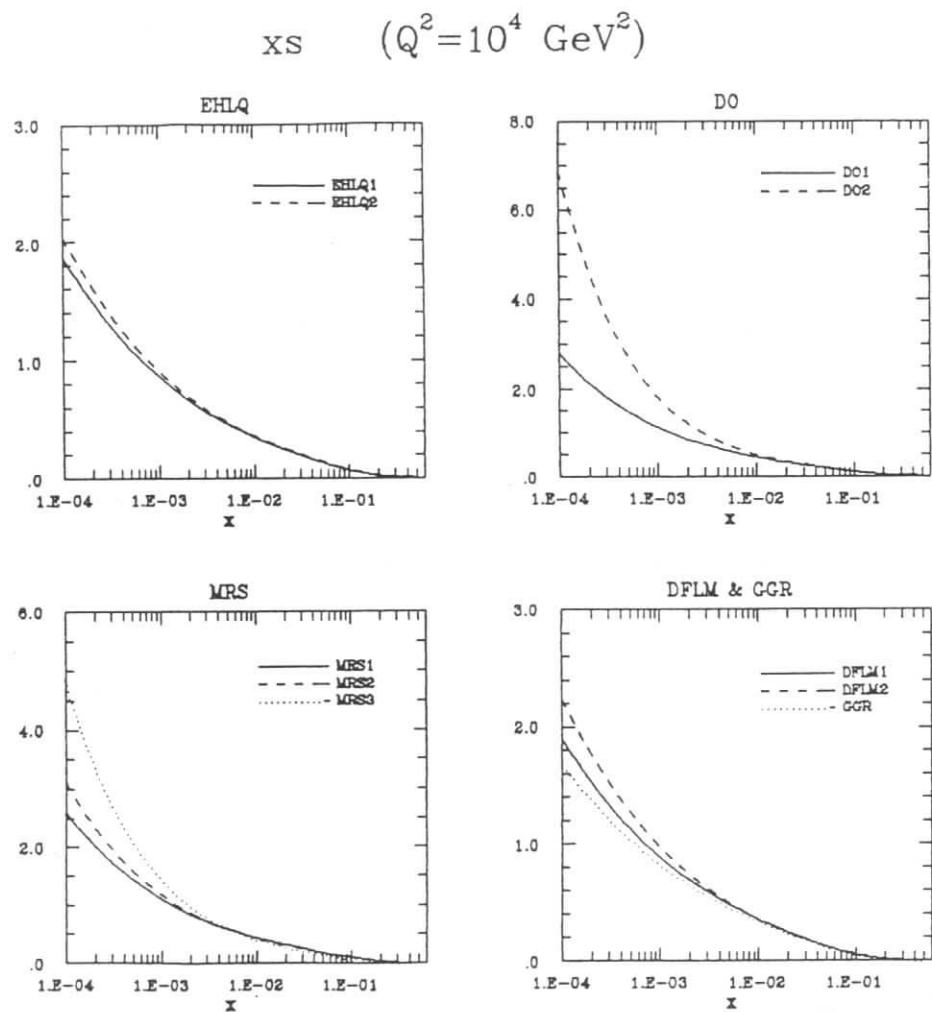


Fig. III.4a. The strange quark distribution $x s(x, Q^2)$ at $Q^2 = 10^4 \text{ GeV}^2$ as a function of x , for various parametrizations: EHLQ1,2, DO1,2, MRS1,2,3, DFLM1,2 and GGR.

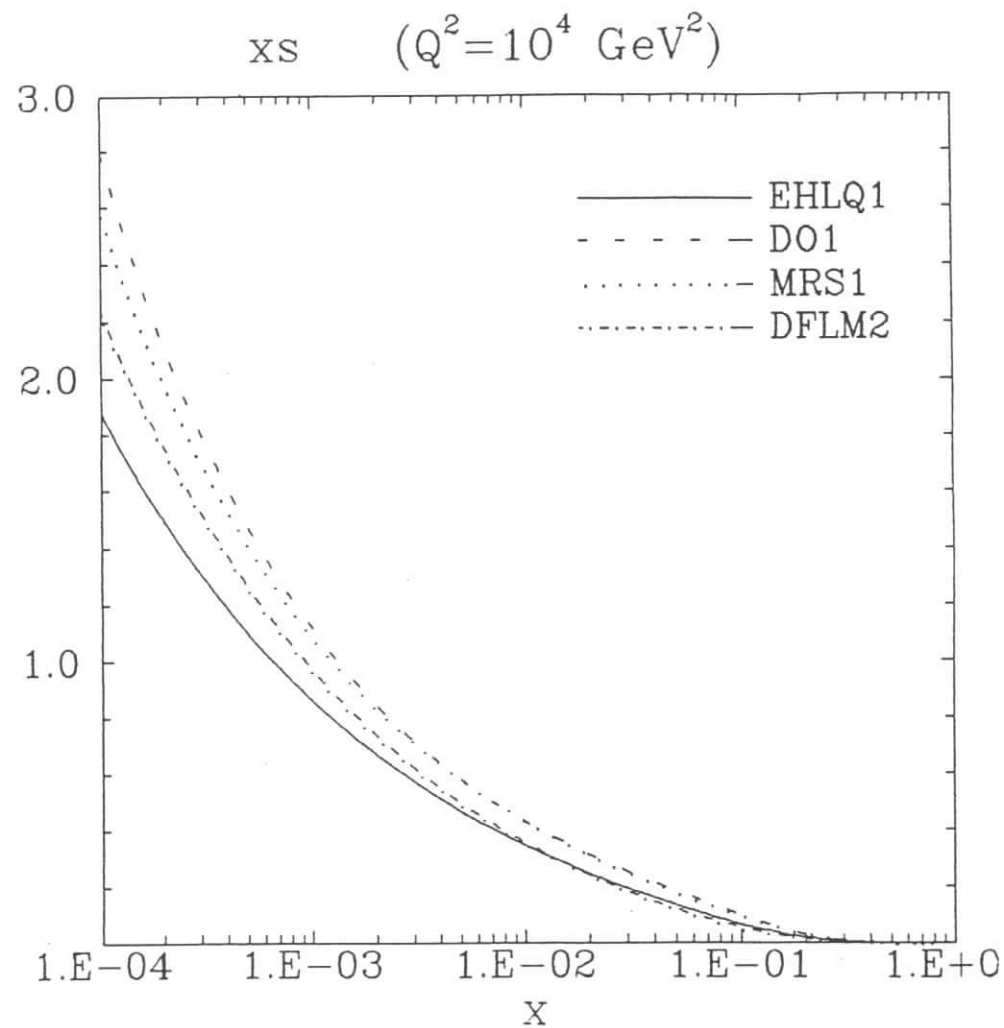


Fig. III.4b. Comparison of the strange quark distributions $x s(x, Q^2)$ at $Q^2 = 10^4 \text{ GeV}^2$ obtained in various parametrizations: EHLQ1, DO1, MRS1, DFLM2.

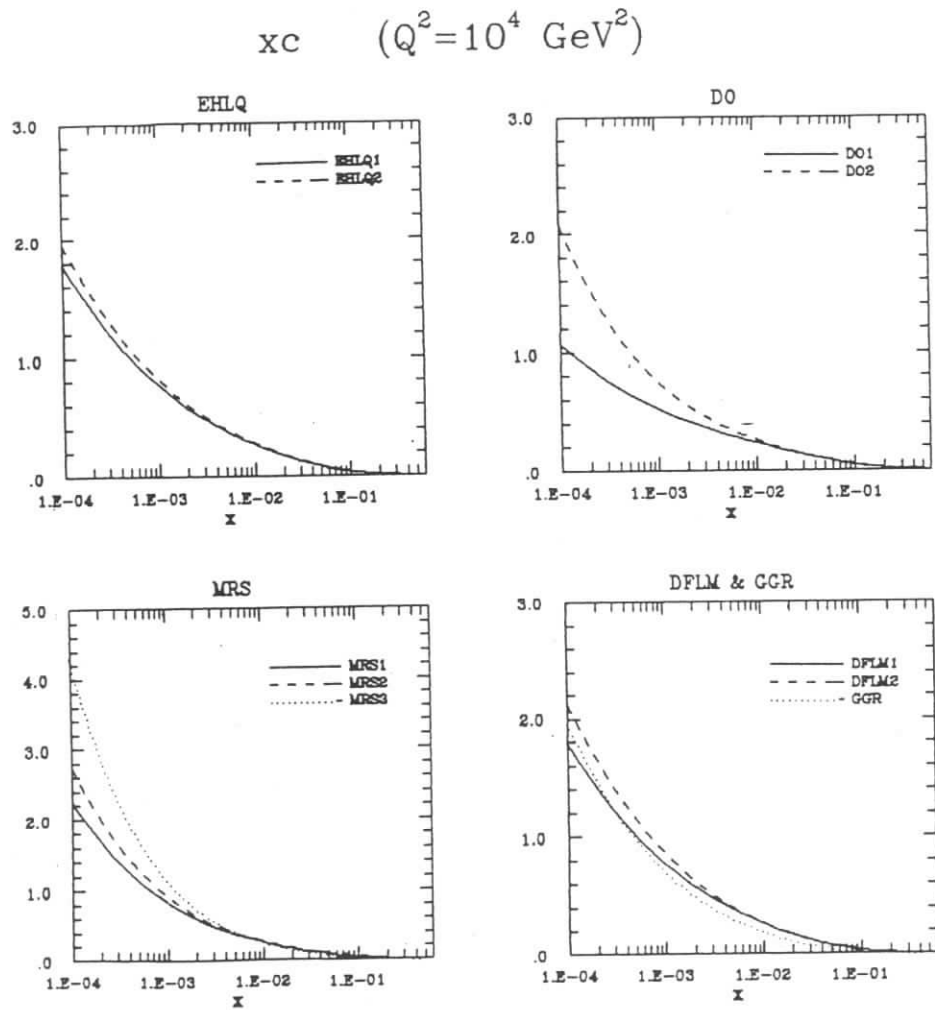


Fig. III.5a. The charm quark distribution $x_c(x, Q^2)$ at $Q^2 = 10^4 \text{ GeV}^2$ as a function of x , for various parametrizations: EHLQ1,2, DO1,2, MRS1,2,3, DFLM1,2 and GGR.

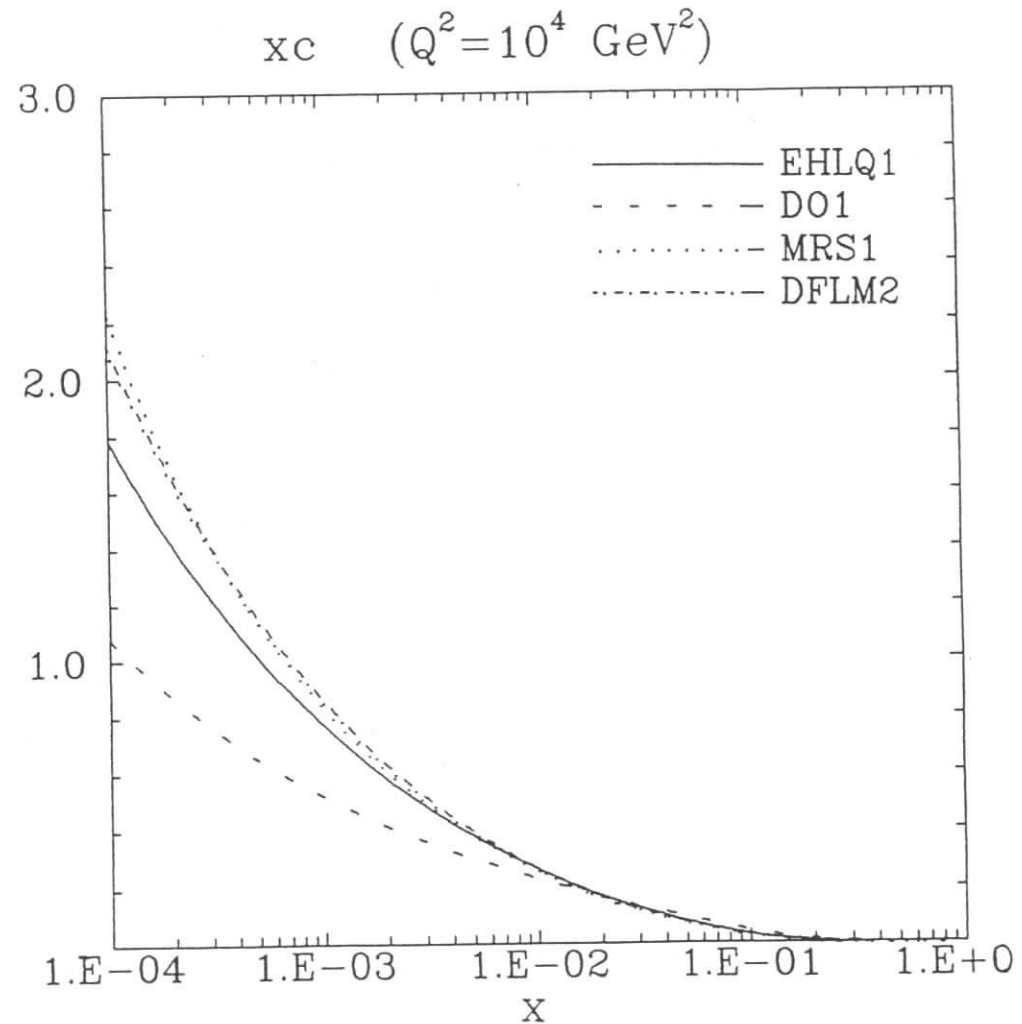


Fig. III.5b. Comparison of the charm quark distributions $x_c(x, Q^2)$ at $Q^2 = 10^4 \text{ GeV}^2$ obtained in various parametrizations: EHLQ1, DO1, MRS1, DFLM2.

$xb \quad (Q^2 = 10^4 \text{ GeV}^2)$

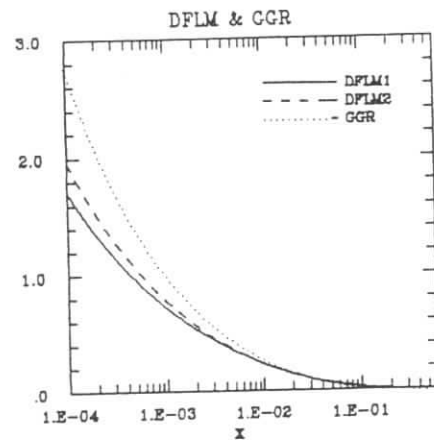
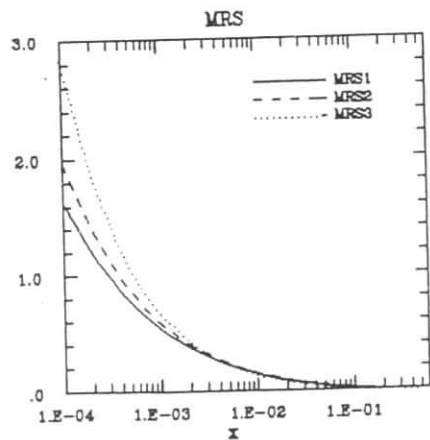
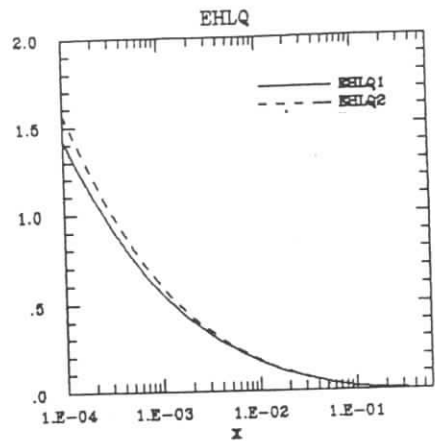


Fig. III.6a. The bottom quark distribution $xb(x, Q^2)$ at $Q^2 = 10^4 \text{ GeV}^2$ as a function of x , for various parametrizations: EHLQ1,2, MRS1,2,3, DFLM1,2 and GGR.

$xb \quad (Q^2 = 10^4 \text{ GeV}^2)$

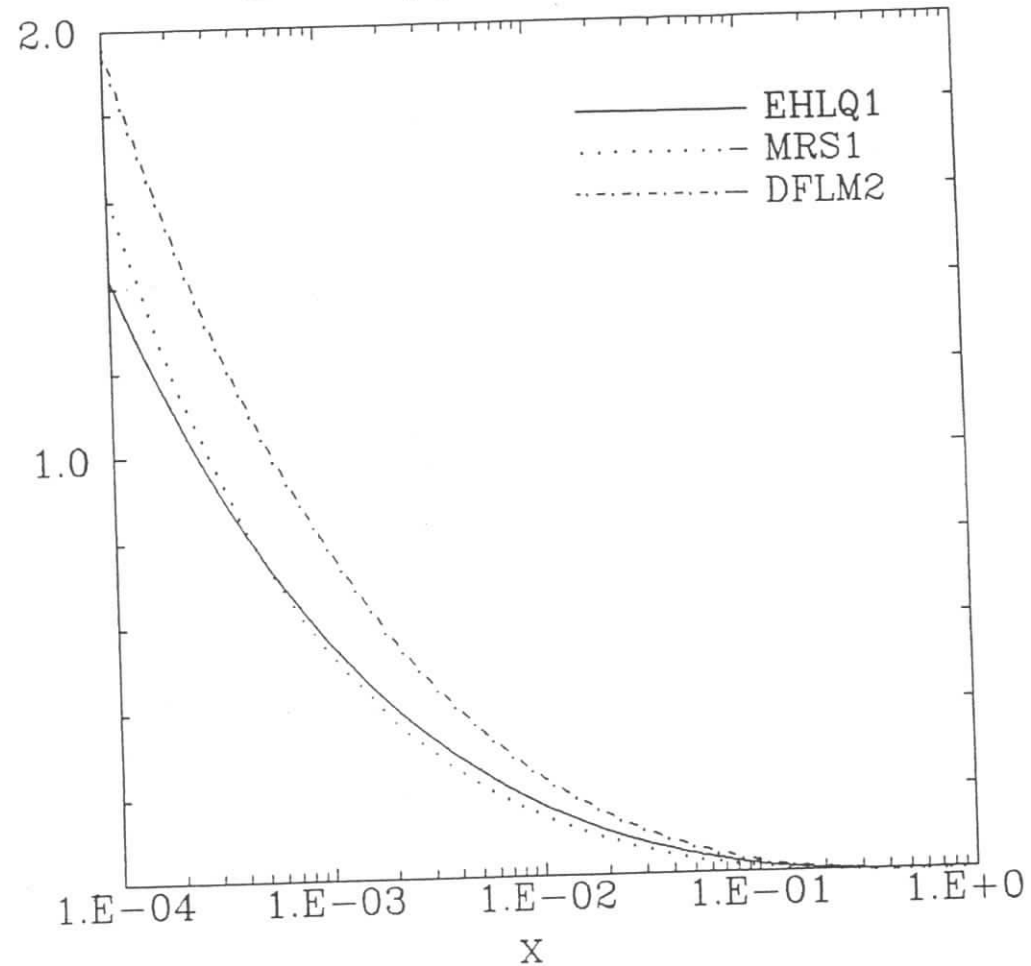


Fig. III.6b. Comparison of the bottom quark distributions $xb(x, Q^2)$ at $Q^2 = 10^4 \text{ GeV}^2$ obtained in various parametrizations: EHLQ1, MRS1, DFLM2.

$xt \quad (Q^2 = 10^4 \text{ GeV}^2)$

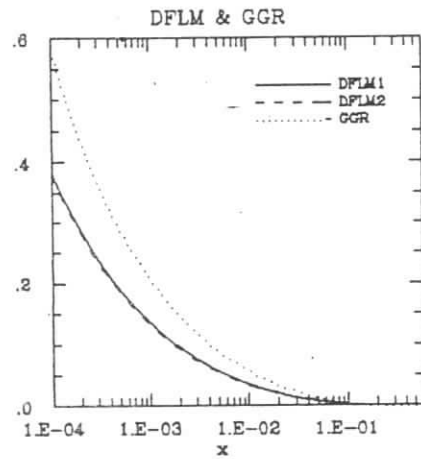
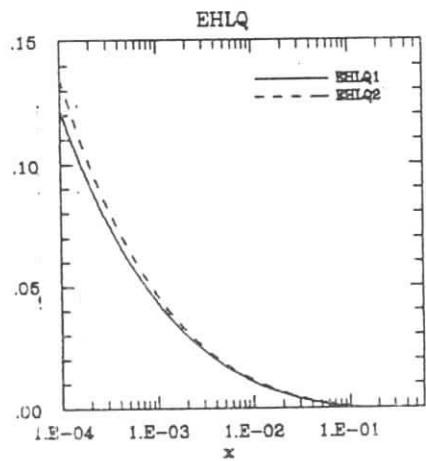


Fig. III.7a. The top quark distribution $xt(z, Q^2)$ at $Q^2 = 10^4 \text{ GeV}^2$ as a function of x , for various parametrizations: EHLQ1,2, DFLM1,2 and GGR.

$xt \quad (Q^2 = 10^4 \text{ GeV}^2)$

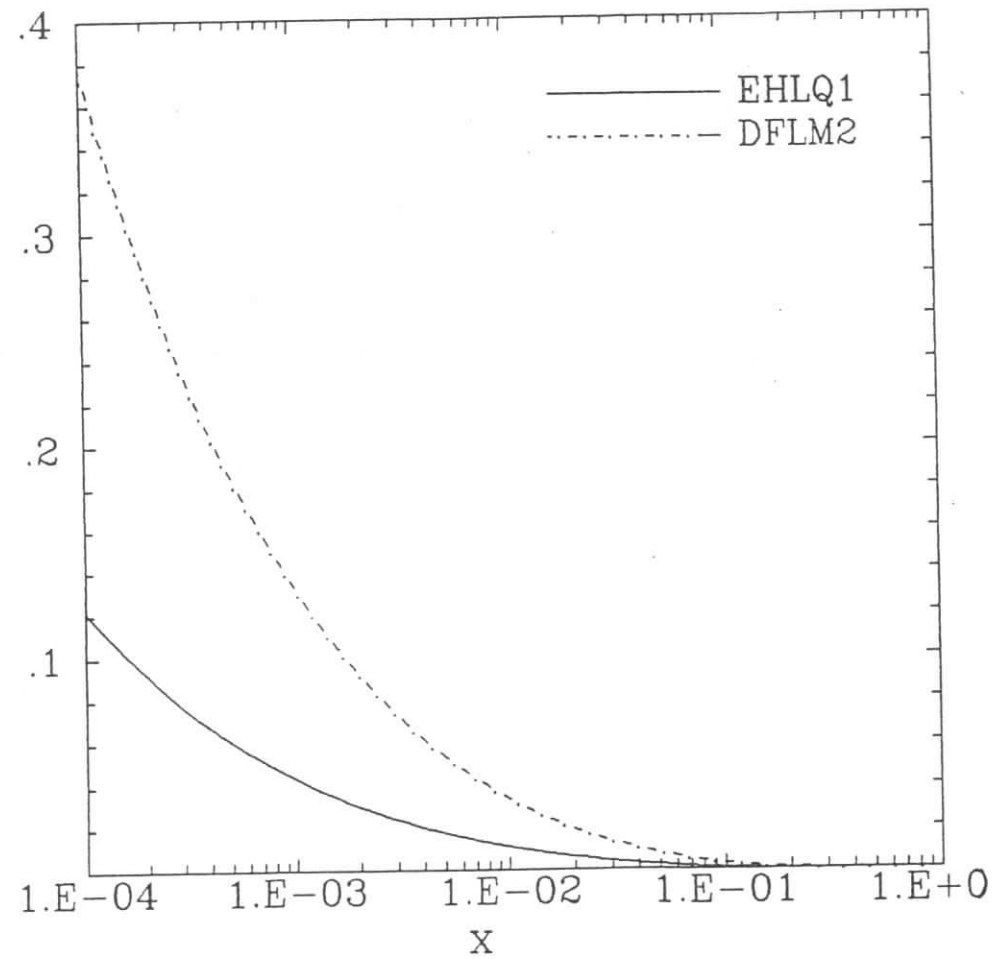


Fig. III.7b. Comparison of the top quark distributions $xt(z, Q^2)$ at $Q^2 = 10^4 \text{ GeV}^2$ obtained in EHLQ1, DFLM2 parametrizations.

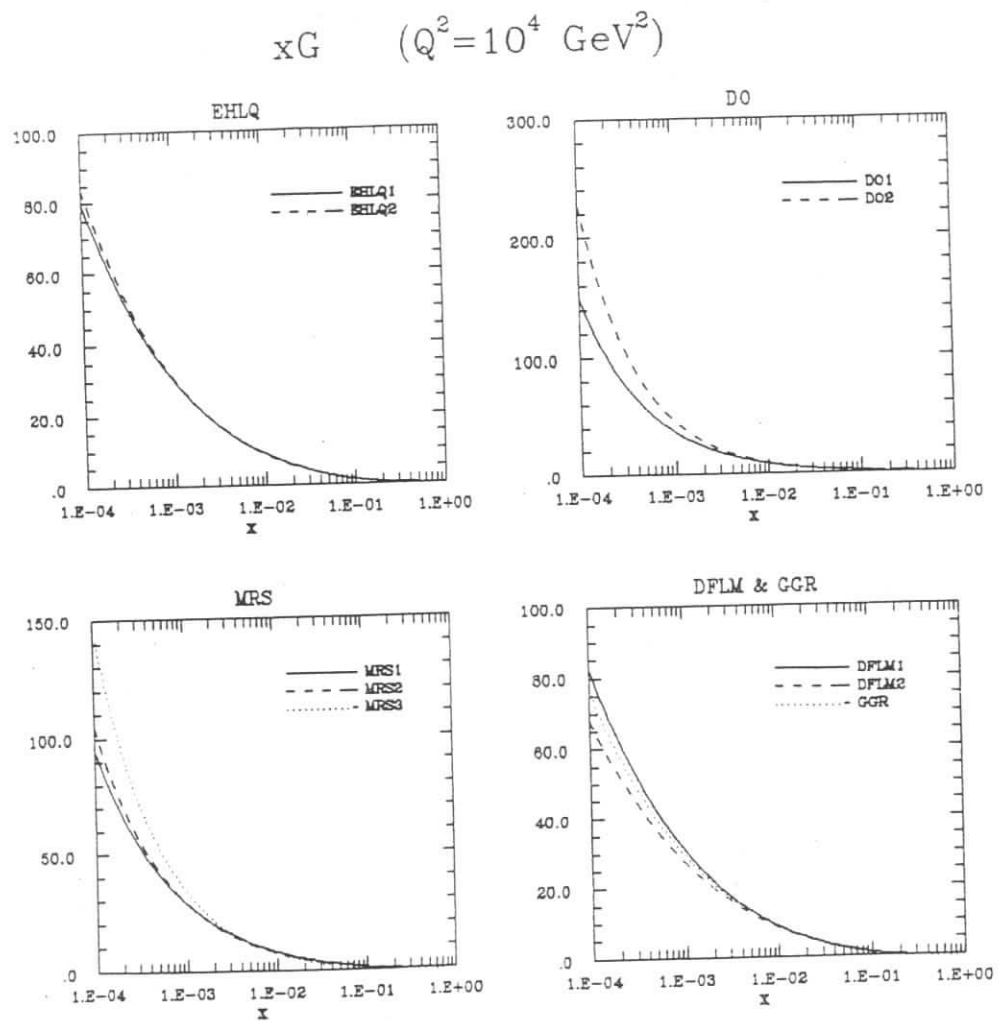


Fig. III.8a. The gluon distribution $xG(x, Q^2)$ at $Q^2 = 10^4 \text{ GeV}^2$ as a function of x , for various parametrizations: EHLQ1.2, DO1.2, MRS1.2.3, DFLM1.2 and GGR.

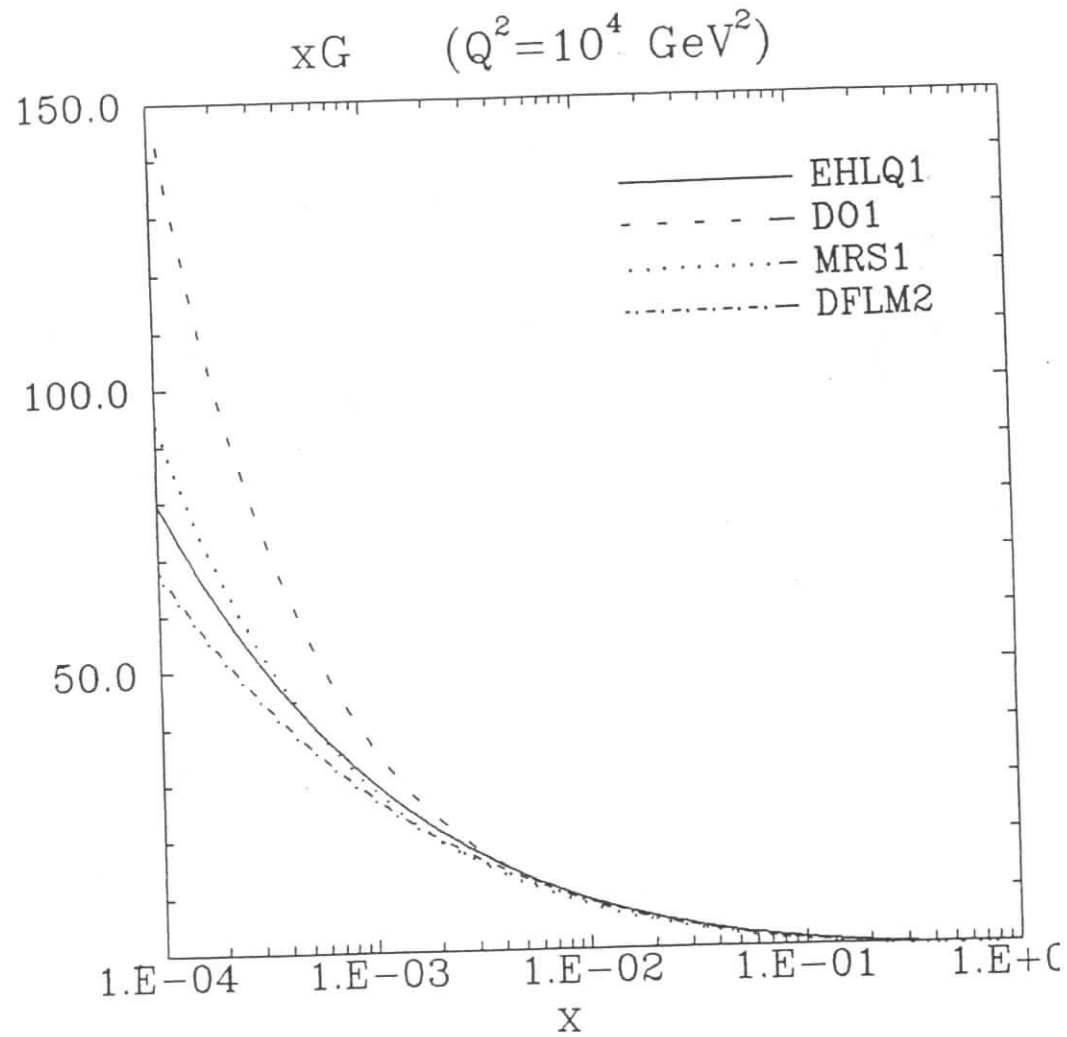


Fig. III.8b. Comparison of the gluon distributions $xG(x, Q^2)$ at $Q^2 = 10^4 \text{ GeV}^2$ obtained in various parametrizations: EHLQ1, DO1, MRS1, DFLM2.

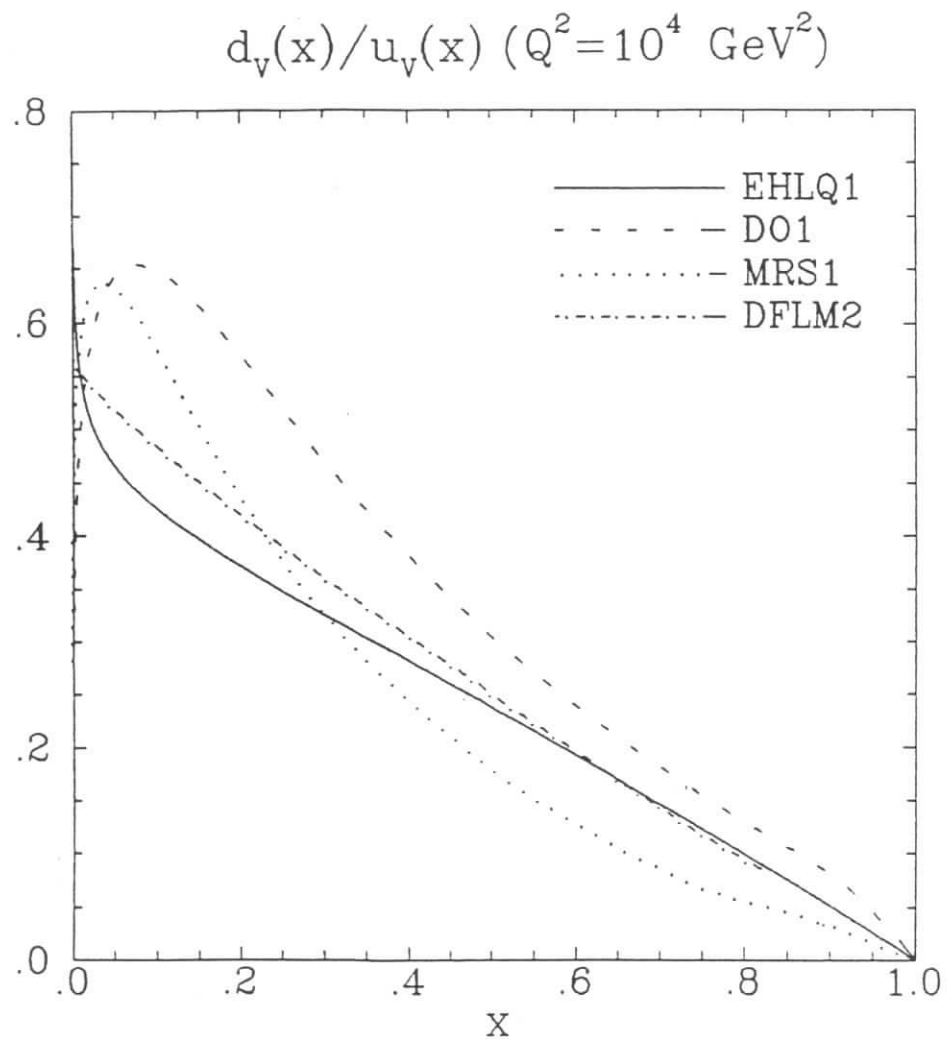


Fig. III.9a. The ratio for valence down and up quarks distributions $d_v(x, Q^2)/u_v(x, Q^2)$ at $Q^2 = 10^4 \text{ GeV}^2$ predicted by various parametrizations: EHLQ1, DO1, MRS1 and DFLM2 — linear x -scale.

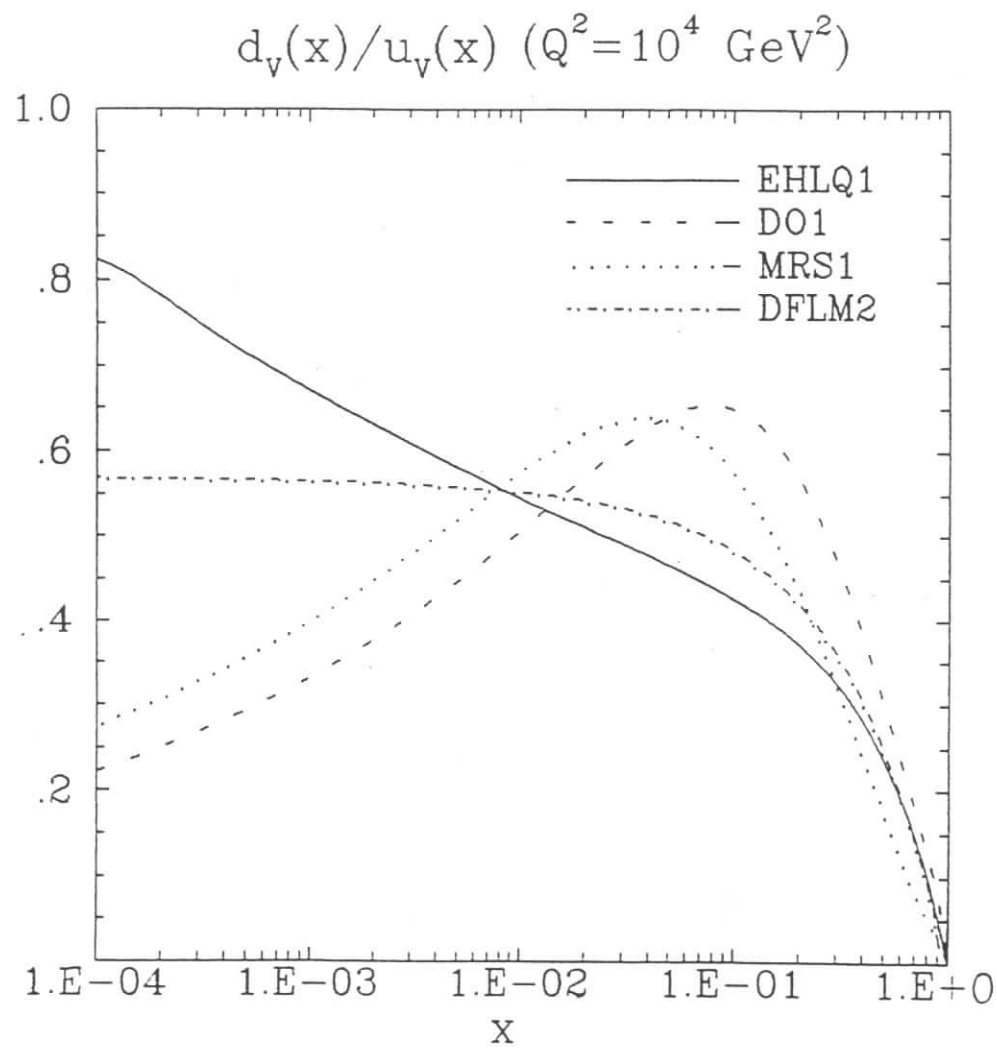


Fig. III.9b. The ratio for valence down and up quarks distributions $d_v(x, Q^2)/u_v(x, Q^2)$ at $Q^2 = 10^4 \text{ GeV}^2$ predicted by various parametrizations: EHLQ1, DO1, MRS1 and DFLM2 — logarithmic x -scale.

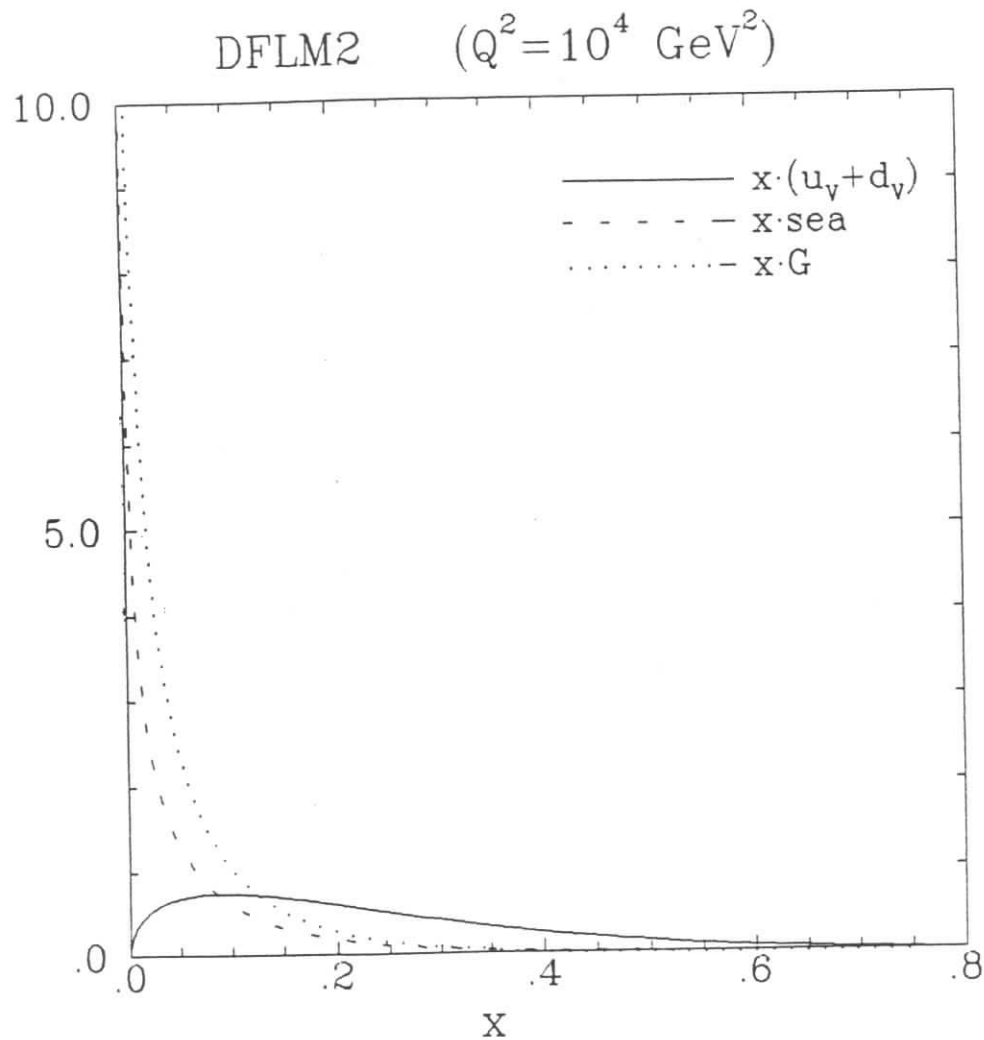


Fig. III.10a. Comparison of the valence quark distribution $x[u_v + d_v]$, the sea quark distribution $2x[\bar{u} + \bar{d} + s + c + b + t]$ and the gluon distribution xG of DFLM2 parametrization at $Q^2 = 10^4 \text{ GeV}^2$ —linear x -scale. There is cut on the y -axis at $y = 10$. True values of gluon and sea distributions at $x = 10^{-4}$ are seen on the next plot.

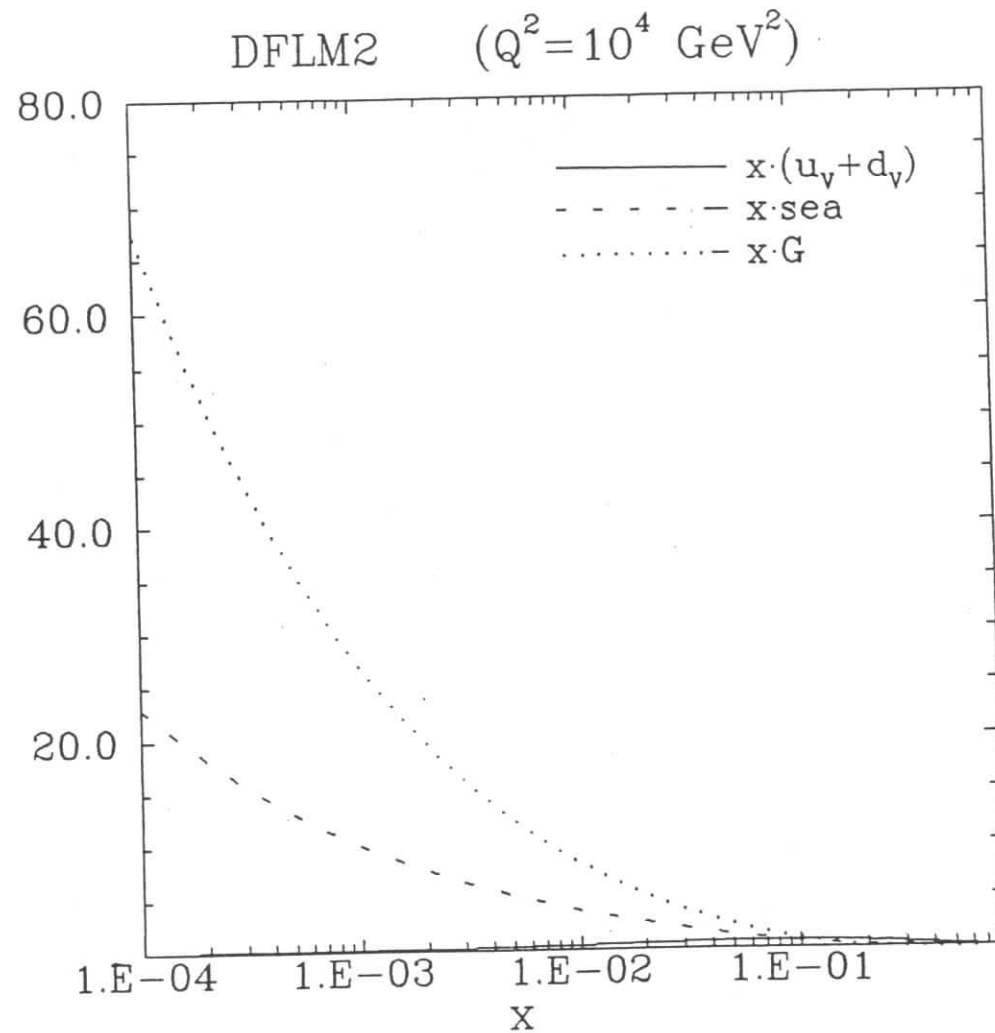


Fig. III.10b. Comparison of the valence quark distribution $x[u_v + d_v]$, the sea quark distribution $2x[\bar{u} + \bar{d} + s + c + b + t]$ and the gluon distribution xG of DFLM2 parametrization at $Q^2 = 10^4 \text{ GeV}^2$ —logarithmic x -scale.

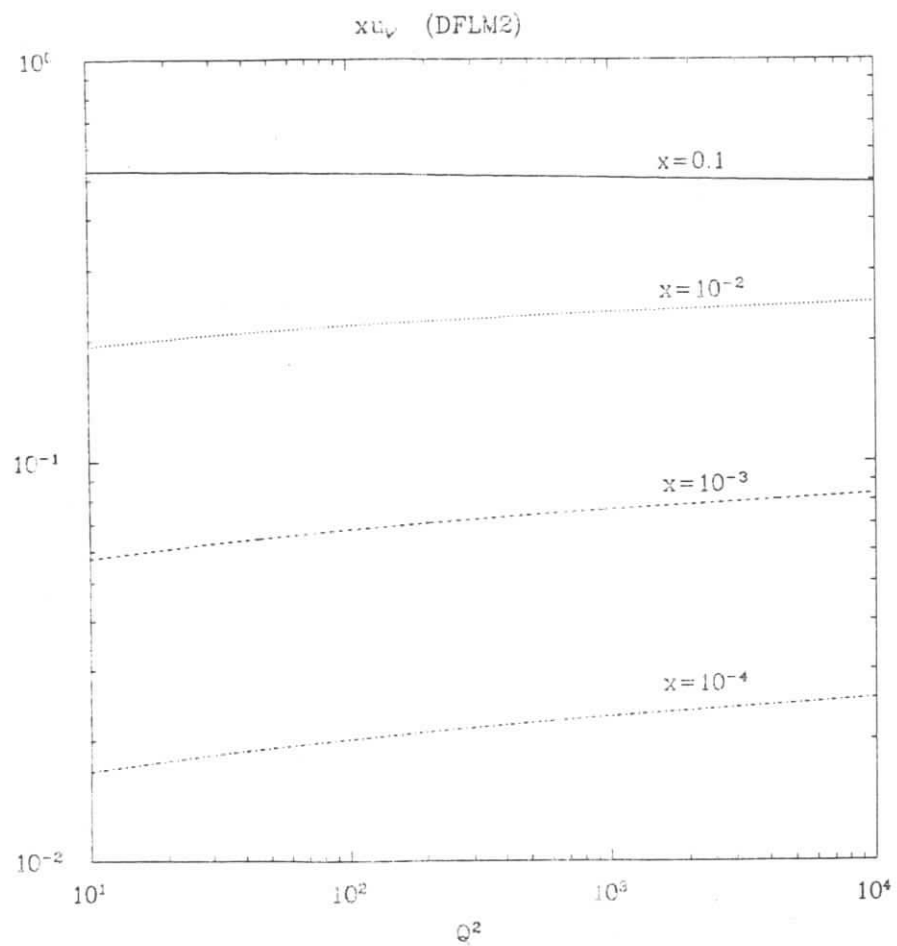


Fig. IV.1. The Q^2 evolution of the up valence quark distribution $x u_v(z, Q^2)$ in the DFLM2 parametrization at $x = 10^{-4}, 10^{-3}, 10^{-2}, 0.1$.

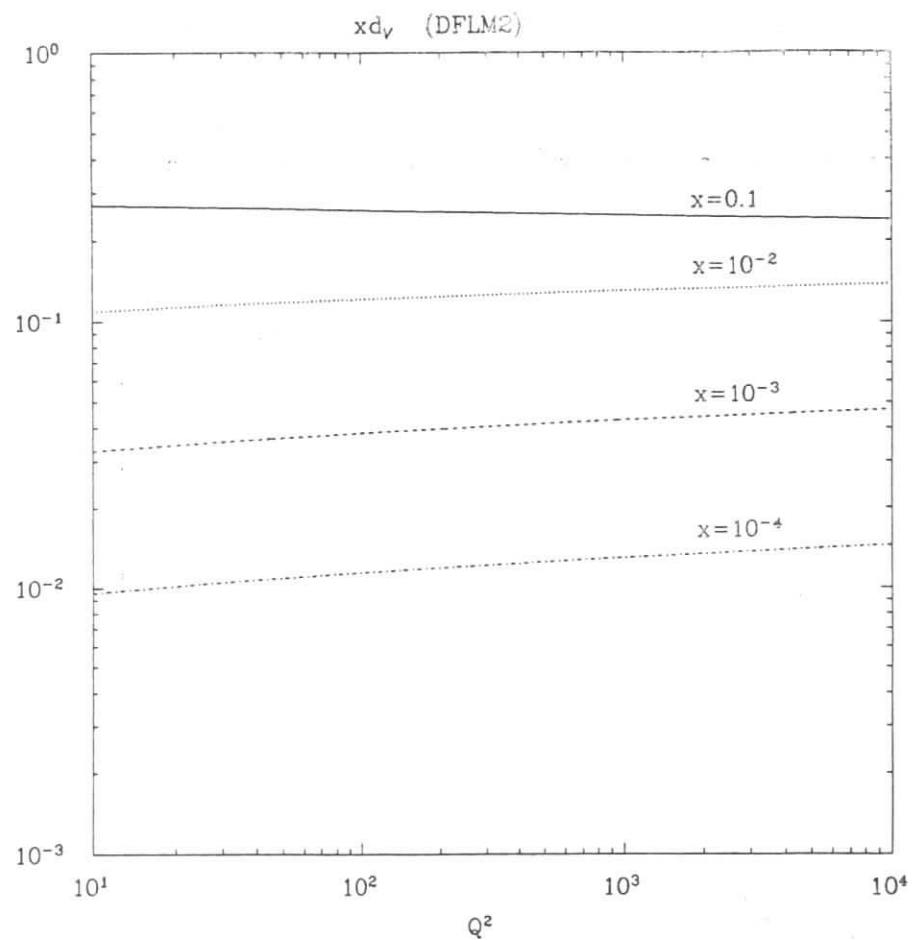


Fig. IV.2. The Q^2 evolution of the down valence quark distribution $x d_v(z, Q^2)$ in the DFLM2 parametrization at $x = 10^{-4}, 10^{-3}, 10^{-2}, 0.1$.

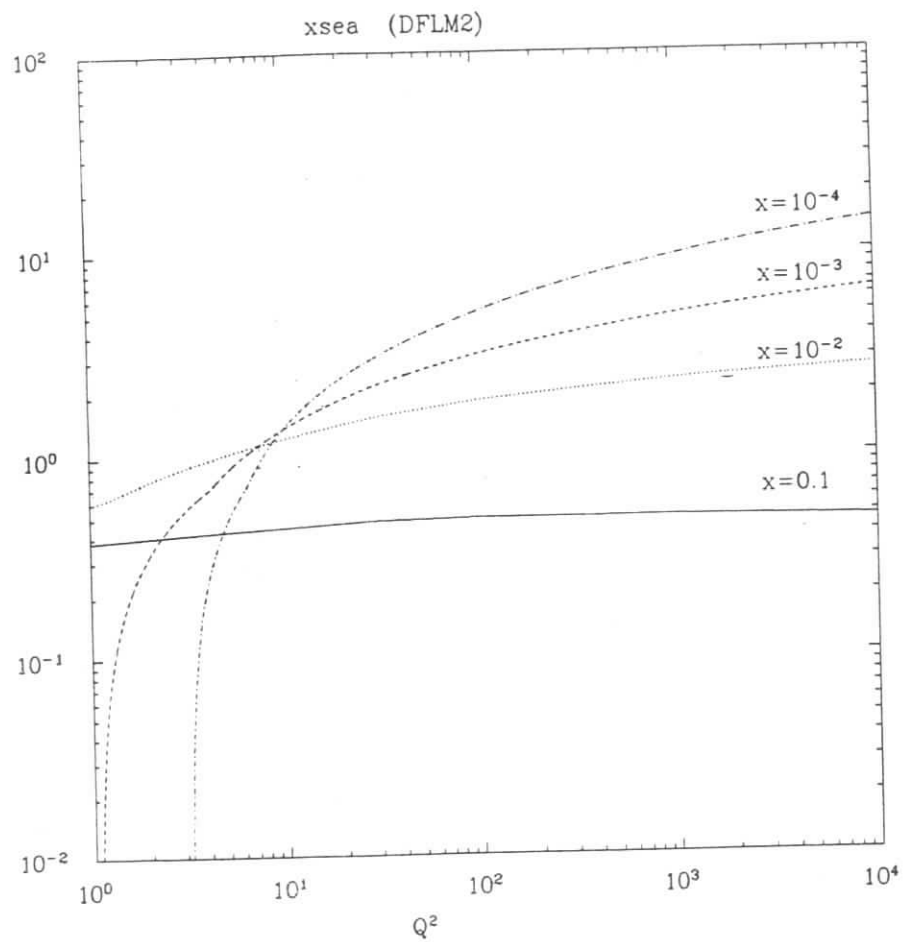


Fig. IV.3. The Q^2 evolution of the light sea distribution $2x(\bar{u} + \bar{d} + s)$ in the DFLM2 parametrization at $x = 10^{-4}, 10^{-3}, 10^{-2}, 0.1$.

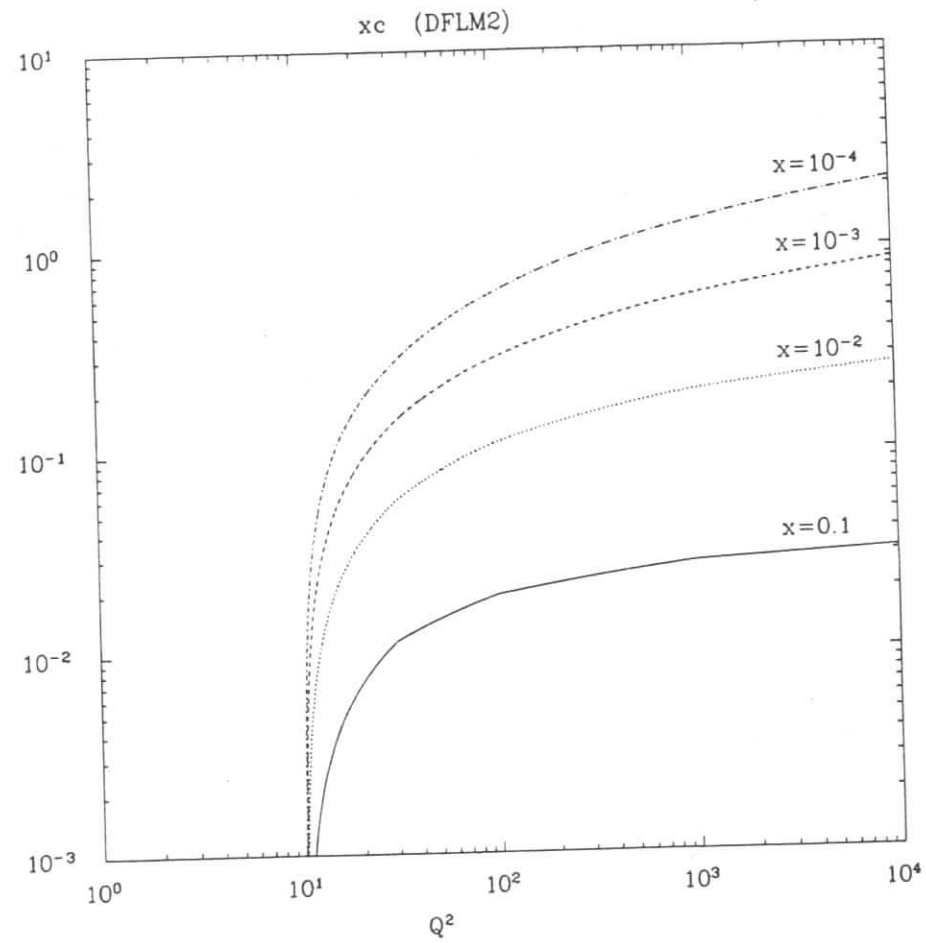


Fig. IV.4. The Q^2 evolution of the charm quark distribution $z_c(z, Q^2)$ in the DFLM2 parametrization at $x = 10^{-4}, 10^{-3}, 10^{-2}, 0.1$.

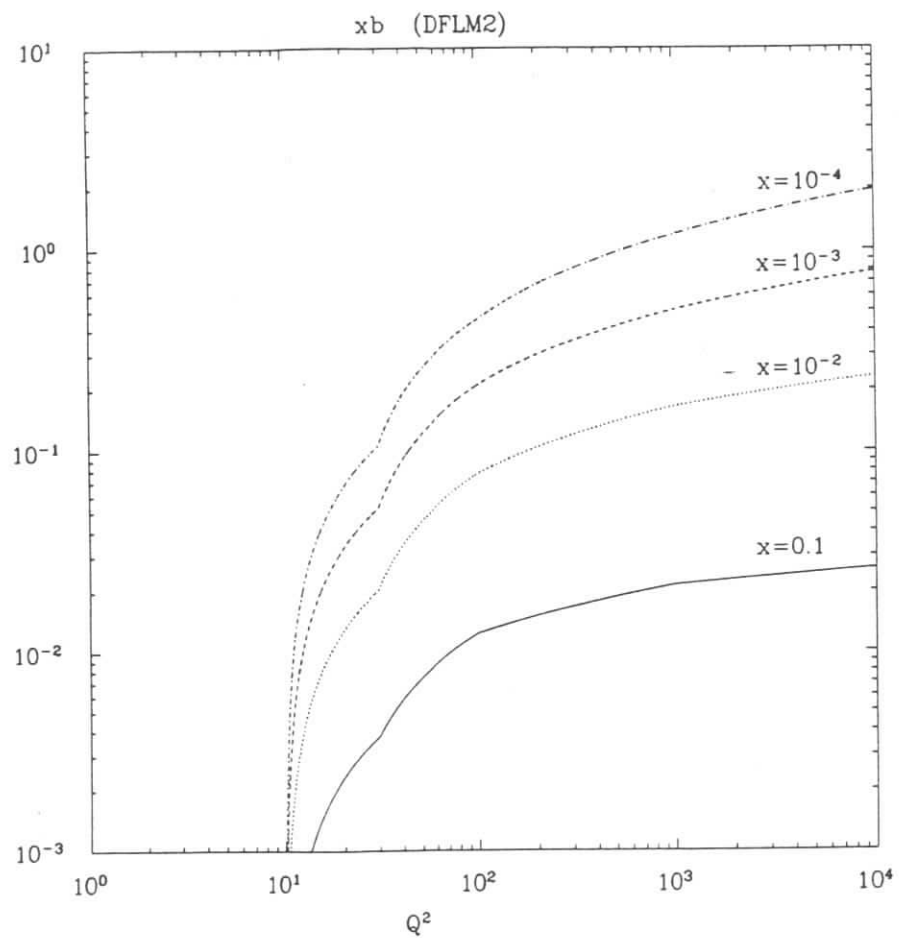


Fig. IV.5. The Q^2 evolution of the bottom quark distribution $x_b(z, Q^2)$ in the DFLM2 parametrization at $x = 10^{-4}, 10^{-3}, 10^{-2}, 0.1$.

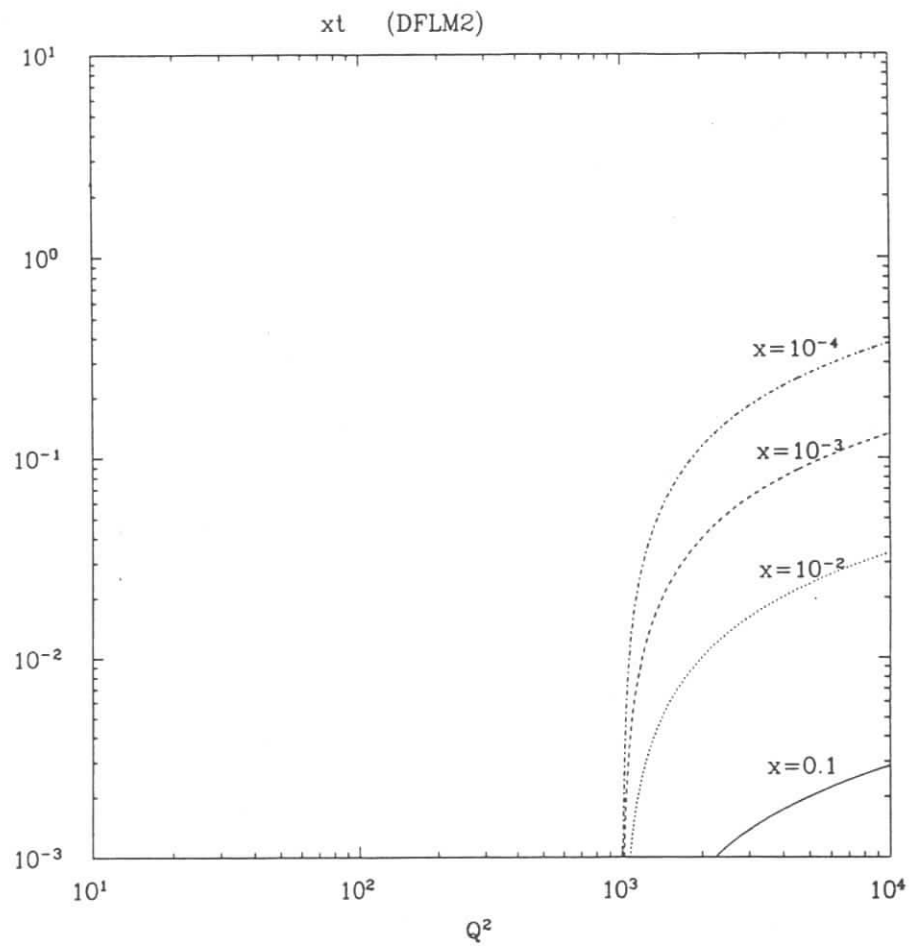


Fig. IV.6. The Q^2 evolution of the top quark distribution $x_t(x, Q^2)$ in the DFLM2 parametrization at $x = 10^{-4}, 10^{-3}, 10^{-2}, 0.1$.

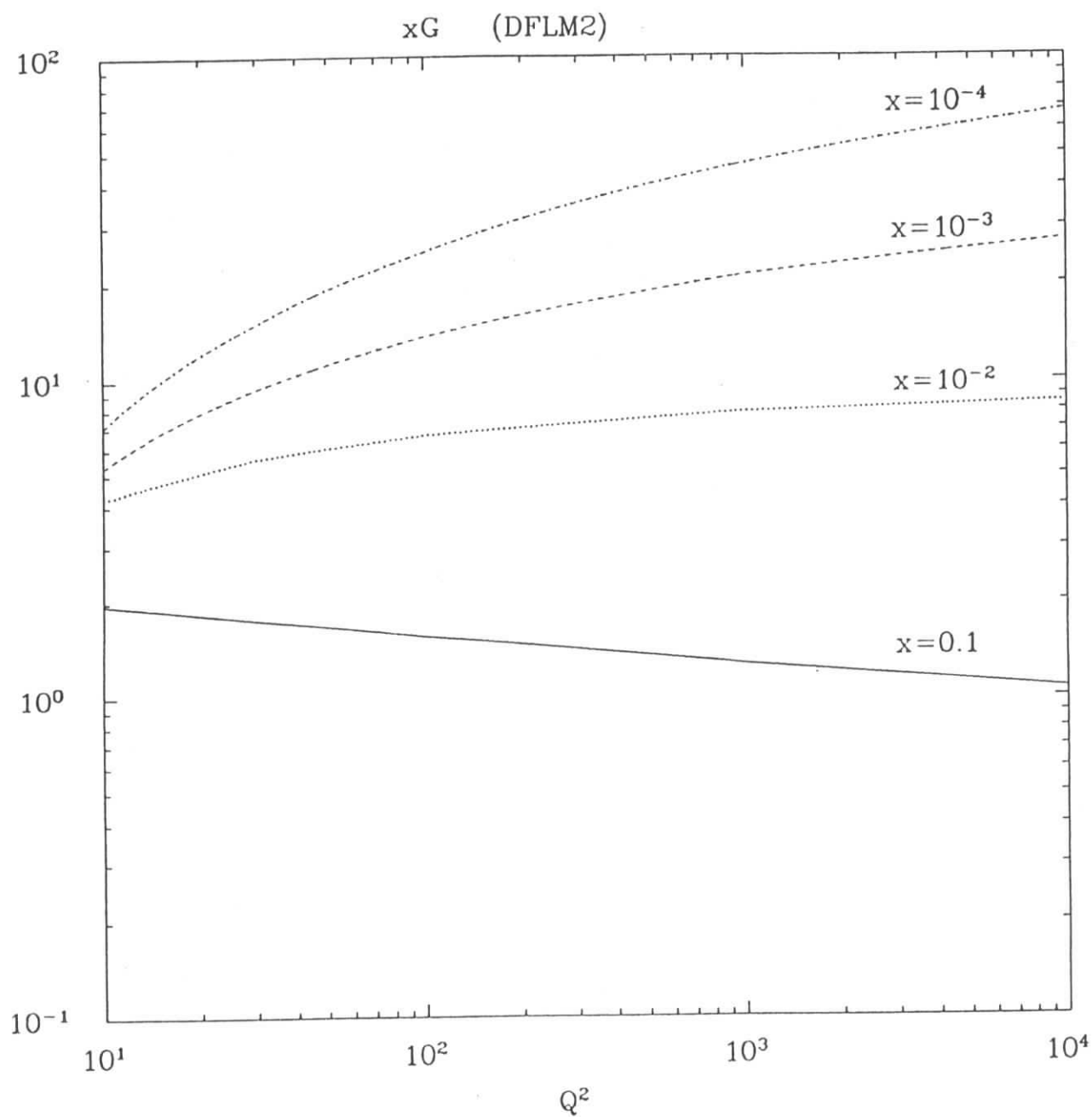


Fig. IV.7. The Q^2 evolution of the gluon distribution $xG(x, Q^2)$ in the DFLM2 parametrization at $x = 10^{-4}, 10^{-3}, 10^{-2}, 0.1$.

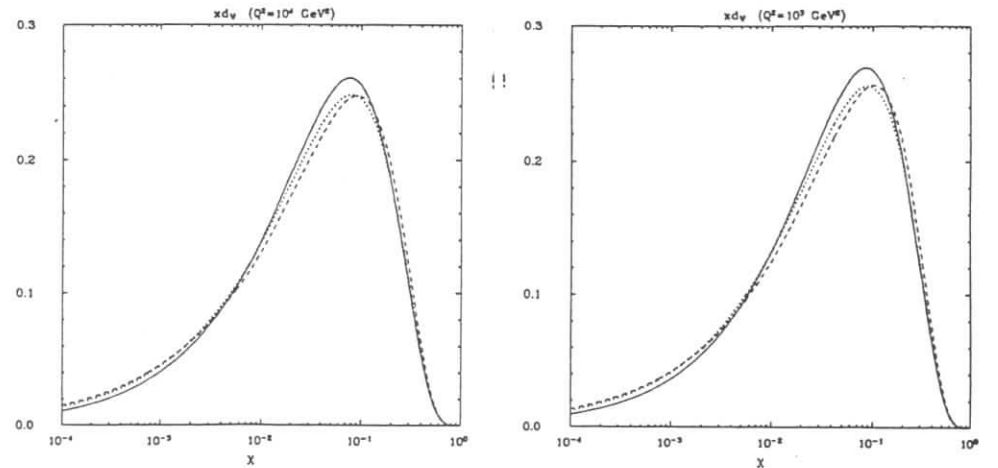
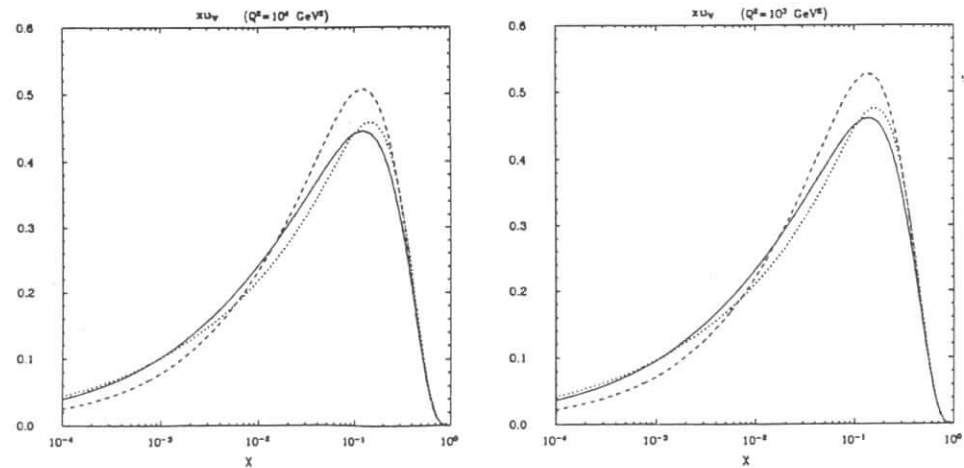
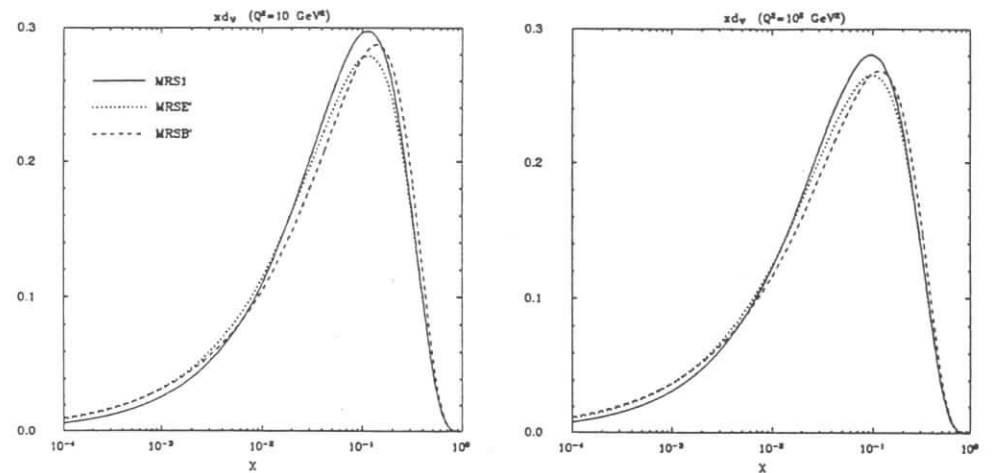
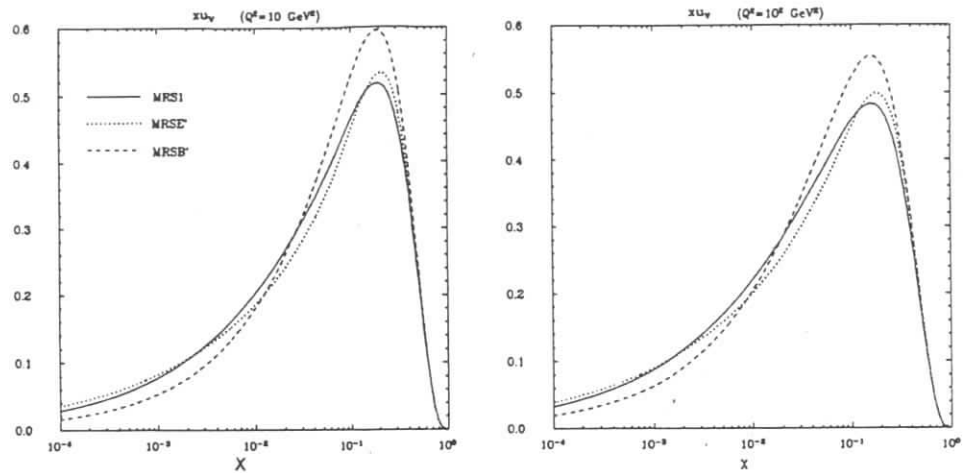


Fig. V.1. Comparison of the old (MRS1) and the new (MRSE' and MRSB') versions of the MRS parametrization for the up valence quark $xu_v(x, Q^2)$ at $Q^2 = 10, 10^2, 10^3, 10^4 \text{ GeV}^2$.

Fig. V.2. Comparison of the old (MRS1) and the new (MRSE' and MRSB') versions of the MRS parametrization for the down valence quark $xd_v(x, Q^2)$ at $Q^2 = 10, 10^2, 10^3, 10^4 \text{ GeV}^2$.

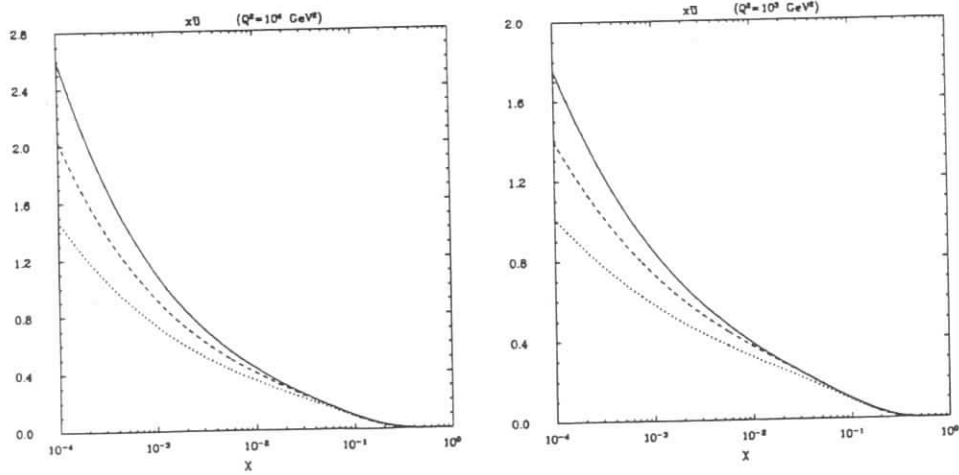
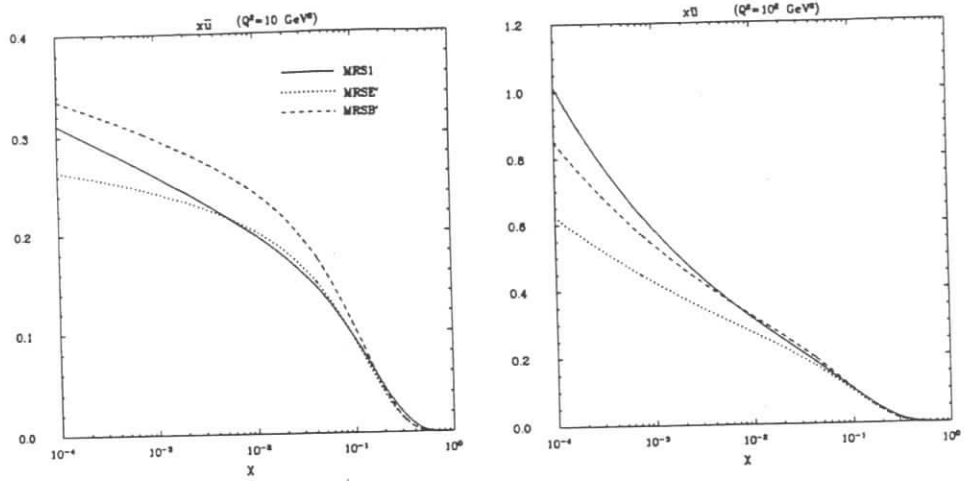


Fig. V.3. Comparison of the old (MRS1) and the new (MRSE' and MRSB') versions of the MRS parametrization for the up antiquark $x\bar{u}(x, Q^2)$ at $Q^2 = 10, 10^2, 10^3, 10^4 \text{ GeV}^2$.

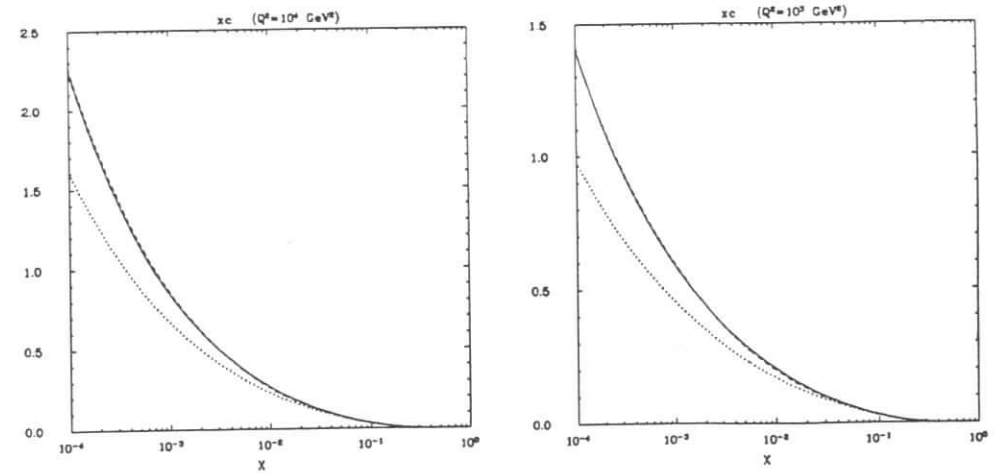
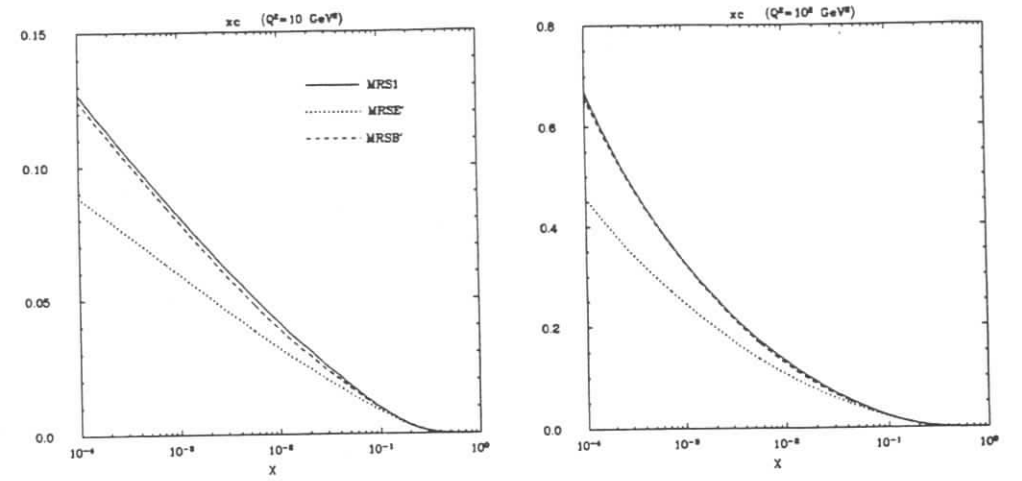


Fig. V.4. Comparison of the old (MRS1) and the new (MRSE' and MRSB') versions of the MRS parametrization for the charm quark $xc(x, Q^2)$ at $Q^2 = 10, 10^2, 10^3, 10^4 \text{ GeV}^2$.

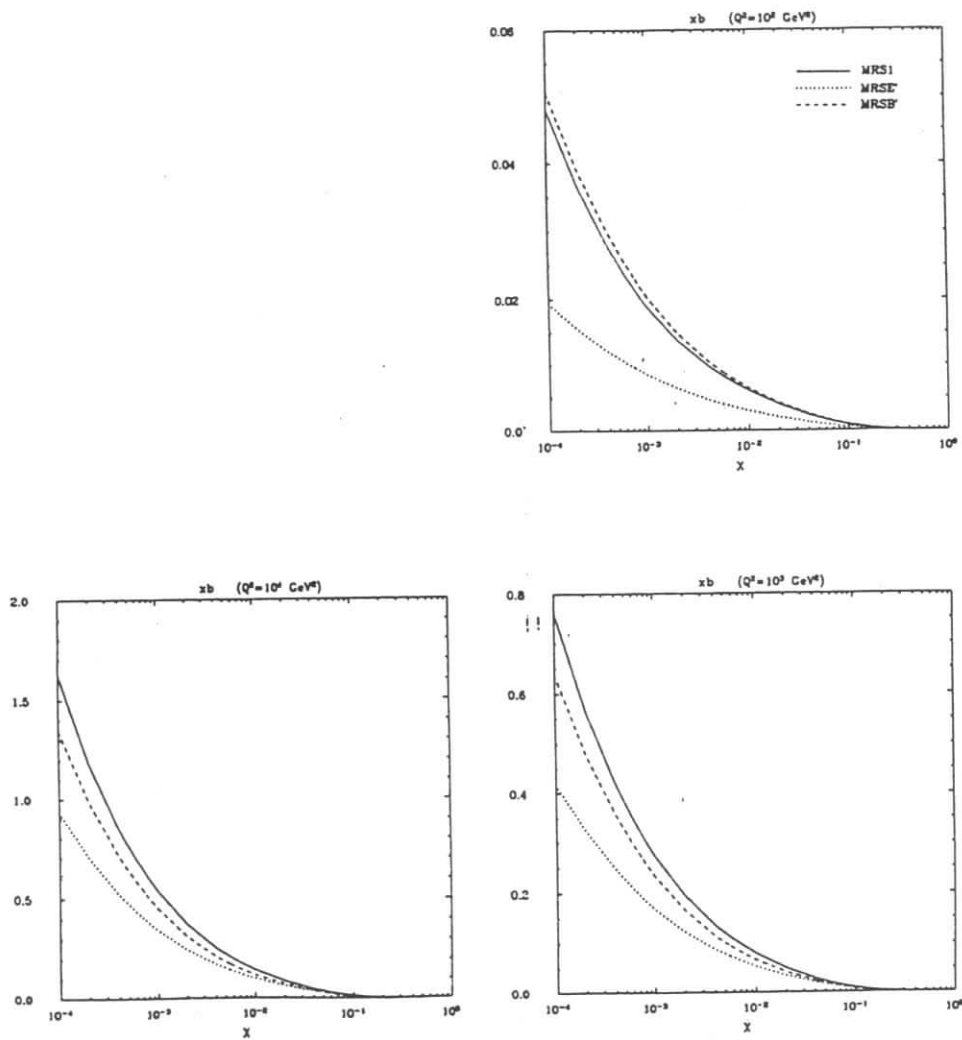


Fig. V.5. Comparison of the old (MRS1) and the new (MRSE' and MRSB') versions of the MRS parametrization for the bottom quark $x_b(x, Q^2)$ at $Q^2 = 10^2, 10^3, 10^4 \text{ GeV}^2$.

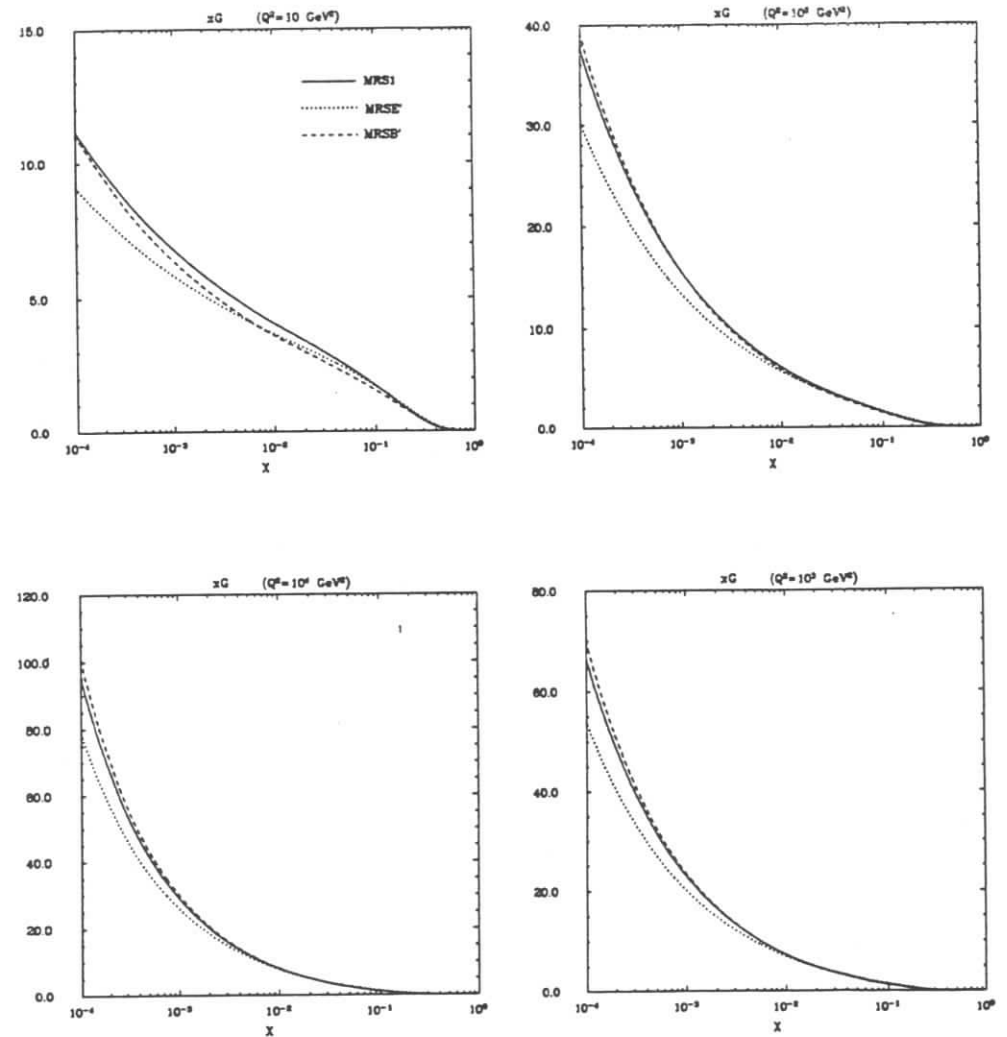


Fig. V.6. Comparison of the old (MRS1) and the new (MRSE' and MRSB') versions of the MRS parametrization for the gluon $x_G(x, Q^2)$ at $Q^2 = 10, 10^2, 10^3, 10^4 \text{ GeV}^2$.

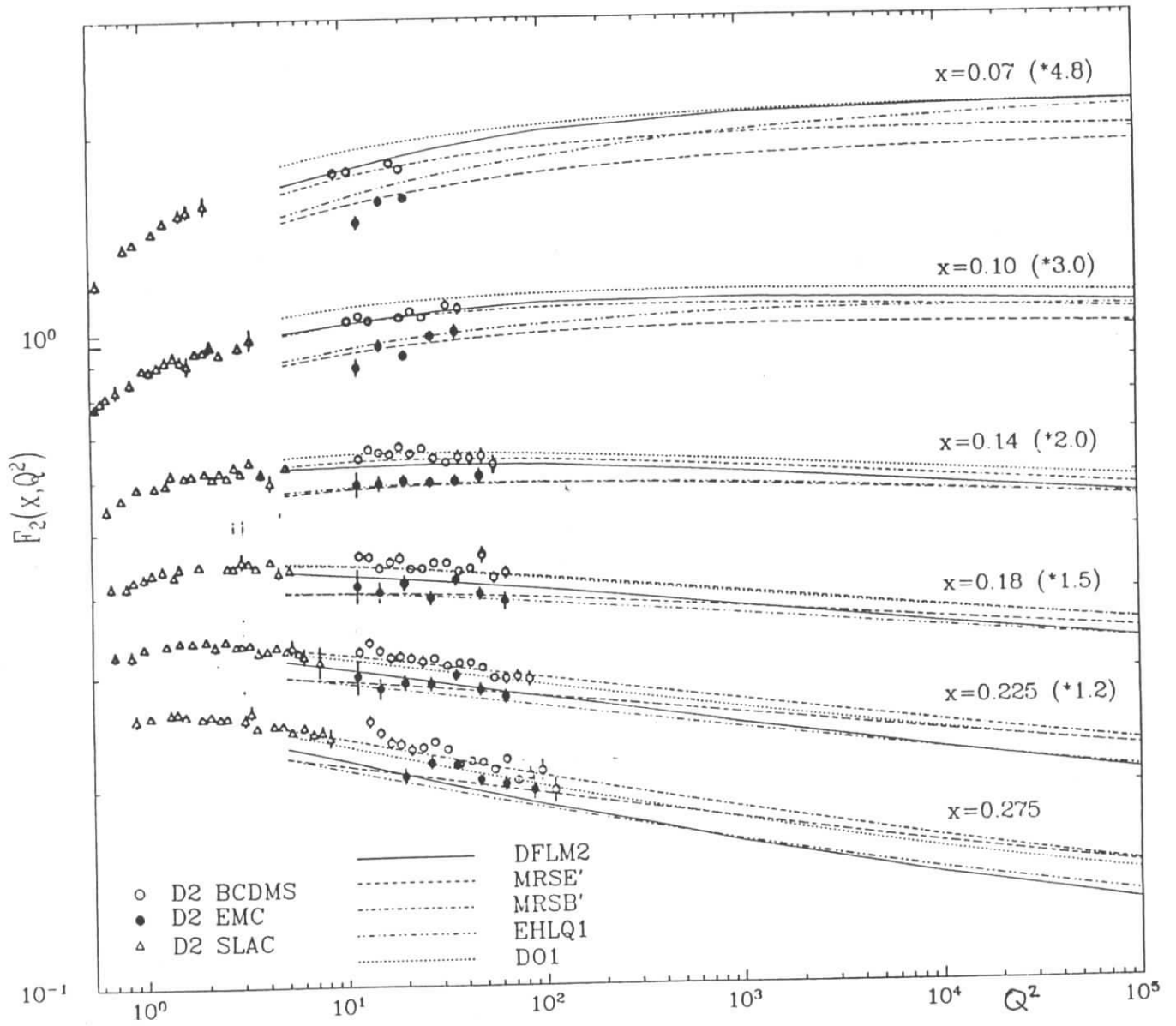


Fig. VI.1a. Comparison between the predictions of parametrizations P1-P5 for F_2^{em} and the data [20] for several values of x .

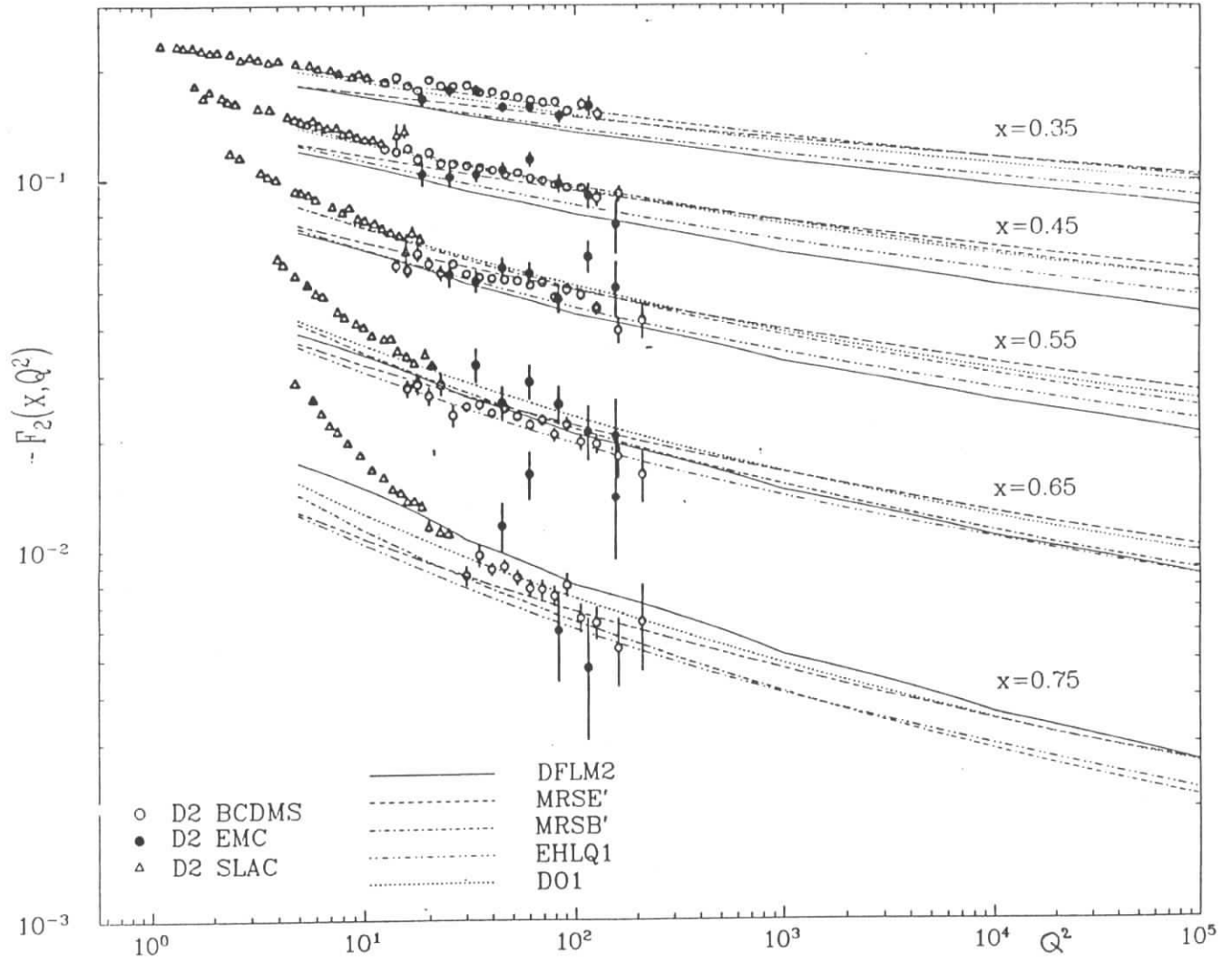


Fig. VI.1b. Comparison between the predictions of parametrizations P1-P5 for F_2^{em} and the data [20] for several values of x .

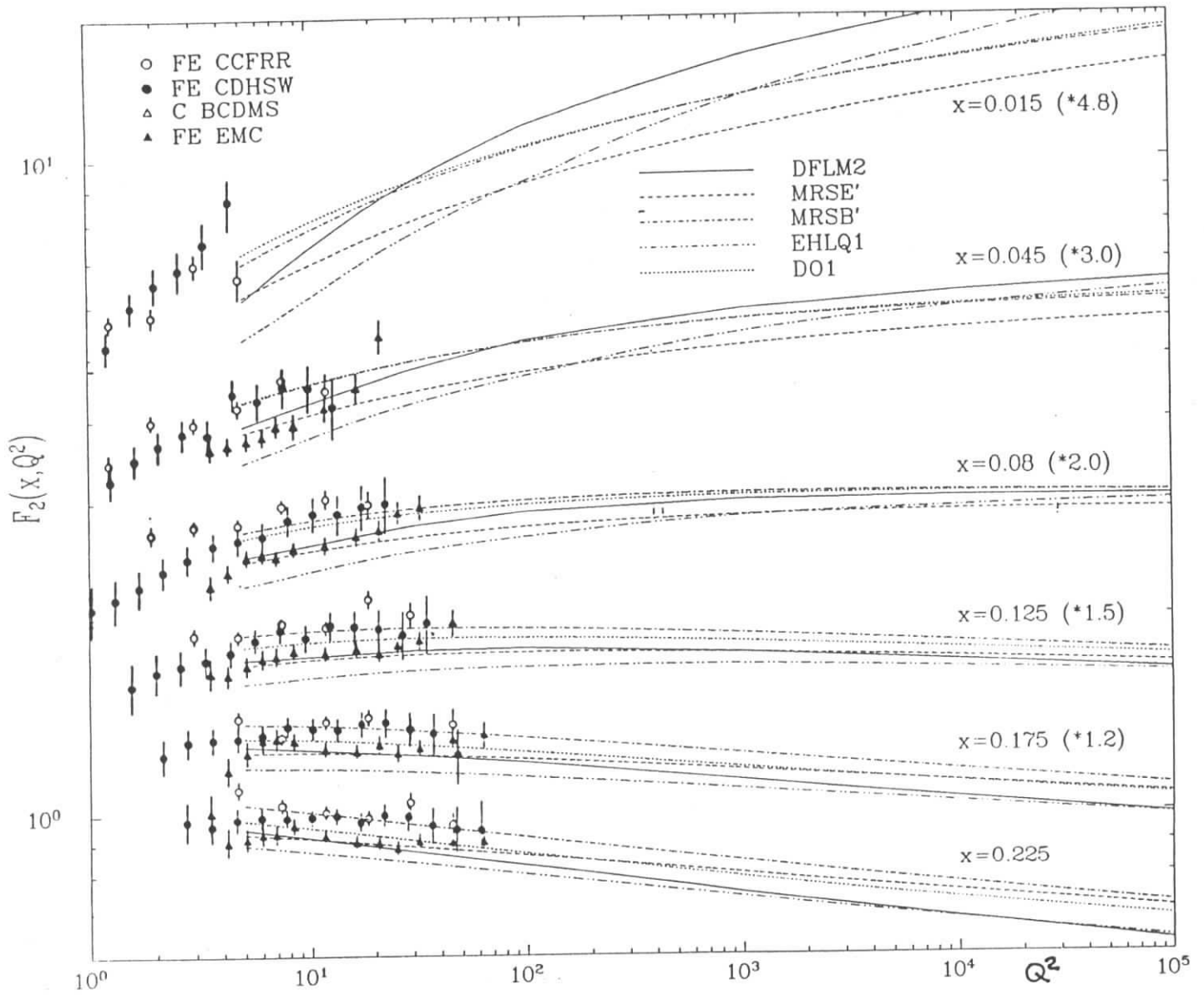


Fig. VI.2a. Comparison between the predictions of parametrizations P1-P5 for F_2^{ν} and the data [20] for several values of x . The data of EMC on iron and of BCDMS on carbon are multiplied by 18/5.

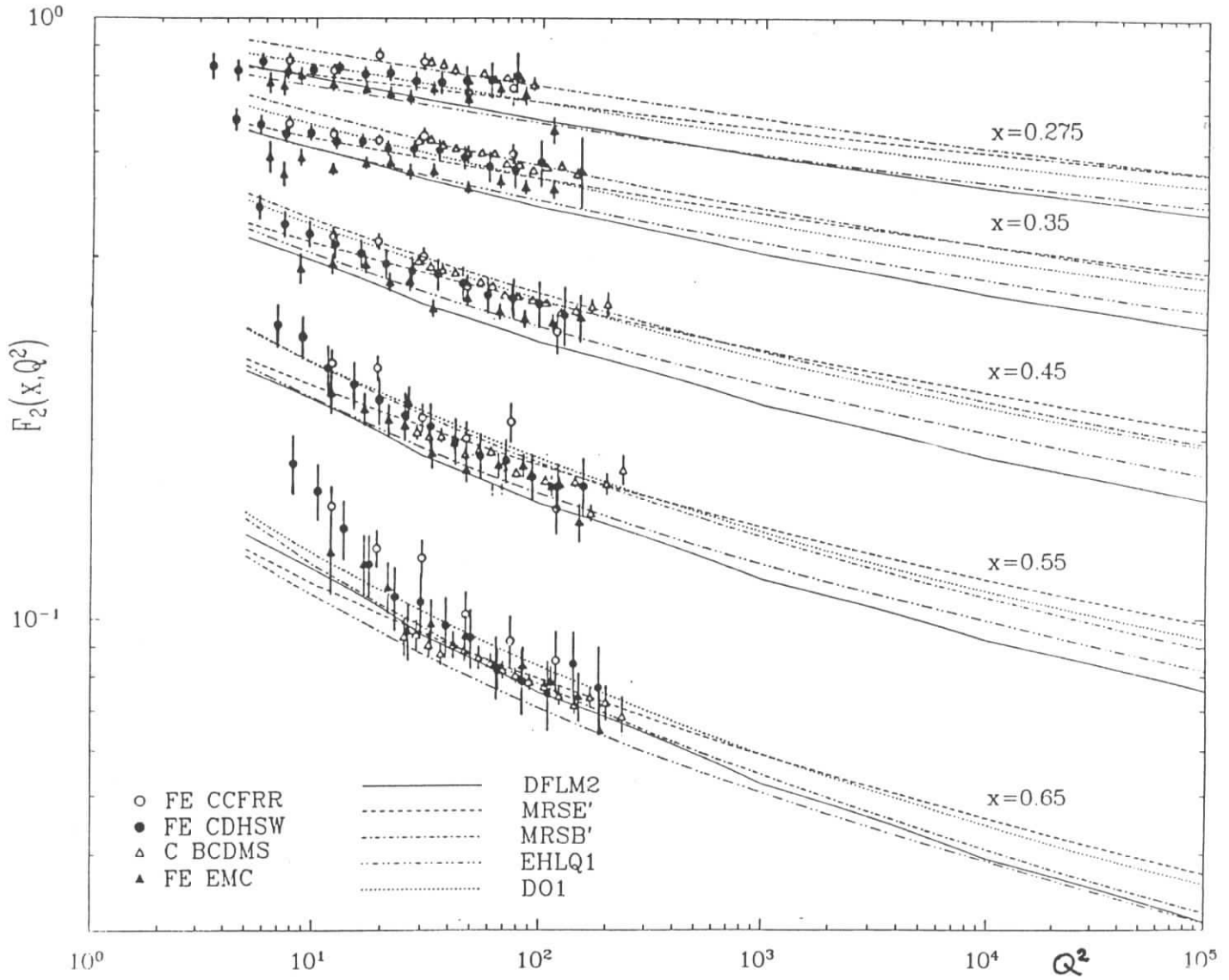


Fig. VI.2b. Comparison between the predictions of parametrizations P1-P5 for F_2^p and the data [20] for several values of x . The data of EMC on iron and of BCDMS on carbon are multiplied by 18/5.